Peptide-Based Strategies of Delivering Semiconductor Nanocrystals into Living Cells

BY
CLAUDIA IVETTE RIVERA VERA
B.Sc., Universidad Veracruzana, 2003
M.Sc., State University of New York at Buffalo, 2009

THESIS

Submitted as partial fulfillment of the requirements
for the degree of Doctor of Philosophy in Chemistry
in the Graduate College of the
University of Illinois at Chicago, 2017

Chicago, Illinois

Defense Committee:

Lawrence W. Miller, Chair and Advisor
Duncan Wardrop
Jung-Hyun Min
Justin Mohr
Ursula Perez-Salas, Physics

This Thesis is dedicated to my family for their endless love and support.

ACKNOWLEDGMENTS

I want to thank my PhD adviser Prof. Lawrence W. Miller for giving me the opportunity to join his lab, for the trust he put on me and for the countless times he vouched for me to support my academic and personal goals. I would also like to thank Prof. Duncan Wardrop for playing a key role in my success in graduate school, and his valuable advice during my job search, as well as Prof. Scott Schippy for being an advocate during my transition to Miller's group. I also want to thank the rest of my defense committee Prof. Jung-Hyun Min, Prof. Wonhwa Cho, Prof. Justin Mohr, and Prof. Ursula Perez-Salas for their valuable feedback and assistance.

Special thanks to my lab members and friends in Miller's group and Gevorgyan's group, to Silvia Solis, Rhonda Staudohar, Prof. George Papadantonakis, Dr. Dan McElheny, colleagues in Lorieau's group, Dr. Troyer, Prof. Gevorgyan, Prof. Qing Lin, Prof. Huw Davies, Prof. Thomas Kalman, Prof. David Hangauer, and Prof. Sherry Chemler.

Also, my eternal gratitude goes to my lab mate and friend Hamid Samareh Afsari for patiently helping me with all the imaging studies, qualitative and quantitative analyses, cell culture techniques and all the cellular biology experiments I am not familiar with since I am a synthetic organic chemist.

Further, I want to thank one of my best friends, Jose Ortiz, Silvia Solis (again), Victoria Helan, Lakmali Waidyarachchi, Geovannie Ojeda and Luz Maria Solis. My gratitude also goes to the four pillars I have strongly relied on at very critical points during my Masters and/or PhD program, Fabiola Barrios-Landeros, Simon Hedley, Silvia Solis and my family.

TABLE OF CONTENTS

TABLE OF CONTENTS (Continued)

Chapter ……..……..**Page**

TABLE OF CONTENTS (Continued)

Chapter …… **Page**

TABLE OF CONTENTS (Continued)

Chapter …… **Page**

LIST OF TABLES

LIST OF FIGURES

LIST OF FIGURES (CONTINUED)

Figure…….. **Page**

LIST OF FIGURES (CONTINUED)

LIST OF FIGURES (CONTINUED)

Figure…….. **Page**

LIST OF FIGURES (CONTINUED)

Figure…….. **Page**

LIST OF SCHEMES

Scheme ……Page

LIST OF SCHEMES (CONTINUED)

Scheme ……..**Page**

LIST OF ABBREVIATIONS

Å	Angstrom
A	Acceptor
Abs	Absorption
AMP	Antimicrobial peptide
Boc	tert-Butyloxycarbonyl
BHQ-2	Black hole quencher 2
$CHCl_3$	Chloroform
CL4	Zwitterionic ligand CL4
CO_2	Carbon dioxide
CPP	Cell penetrating peptide
CTC	Chlorotrityl chloride
D	Donor
Da	Daltons
DAPI	4',6-diamidino-2-phenylindole
DCC	*N,N′*-dicyclohexylcarbodiimide
DCE	1,2-Dichloroethane
DCM	Dichloromethane
DHLA	Dihydrolipoic acid
DIC	Differential interference contrast
DIEA	N,N-diisopropylethylamine
DMAP	4-(Dimethylamino) pyridine
DMEM	Dulbecco's modified Eagle's medium
DMF	Dimethylformamide
DMSO	Dimethylsulfoxide
DNA	Deoxyribonucleic acid
DPBS	Dulbecco’s phosphate buffered saline
EDC	1-Ethyl-3-(3-dimethylaminopropyl)carbodiimide
e-DHFR	Enhanced dihydrofolate reductase
EDT	1,2-ethanedithiol
EDTA	Ethylenediaminetetraacetic acid
EE	Endosomal escape
ELISA	Enzyme-linked immunosorbent assay
Em	Emission
Equiv	Equivalents
ESI-MS	Electrospray ionization mass spectrometry
EtOAc	Ethyl acetate
EtOH	Ethanol
FACS	Flow cytometry cell sorting

LIST OF ABBREVIATIONS (CONTINUED)

FBS	Fetal bovine serum
FDA	Food and Drug Administration
Fmoc	Fluorenylmethyloxycarbonyl
FRET	Förster resonance energy transfer
GC	Gas chromatography
GFP	Green fluorescent probe
GSH	Glutathione
H_2	Hydrogen gas
H_2O	Water
HA	Influenza hemagglutinin glycoprotein
HA2	Influenza hemagglutinin glycoprotein subunit 2
HAfp23	Hemagglutinin glycoprotein fusion protein 23
HBTU	O-(Benzotriazol-1-yl)-N,N,N',N'-tetramethyluronium hexafluorophosphate
HCCA	α-Cyano-4-hydroxycinnamic acid
HCL	Hydrochloric acid
HeLa	A cancer cell from a human uterine cervical carcinoma
HEPES	*N*-2-hydroxyethylpiperazine-*N'*-2-ethanesulfonic acid
His_6	Hexahistidine
HIV-1	Human immunodeficiency virus
HPLC	High pressure liquid chromatography
IFP	Intracellular fluorescence pattern
J	Spectral overlap integral
K_a	Equilibrium constant
K_d	Dissociation constant
$KMnO_4$	Potassium permanganate
LC	Liquid chromatography
LC/MS	Liquid chromatography mass spectrometry
LED	Light emitting diode
LiOH	Lithium hydroxide
MALDI	Matrix-assisted laser desorption/ionization
MEM	Minimum Essential Medium
mM	Millimolar
mRNA	Messenger ribonucleic acid
MeOH	Methanol
Mtt	4-Methyltrityl
N_2	Nitrogen gas
$NaBH_4$	Sodium borohydride
$NaHCO_3$	Sodium bicarbonate

LIST OF ABBREVIATIONS (CONTINUED)

NHS	*N*-hydroxysuccinimide
nM	Nanomolar
nm	Nanometer
NMR	Nuclear magnetic resonance
NPys	3-nitro-2-pyridinesulfenyl
MS	Mass spectrometry
MW	Molecular weight
OPC	Oligonucleotide Purification Cartridge
Oxyme	Ethyl Isonitrosocyanoacetate
PAMAM	Polyamidoamine
PBS	Phosphate-buffered saline
PCR	Polymerase chain reaction
PEG	Polyethyleneglycol
PEI	Polyethyleneimine
PL	Photoluminescence
PVC	Poly (vinyl chloride)
QD	Quantum dot
Qd	Quantum dot
QSY-7	Dark quencher commercial name
QSY-21	Dark quencher commercial name
Rpm	Revolutions per minute
RT-PCR	Reverse transcriptase polymerase chain reaction
R_9	Nonarginine
siRNA	Small interference ribonucleic acid
SPPS	Solid phase peptide synthesis
TAT	Trans-activator protein that regulates viral transcription
Tb	Terbium
TCEP	Tris-(carboxyethyl)phosphine hydrochloride
TEAA	Triethylammonium acetate)
Tf	Transferrin
TFA	Trifluoroacetic acid
THF	Tetrahydrofuran
TIPS-H	Triisopropylsilane)
TMP	Trimetropin
TOP	Trioctylphosphine
TOPO	Trioctylphosphine oxide
Trt	Trityl
µL	Microliters

LIST OF ABBREVIATIONS (CONTINUED)

μM	Micromolar
UV/vis	Ultraviolet/ Visible

AMINO ACIDS ABBREVIATIONS

Name	Abbreviation (3 Letter)	Abbreviation (1 Letter)
Aminoisobutyric acid	Aib	Aib
Alanine	Ala	A
Arginine	Arg	R
Asparagine	Asn	N
Aspartate	Asp	D
Asparagine	Asn	N
Cysteine	Cys	C
Diaminopropionic	Dap	Dap
Glutamate	Glu	E
Glutamine	Gln	Q
Glutamic acid	Glu	D
Glycine	Gly	G
Histidine	His	H
Isoleucine	Ile	I
Leucine	Leu	L
Lysine	Lys	K
Methionine	Met	M
Palimitic acid	Palm-OH	Palm-OH
Phenylalanine	Phe	F
Proline	Pro	P
Serine	Ser	S
Threonine	Thr	T
Tryptophan	Trp	W
Tyrosine	Tyr	Y
Valine	Val	V

Dissertation Advisor: Prof. Lawrence W. Miller Claudia I. Rivera Vera

Peptide-based strategies of delivering semiconductor nanocrystals into living cells

Abstract

Semiconductor nanocrystals or quantum dots (QDs) possess exceptional optical and physicochemical properties, for instance, their brightness and long fluorescence lifetimes, which makes them valuable for live-cell imaging. Due to their large size, QDs do not cross cell membranes passively, fortunately, this issue can be addressed by coating QDs with cell penetrating peptides (CPPs) such as the TAT sequence or polyarginine as it has been reported by several studies from different labs. We could intracellularly deliver CPP coated red and green emitting QDs, however, as many others have shown, we also found that endocytosis was the major mechanism of intracellular uptake in HeLa cells, and consequently, QDs remained trapped inside the endosomes without being able to reach the cytosol.

In this thesis, I designed and synthesized a few peptides with purported potential endosomal escape activity. These peptides were conjugated to the QD surface, and we showed that a peptide derived from Aurein 1.2 and a polyamine derivative significantly enhanced the endosomal escape of our QD bioconjugates in live cell studies. Further, we developed a FRET (Forster resonance energy transfer)-based method to quantify the endosomal escape triggered by the Aurein 1.2, polyamine, and palmitoyl peptides respectively, along with a small protein (HA2) derived from the influenza virus. Our FRET

sensor system is comprised of a QD (as the FRET donor) linked to a rhodamine labeled peptide (as the FRET acceptor) through a disulfide bond, and thus, rendering a ratiometric FRET system that measures the extent of endosomal escape by the change in red/green signal upon disulfide bond cleavage by cytosolic glutathione.

Collectively, our qualitative and quantitative microscopy studies indicate that both, Aurein 1.2, as well as a polyamine peptide I designed from scratch, do enhance endosomal escape of QDs in live-cell studies. I also performed more than 95% of the synthetic work displayed in this thesis.

1 Introduction

1.1 Introduction

Therapeutic and imaging nanoparticles are part of a new growing field in nanomedicine, in fact, by 2016 the FDA had already approved 51 nanomedicines, among them liposomal, polymeric and nanocrystal formulations.[1]

Nanoparticle size (1-100 nm), shape, and surface chemistry directly affect the potential for accumulation in different tissues and for cellular uptake. It is well known that endocytosis is the major mechanism of internalization of nanoparticles, thus, to realize the intended therapeutic effect, nanoparticles must escape the endosomes to reach the cytosolic environment. Since nanoparticles have a large surface area, and given the large amount of bioconjugation chemistries available, it is possible to tailor their design at the synthetic stage to include ligands that enhance or trigger their escape from the endolysosomal system, however, a major obstacle is the lack of methods to quantify endosomal escape. In this chapter, I present an overview of the properties of quantum dots and their ability to act as imaging agents, nanoscaffolds for bioconjugation and Förster Resonance Energy Transfer (FRET) donors.

Then an overview of methods used for their intracellular delivery is described, followed by a review on the endocytosis of nanoparticles and mechanisms of endosomal escape. Last, I describe current procedures used to measure endosomal escape and the need to develop a method to quantify (section 1.10) and compare (section 1.11) the endosomal escape abilities of different bioconjugatable endosomolytic ligands.

1.2 Quantum dots and their application in microscopy.

Quantum dots (QDs) are semiconductor nanocrystals with unique optical and physicochemical properties due to quantum confinement effects.[2] For example, they have broad absorption spectra, large extinction coefficients , tunable and narrow photoluminescence (PL) as a function of their size, improved resistance to photobleaching high emission quantum yields, and long fluorescence lifetimes, which makes them useful for bioimaging and biosensing applications in cellular biology[3] (Figure 1.1).

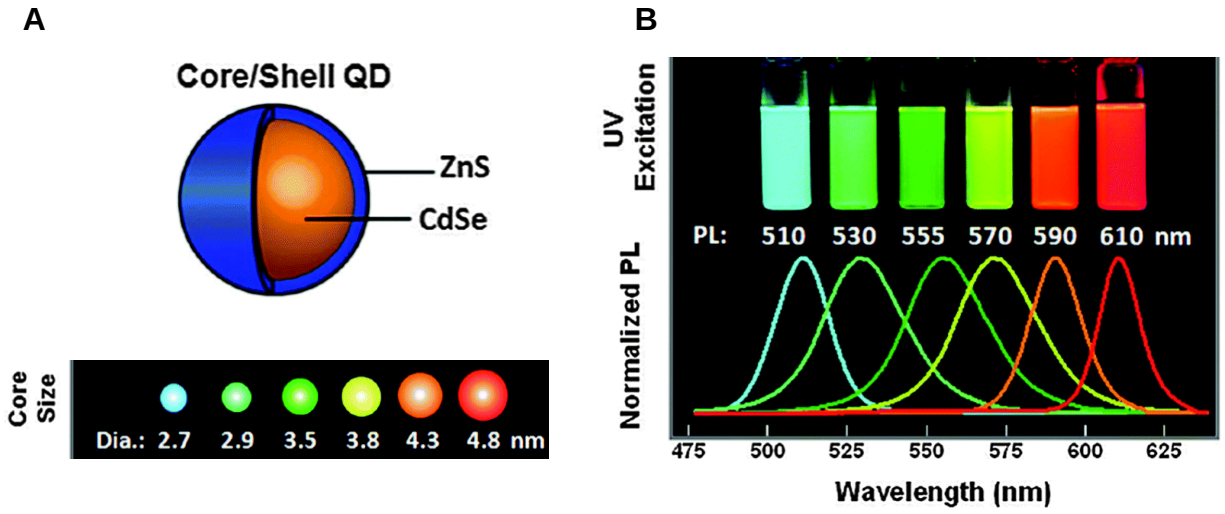

Figure 1.1. (A) Schematic drawing of core-shell QD. (B) The smaller QDs of the same material emit lower PL wavelengths. Figure adapted from Chem. Soc. Rev., 2015, **44**, 4792-4834).

QDs are composed of 10^2– 10^4atoms, are roughly spherical in shape, and their size typically ranges from 1–10 nm in diameter[4-6]. In this work, we employed QDs with a CdS core and ZnS shell due to their well-known properties and established synthetic methods[7-10], although there are several other choices such as core CdS and CdTe, whose synthetic methods are well developed. The large surface area of QDs allows them to assemble and display multiple copies of biomolecules to either reach a target or to sense a biological event upon their intracellular delivery (methods of delivery discussed further in section 1.6). By choosing the appropriate surface ligands QDs are made biocompatible and even resistant to a wide pH range (Figure 1.2).

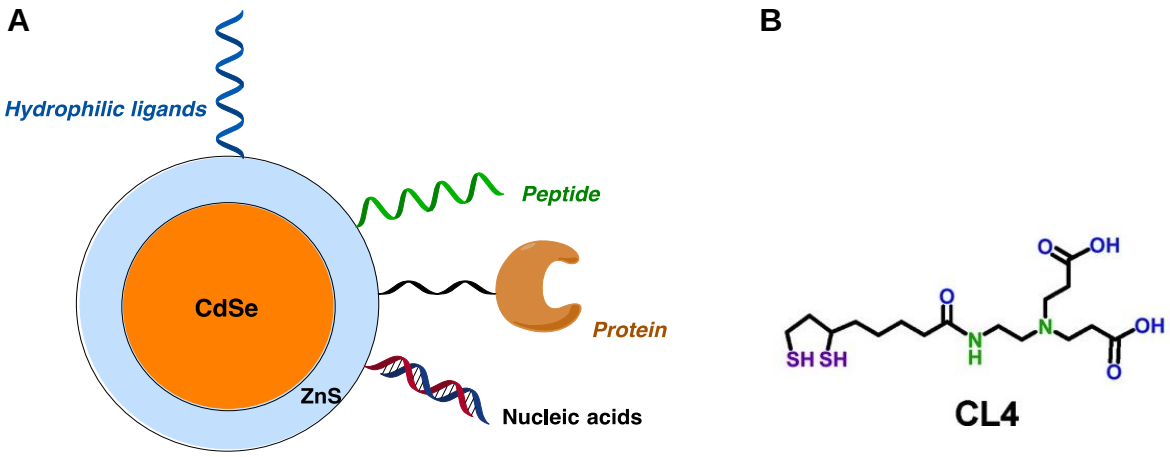

Figure 1.2. QDs can be made biocompatible (A). An example of a coating ligand that makes QDs stable at low pH (B).

Besides their ability to be bioconjugated, in this work we have exploited the ability of green emitting QDs to act as FRET donors when coupled with a matching red rhodamine FRET acceptor to sense and report an intracellular event by a change in their emission wavelength.

1.3 The FRET Principle

Förster Resonance Energy Transfer (FRET) is a physical phenomenon that relies on the radiationless transmission of excitation energy from a donor to an acceptor molecule. This transfer of energy is highly distance-dependent and occurs over distances of 10-100 Å between donor and acceptor, without any molecular collision and without conversion to thermal energy. The electronic excitation energy of a donor (D) is transferred -without photons being involved-to a ground state acceptor (A) via dipole–dipole interactions. The dipoles of interest are the transition moments associated with donor relaxation and acceptor excitation.[11] In general, a pair of entities or molecules that interact in a such a way that FRET occurs is referred to as a donor/acceptor pair. The primary conditions that need to be met for FRET occur are the following: a) The donor and acceptor molecules must be near one another (10-100 Å). b) The absorption or excitation spectrum of the acceptor must overlap the fluorescence emission spectrum of the donor, and the degree to which they overlap is referred to as the spectral overlap integral (J) (Figure 1.3) and c) The donor and acceptor transition dipole orientations must be approximately parallel[11].

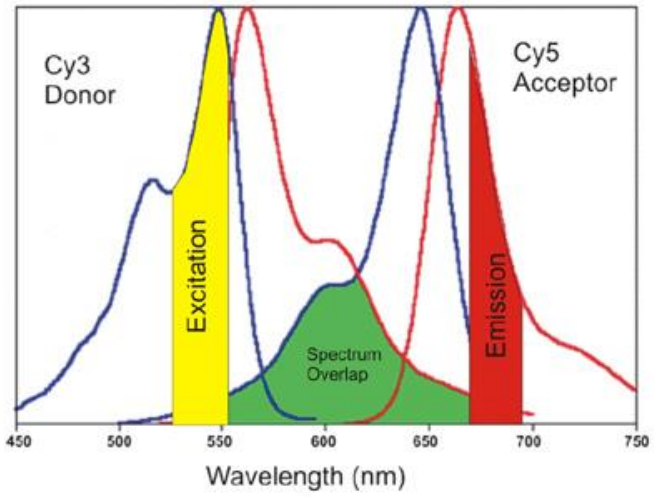

Figure 1.3. Schematic representation of the spectral overlap integral[12]

If the donor-acceptor pairs are compatible (as shown in Figure 1.3) , the most critical element necessary for FRET to occur is proximity of the pairs. The FRET efficiency of the process (E) depends on the inverse sixth-distance between the donor and acceptor (Equation 1)[13]

$$E = Ro^6/ (Ro^6 + r^6) \qquad \text{(Eq. 1)}$$

Where Ro is the Förster distance at which half the energy is transferred, and **r** is the actual distance between donor and acceptor. Also, Ro is dependent on the fluorescence quantum yield of the donor in the absence of the acceptor (fd), the refractive index of the solution (n), the dipole angular orientation of each molecule (k^2), and the spectral overlap integral of the donor and acceptor (J). (Equation 2) [13]

$$Ro = 9.78 \times 10^3(n^{-4} * fd* k^2*J)^{1/6} \text{ Å} \qquad \text{(Eq. 2)}$$

FRET can be detected by the appearance of fluorescence of the acceptor oy by quenching of the donor fluorescence. The way fluorophore donors emit a photon in the absence of a FRET acceptor is as follows: with appropriate excitation, the electrons of the donor jump from the ground state (S0) to a higher vibrational level. Within picoseconds these electrons decay to the lowest vibrational level (S1) and eventually, within nanoseconds they decay back to the S0 state and a photon of light is emitted (Figure 1.4).

In contrast, when there is a fluorescent donor in the presence of a matching FRET acceptor, two processes will compete for the decay of excitation energy; the donor fluorescence decay and the energy transfer to the acceptor. With Förster resonance energy transfer, the photon from the fluorescent donor is not emitted, but instead, the energy is transferred to the acceptor, exciting its electrons and emitting a photon after returning to their ground state.

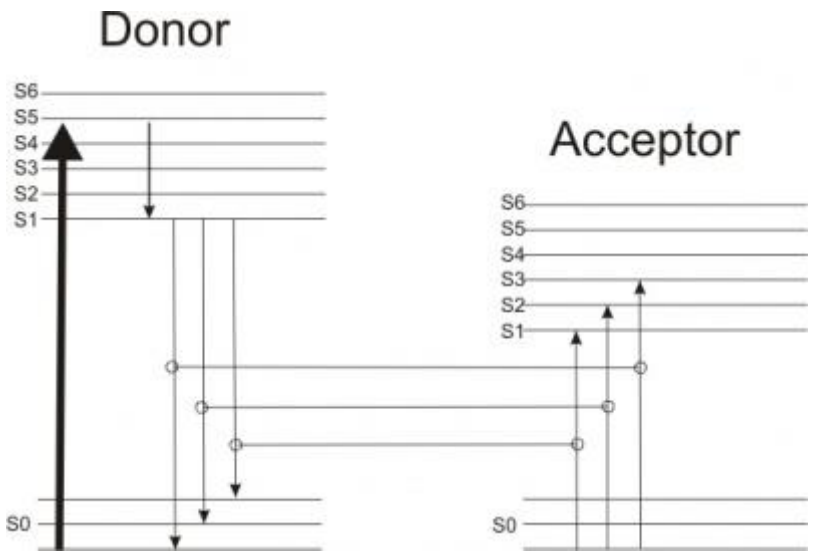

Figure 1.4. Schematic depicting electron vibrational energy states that occur during FRET[12]

1.4 QDs as FRET donors

QDs are continuously used as FRET donors because of the following features: (*i*) their broad absorption spectra and large molar absorption coefficients, (*ii*) their narrow, size tunable PL with good quantum yields and (*iii*) their large and biochemically accessible area.[11] QDs capacity to absorb energy increases as the excitation moves towards shorter wavelengths. This attribute is desirable because it decreases the chances of directly exciting the acceptor dye by choosing a QD excitation wavelength as far as possible from the acceptor absorption band.

Besides their size-tunable PL, QDs are ideal donors because the rate of FRET and its overall efficiency becomes larger due to their much higher quantum yield when compared to regular fluorophore donors. Also, their narrow PL allows to maximize the resolution of the FRET sensitized emission from the acceptor with minimal overlap between the QD emission and the acceptor emission. It is also possible to simultaneously excite different colors of QD donors at a single wavelength and therefore, transfer energy to their corresponding FRET acceptors to allow for highly multiplexed studies.[2, 14-20]

Since QDs have a large surface area, it is possible to use bioconjugation to assemble multiple FRET acceptors around a single QD donor, however, there are some alterations to the standard FRET model (Equation 2, Section 1.3) that should be considered when a single QD donor simultaneously interacts with multiple (*a*) acceptors.

Thus, if all acceptors are located at the same distance from the QD donor, the FRET efficiency is expressed as shown in Equation 3:

$$E = a\,Ro^6/(a\,Ro^6 + r^6) \quad \text{, where } a = \text{number of acceptors} \qquad \text{(Eq. 3)}$$

The rate of FRET between the QD donor and dye acceptor is still the same, however, since multiple acceptors are introduced, according to Equation 3, the net rate of FRET from the QD donor to any acceptor increases.[11]

Any process that affects the energy transfer rate from QD donor to a FRET acceptor(s) can be quantified,[21] therefore, the transfer of energy from a green QD donor to a red rhodamine acceptor would lead to a reduction in the donor fluorescence (and excited lifetime), and an increase in the rhodamine acceptor emission intensity. This last process can be quantified, and therefore provide information about biochemical events such as the disulfide bond reduction of the red rhodamine acceptor from the green QD donor by cytosolic glutathione.

1.5 Our bioconjugation method

Bioconjugation is the process by which biological molecules are assembled on to the QD surface. This is a critical step as it directly impacts the QD-bioconjugate's final function, structure and hydrodynamic radius.[22] There are plenty of QD bioconjugation chemistries described to date,[19, 22-31] regardless the technique used it should provide control over (1) the ratio of biological per QD (valence); (2) the orientation of the biological on the QD; (3) the separation distance between QD and biological; (4) affinity of their interaction; moreover, (5) the orientation should be homogeneous for most biologicals; and (6) the chemistry used should be broadly applicable with most forms of QDs and biologicals.[32]

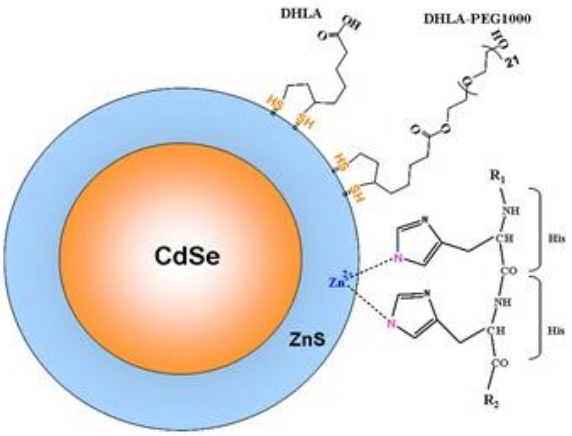

Figure 1.5. Metal-Affinity Driven Self-Assembly between Proteins or Peptides and CdSe - ZnS QDs.[33]

In this work we chose polyhistidine-based self-assembly as our bioconjugation platform of peptide ligands to the QD surface (Figure 1.5) , for several reasons; the self-assembly occurs rapidly within minutes after mixing, it is equally efficient when using QDs capped

with small, negatively charged DHLA or neutral PEG ligands, has a high affinity equilibrium constant in solution (K_a ~ 1 nM), and allows for control over the number of ligands arrayed on a single QD through modulation of the molar ratios of the QDs and ligands mixed.[34] This bioconjugation relies on the strong affinity coordination of Zn (from the ZnS QD surface) to the nitrogen atoms on the peptide polyhistidine tag[33], and it has already been proved to be effective multiple times on the assembly of peptides, DNA conjugates and proteins on QDs to generate sensor systems.[35-38]

1.6 Methods utilized for intracellular delivery of QDs

Several strategies have been used for the intracellular delivery of QDs for bioimaging, based on their physicochemical nature these strategies are classified in three major categories; *Passive QD* delivery utilizes the inherent physical properties of the QD material such as surface coating and charge, to enable uptake. *Facilitated QD* delivery relies on the decoration of the QD surface with a polymer or biological (e.g., peptide, protein), to drive initial interactions of the QD with plasma membrane and ultimately its internalization, mostly by endocytosis. *Active QD delivery* which involves the direct, physical manipulation of the cell (e.g., microinjection) to introduce the QD to the cellular environment.[32]

In this work, we used CPPs to mediate the facilitated delivery of QD-bioconjugates. For an overview of the methods reported to date and targeted cell lines Table 1.1 is presented in the next page.

Strategy	Mechanism	Examples	Targeted Cells
Facilitated delivery	Peptide-mediated	His-Arg-rich peptide	A549 (lung adenocarcinoma; cytosol)
		gH625 (Herpes simplex virus derived-peptide)	HeLa (cervical adenocarcinoma; cytosol)
		JB577 peptide (palmitoylated)	HEK, COS-1, A549, primary fibroblast, chick embryo, rat hippocampal neurons (cytosol)
		Hph-1 (Arg-rich)	MDA-MB-435 (breast carcinoma)
		LAH, sweet arrow peptide	COS-1 (African green monkey kidney)
		Chemoselective peptides	A549
	Protein	Positively charged protein domains	$CD133^+$, $CD34^+$, $CD14^+$, mesenchymal stem cells
		SV40 virus particles	Vero cells
		Baculovirus	U87 human glioma
	Polymer	Cross-linked methacrylte	HeLa
		Chitosan	L929 (murine fibrosarcoma)
			MDA-MB-231, MCF-7 (breast carcinoma)
		Liposomes	B16F10 (mouse melanoma)
		Triblock copolymer	Panc-1
	Small molecule	Lactose	HeLa, Araki Sasaki (human corneal epithelium)
		Galactose	HepG2 (hepatocyte), MCF-7
		Gambogic acid	HepG2
Active delivery	Nanoneedle injection		HeLa
	Reversible membrane permeabilization		Rat cardiomyocyte (H9C2)
	Nanochannel electroporation		A549
	Nanoblade		HeLa
	Microfluidic cell ‘squeezing’		HeLa
Passive uptake	QD surface character/charge		Human primary epithelial
			Mouse primary chromaffin cells
			THP-1, HEp-2, AGS, A549
			Mouse HT-1080 tumor model

Table 1.1. Methods Utilized for the Intracellular Delivery of Quantum Dots.[32] (adapted from reference 32, page 136.

1.7 Endocytosis of Nanoparticles

Unless QDs are introduced to the cytosol by an active delivery method such as microinjection, the main internalization route will include some type of endocytosis. Endocytosis is a natural biological process that starts with the invagination of the plasma membrane to form vesicles or endosomes (through membrane fission) that internalize extracellular fluid, macromolecules, solutes, receptors, particles and plasma membrane components into the cytosol. These vesicular endosomes traffic and deliver to organelles, recycle, and discard unwanted components. Endocytosis is a vital function that regulates numerous pathways in the cell by sorting, processing, recycling, storing, activating, silencing, and degrading incoming materials and receptors.[39]

Because endocytosis is the leading mechanism of uptake for nanoparticles into cells, [40-42] it is important to understand the major endocytic mechanisms among them, those that are clathrin-dependent / independent, mediated by caveloae or involve some form of pinocytosis or phagocytosis.[43-46]

It is well-known that almost all QD-bioconjugates internalized by peptide-mediated delivery are taken up into cells by endocytosis and consequently remain trapped in the endolysosomal system without access to the cytosol.[44, 47-50]

To better design QD-bioconjugates that can reach the cytosol by their facilitated delivery, it is necessary to review the basic mechanisms of endocytosis. A general overview is described in **Figure 1.6**.

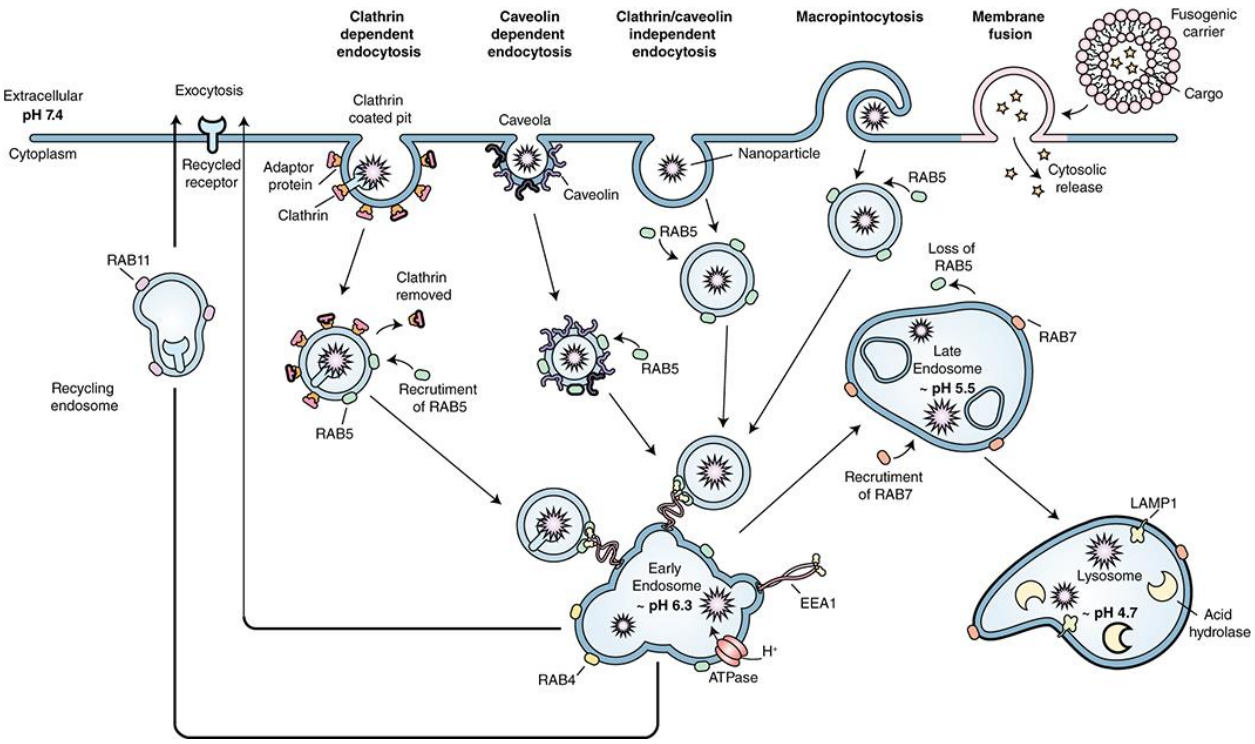

Figure 1.6. **Multiple entry endocytic mechanisms operate in the cellular uptake of nanoparticles.** Particles are internalized into clathrin or caveolin coated vesicles, or by using a clathrin/caveolin-independent mechanism. EEA1 binds to RAB5 on the vesicle surface, and tethers them to RAB5-positive early endosomes. The pH drops to ~6.3 and cargo is either recycled back to the surface or transferred to RAB7-positive late endosomes (pH ~ 5.5). Consequently, trapped particles are trafficked to the lysosome (pH ~ 4.7) where they are broken down by acid hydrolases. On the other hand, membrane fusion and direct translocation across the membrane, are alternative non-endocytic entry mechanism that bypass endocytosis.[51] Adapted from reference 51.

As Figure 1.6 depicts, succeeding endocytosis at the cell membrane, a signaling protein termed Rab 5 binds to the endocytic vesicle on the cytoplasmic side. Rab 5 then interacts with EEA1 on early endosomes, which tethers to the surface of the vesicle and draws it in to fuse with the early endosome.[52]

V-type H+ ATPases rapidly acidify the endocytic vesicles,[53] lowering the pH from an extracellular pH of 7.4 down to ~6.3.[54] The initial fate of clathrin-and caveolin dependent or -independent vesicles is similar in most cell lines, with fusion to early endosomes taking place within minutes of internalization.[55]

Endosomes can follow either of two pathways, where they get recycled back to the cell surface or they continue to acidify to pH 5.5 in late endosomes and vesicular bodies before undergoing fusion with lysosomes where the pH = 4.7.[54] Lysosomes contain a range of acid hydrolases, including nucleases, esterases, proteases and lipases, as their main function is to degrade incoming material, [56] as a consequence, nanoparticles that are transferred to the lysosome are subjected to these enzymes, degrading their cargo.[57]

1.8 Mechanisms of endosomal escape

There are several reported mechanisms to induce endosomal escape,[58] the three major strategies are described in the subsequent sections. For efficient delivery to the cytoplasm, it is very probable that more than one mechanisms of endosomal escape are required.

1.8.1 Proton Sponge Effect and Osmotic Lysis

This is the mechanism by which basic and polycationic materials such as PAMAM dendrimers[59], PEI,[60] and chloroquine[61-62] are theorized to escape the endosomes, however, this mechanism is currently highly debated. The proton sponge theory is founded on the buffering effect of polymers with a p*K*a in a physiologically relevant pH. Thus, it is conceived that when polyamines get endocytosed, H^+ ions are pumped into the endosomes/lysosomes, while also transporting Cl^{-1} anions to attain a charge balance. As a result, the osmotic pressure inside the endocytic vesicle increases until it eventually bursts the endosome/ lysosome, (**Figure 1.7 a**).[58]

Although this has been demonstrated to be the operating mechanism for the endosomolytic base chloroquine, this theory is not general as there are several reported polymers with buffering capacity within the 5-7 pH range that are incapable on inducing endosomal escape.[63] Which means that while a change in pH is a key step, it should not be considered as the only event responsible for osmotic lysis, instead consequent events induced by a drop in the pH must be accounted for, such as conformational changes and membrane interactions of the trapped material.

The role of osmotic pressure upon the disassembly of nanoparticles trapped in endosomes has been described in an alternative way,[64] in which the authors explain that the rupture of endosomes by some nanoparticles is due to the osmotic shock generated upon their disassembly into their polymer unit components, rather than due to protonation and swelling of the polymer.[65]

1.8.2 Membrane Fusion

Enveloped viruses escape from endosomes by triggering the fusion of their viral membranes with the endosomal membrane as a strategy to internalize their viral capsid into the cytoplasm.[66] Liposomes are assembled from lipids or amphiphilic materials, and also have a phospholipid bilayer that can fuse with the endosomal membrane by inverting their structure and delivering the cargo to the cytoplasm[67-68] **(Figure 1.7 b).**

1.8.3 Membrane Disruption and Pore Formation

There are reports of polymers,[69] and peptides[70] that can directly interact and destabilize the endosomal membrane by creating defined pores, therefore releasing a trapped cargo. Peptides that self-assemble across the membrane also create defined pores,[71-72] however, this technique is somewhat limited as transmembrane pores are within 1~2 nm.[73] An alternative is the non-natural designed peptide GALA which can induce the release of larger cargos (~ 5000 Da).[71] **(Figure 1.7 c)**

A growing amount of data supports the theory that polymers induce escape by direct interaction with membranes **(Figure 1.7 d)** by either insertion into membranes (and therefore with asymmetry interference),[74] by membrane thinning[75] or by hole formation.[75-76] The membrane insertion and subsequent membrane disruption observed in polyanionic polymers is ascribed to an increase in lipophilicity by protonation of carboxylate groups the acidic endosomal environment.[69]

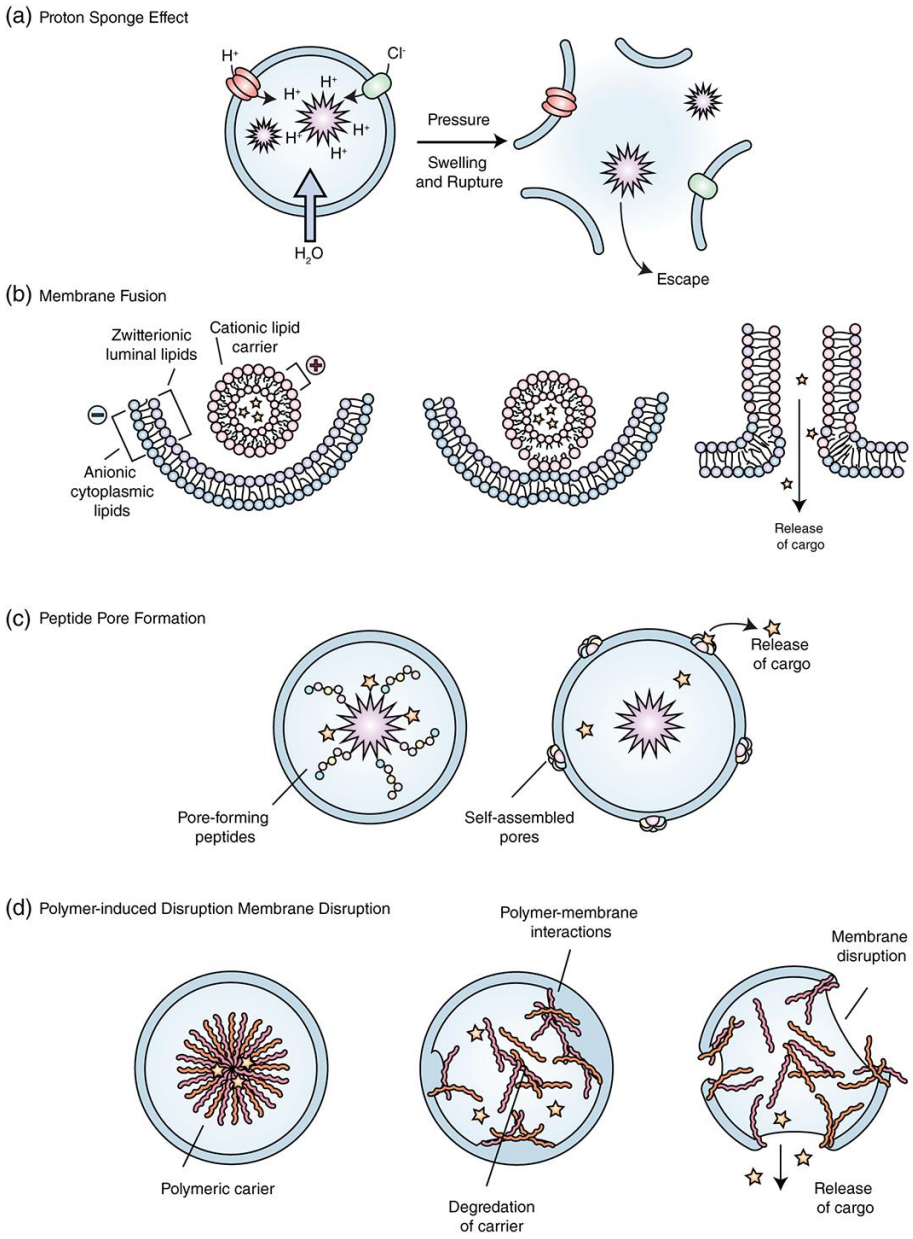

Figure 1.7. Mechanisms of endosomal escape. (a) Proton sponge effect—Buffering polymers get protonated, as protons are driven into endosomes by ATPases. Chloride ions are also pumped in to maintain the charge balance. As ion concentration increases, the endosome swells and the osmotic pressure eventually ruptures the membrane. (b) Membrane fusion—Anionic lipids on the cytoplasmic side of the endosomes reorganize to form a neutral ion pair with positively charged lipids of the carrier, causing membrane destabilization. The membranes fuse and let the cargo move into the cytoplasm.(c) Pore formation—Some peptides self-assemble in the lipid membrane shaping pores that enable small size therapeutics to escape. (d) Membrane disruption—Polymers or peptides cause endosome disruption by directly interacting with the inner membrane, allowing cargo to escape.[51] Adapted from reference 51.

1.9 Current methods to quantify endosomal escape

To date, there are five major methods by which endosomal escape efficiency is quantified regardless the mechanism of endocytosis. These methods are biological activity in cytosol, cellular fractionation, intracellular fluorescence profile, fluorescent microenvironment sensors, real-time visualization of endosomal escape, colocalization and visual assessment by electron microscopy. They are all described in more detail in the following sections.

1.9.1 Biological Activity

This method can be used as an indirect measurement of endosomal escape. After cellular uptake by endocytosis, followed by endosomal escape, the cargo must dissociate from its carrier to reach an intracellular target, and in the case of DNA, continue the path to translocate from the cytosol to the nucleus, to undergo transcription, translation and eventually cause a measurable change on the host cell. Examples of measurable changes are: expression levels of a reporter gene, knockdown of a reporter gene, or enzymatic activity.

The measurable change is the last in a chain of sequential events after cargo uptake, and it cannot occur without endosomal escape, which is why it is considered an indirect way to quantify escape. Biological activity has been used to quantify the escape of different biological cargoes such as: mRNA,[77] siRNA,[78] β-galactosidase,[79] and antigenic proteins.[80] (See Table 1.2 as a reference for measuring techniques).

1.9.2 Cellular fractionation

After endocytosis of the cargo, cells are processed by separation of their cytosolic and endosomal components. After that, the amount of cargo in the separated fractions is analyzed in vitro. Some examples of cargoes quantified by cellular fractionation are: nucleic acids,[81] siRNA,[82] fluorescently labeled dextrans, [83] radioactive pDNA[84] and proteins.[85] This methodology is useful if the cargo is measurable (Table 1.3).

Although high throughput quantification is feasible, the process of cellular fractionation requires intensive labor and extreme care to not cross contaminate endosomal and cytosolic fractions.

1.9.3 Fluorescence microscopy

This is the most used method to estimate the efficiency of endosomal escape since it has become relatively easier to label cargos and carriers with fluorescent dyes. If the material being endocytosed is small, the *Intracellular fluorescence profile* provides useful information on its escape ability , for example, a diffuse fluorescent pattern is an indication of endosomal escape and diffusion throughout the cytosol, in contrast, a punctate pattern is an indication of either particle aggregation or endosomal entrapment. The intracellular fluorescent profile is a preliminary qualitative assay. There have been a few reports[86-88] of methods that attempted to quantify endosomal escape in a mixed punctate and diffuse fluorescence pattern, however they are hard to implement (Table 1.4).

Fluorescent probes that are sensitive to their microenvironment, can reveal information on relevant physiological events such as a change in pH, or a change in reductive environment. *Fluorescent microenvironment sensors* are useful ratiometric probes since their emission is affected by their environment, such change in emission can be measured and compared to a standard curve. Because the cytosolic pH is different from the endolysosomal pH , *fluorescent microenvironment sensors* have been used to indirectly measure endosomal escape, however, to relate fluorescence emission ratio to pH a standard curve is needed. [89] (Table 1.4).

Different techniques used to monitor cargo displacement to the cytosol (endosomal escape)				
Method	**Measuring technique**	**Use**	**Pro's**	**Con's**
Biological Activity in cytosol	RT-PCR	Knockdown of reporter or house-keeping gene by siRNA	-In vivo measurements -Easy high-throughput quantification	- Indirect measure - Fixed end time-point - Limited to siRNA
	Spectro/luminometer	- Expression or knockdown of reporter gene	- Applicable to different cargo - Easy read-out	- Indirect measure - Population average - Fixed end time-point
		- Enzyme activity	- Easy high-throughput quantification	
	Flow cytometry	- Expression or knockdown of reporter gene	- Applicable to different cargo - Fast and easy read-out - Easy high-throughput quantification - Single-cell measurements	- Indirect measure - Fixed end time-point
	ELISA	- Detection of IL-2 secretion as antigen presentation assay	- Live-cell measurement - Easy high-throughput quantification	- Indirect measure - Limited to antigen delivery to APCs
	Immunofluorescence microscopy	Immunostaining of SIINFEKL as antigen presentation assay	- Easy high-throughput quantification	Indirect measure - Limited to antigen delivery to APCs - Fixed end time-point

Table 1.2. Biological activity methods to measure endosomal escape.[90] Adapted from ref. 90

Different techniques used to monitor cargo displacement to the cytosol (endosomal escape)				
Method	**Measuring technique**	**Use**	**Pro's**	**Con's**
Cellular fractionation	Quantitative PCR	- Amount of DNA	- Cytosol <> endosomes - Easy high-throughput quantification - In vivo measurements	- Labor-intensive cellular fractionation - Carrier-bound DNA? - Fixed end time-point
	Stem-loop PCR	- Amount of biologically active siRNA bound to RISC	- Cytosol <> endosomes - Easy high-throughput quantification - In vivo measurements - Only active cargo	- Labor-intensive cellular fractionation - Immunoprecipitation step necessary - Fixed end time-point - Limited to siRNA
	Radio-activity	- Amount of DNA	- Cytosol <> endosomes - Easy high-throughput quantification - In vivo measurements	- Labor-intensive cellular fractionation
		- Amount of proteins		

Table 1.3. Cellular fractionation methods to measure endosomal escape.[90] Adapted from ref. 90

Different techniques used to monitor cargo displacement to the cytosol (endosomal escape)					
Method		**Measuring technique**	**Use**	**Pro's**	**Con's**
Fluorescence Microscopy	**Intracellular fluorescence profile**	Wide field epi-fluorescence or confocal microscopy	- Visual scoring	- Cytosol <> endosomes - Easy read-out - Specific labeling	- Limited to small cargo - Difficult quantification - Fluorescent labeling
			- Quantification		
	Fluorescent microenvironment sensors	Fluorescence microscopy	- Measure reductive environment	- Easy read-out - Specific labeling - Live cells	- Indirect measure - Standard curve necessary - No quantification - Fluorescent labeling
			- Measure difference in pH		
	Real-time visualization of endosomal escape	Live-cell video microscopy	- Visualize bursting of endosomes	- Cytosol <> endosomes - Mechanism of endosomal escape - Live cells - Specific labeling	- Limited to small cargo - Low throughput quantification - Fluorescent labeling
			- Visualize fusion with endosomes		
	Colocalization	Confocal microscopy	- Visual scoring	- Cytosol <> endosomes - Easy read-out - Specific labeling - All cargo	Difficult quantification - Fluorescent labeling - Limited temporal resolution - Fixation sometimes necessary
			- Quantification		
Visual assessment		Electron microscopy	- Visual scoring	- Very high resolution - Labeling not always necessary	- Fixation artifacts - Low throughput quantification

Table 1.4. Fluorescence microscopy methods to measure endosomal escape. [90] Adapted from ref.90.

1.10 The need to develop a method to assess endosomal escape efficiency

As described in the previous section, there are a few methods that directly or indirectly measure endosomal escape, for example indirect measurements, such as the biological activity of a biologically active cargo, must trigger the expression or knockdown of a reporter gene upon delivery, which can be measured by RT-PCR, spectrometer or flow cytometry techniques.[91] Direct methods such as cellular fractionation, require labor intensive cellular fractionation and caution should be taken not to cross-contaminate cytosolic with vesicular fractions.[81] Visual assessment of endosomal escape by a high-resolution technique such as electron microscopy,[92] although reliable, it is not scalable for high throughput analysis.

Since most nanoparticles can be fluorescently labeled, analysis by fluorescent microscopy methods is highly preferred for discriminating cytosolic from endosomal cargo, however the quantitative analysis of escape by nanoparticles is still difficult (Tables 1.2-1.4), hence the need for a quantitative method that can report when a delivered nanoparticle probe escapes the endosome and reaches the cytosol. Taking advantage of QDs intrinsic fluorescence, their ability to serve as nanoscaffolds for bioconjugation, and their capacity to participate in FRET, we have developed a ratiometric-FRET sensor that allows us to detect, quantify and compare the amount of escape facilitated by endosomolytic peptides. The change of QD emission is caused by the disulfide bond cleavage between the QD FRET donor and a Rhodamine FRET acceptor by the reductive environment in the cytosol.

1.11 Aim and scope

We aim to design, develop and test a ratiometric FRET system -where QD is the FRET donor and rhodamine is the FRET acceptor- that allows to measure the extent of endosomal escape by the change in red/green signal upon disulfide bond cleavage by cytosolic glutathione. In this study we tested three peptides, one protein derived from the influenza virus and a highly endosomolytic small molecule (chloroquine) as a control to evaluate our ratiometric sensor (Figure 1.8).

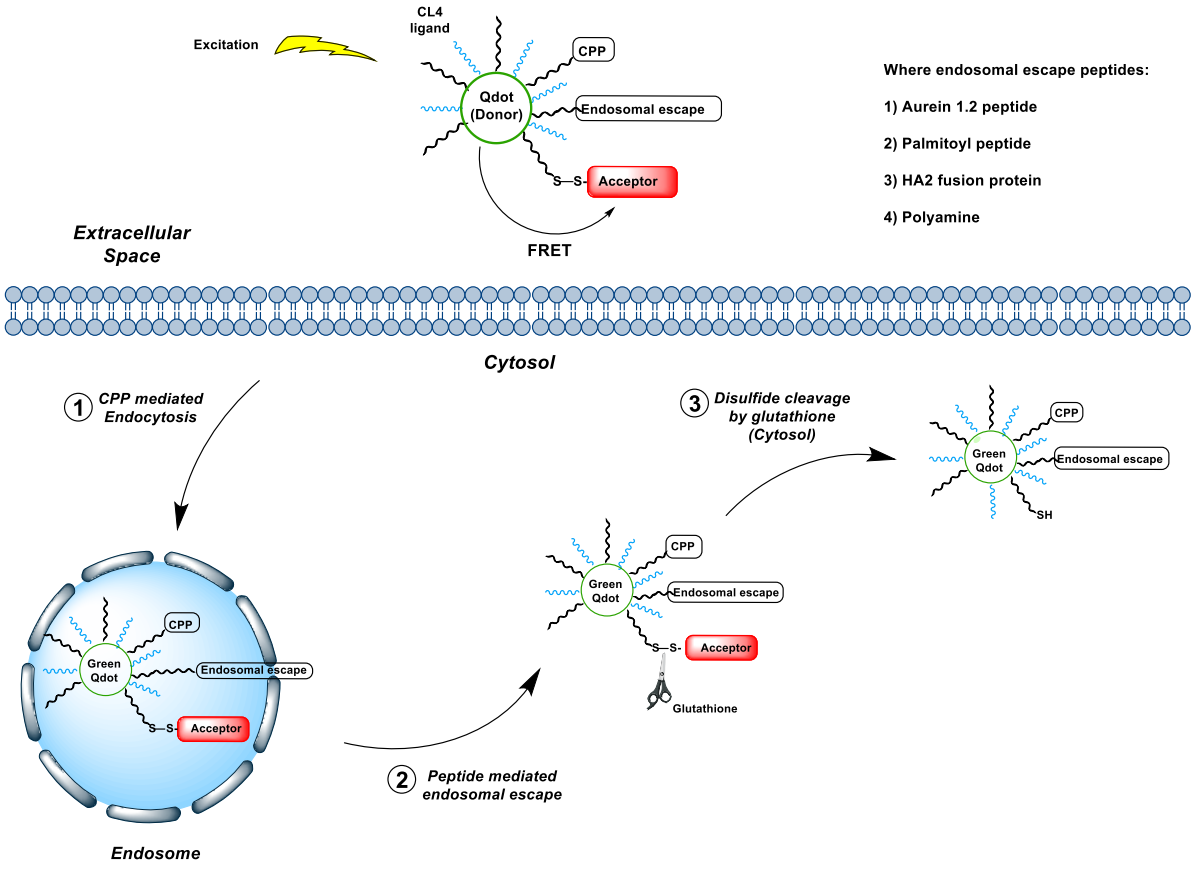

Figure 1.8 Our ratiometric FRET sensor design.

1.12 Significance

We have developed a ratiometric-FRET sensor that allows us to detect, quantify and compare the amount of endosomal escape facilitated by different peptides. Our sensor is equipped with a green QD FRET donor with a large surface area to conjugate peptide ligands; a cell penetrating peptide to facilitate intracellular delivery; an endosomolytic peptide to facilitate endosomal escape; a red rhodamine FRET acceptor linked to the QD through a reducible disulfide bond. When our ratiometric sensor escapes the endosomes, the disulfide bond between donor and acceptor gets cleaved by cytosolic glutathione, as a result, the red/green signal ratio changes. This ratiometric analysis can be detected and quantified at different time points in live-cells, therefore, providing information on escape events regardless the cellular uptake or endosomal escape mechanism.

1.13 Thesis overview

In this thesis, I describe the different stages involved in the development of a ratiometric FRET sensor capable of detecting and quantifying the endosomal escape ability of four different purported endosomolytic biomolecules and a small molecule positive control (chloroquine). Overall, I provide the pertinent supporting information from conception to development to the final prototype of our ratiometric FRET sensor.

In Chapter 2, I demonstrate that we can reproduce what has been published in other reports regarding the facilitated CPP-mediated delivery of QD bioconjugates to live cells. Micrographs show that our QD-bioconjugate colocalize with a red-transferrin endosomal marker, supporting that our QD probe gets internalized through endocytosis. I also

provide preliminary data from confocal microscopy analysis (Chapter 2) that suggests that the active membrane peptide Aurein 1.2 and the fusion protein HA2 may serve as endosomal escape agents.

In Chapter 3, I provide data that shows the spectral match between green QD donor and red rhodamine acceptor, and their ability to participate in FRET. I also demonstrate the recovery on green QD emission upon disulfide bond cleavage of the QD-Rhodamine FRET pair, therefore validating our sensor system. Additionally, in Chapter 3, from spectrofluorimetric data, I show the extent to which several dark quenchers participate as FRET acceptors with green and red QD donors.

It is worth to mention that synthesis was a major component of this project. Along the way, I found countless roadblocks to successfully synthesize all the peptide ligands presented in here, therefore, in Chapter 4, I show a sample of unproductive but informative synthetic routes that gave me the necessary input to re-design and execute new approaches to afford all peptides discussed throughout this dissertation, mass spectrometry data is also provided.

2 Testing the peptide-facilitated delivery of quantum dots to the cellular cytosol

2.1 Introduction

Our group has demonstrated that cell penetrating peptides, CPPs, (including Arg_9 and Tat) can facilitate the delivery of trimethoprim-terbium complexes to an intracellular protein target (eDHFR).[93] Due to the useful properties of lanthanides (narrow, multiwavelength emission, and long-luminescent lifetime), the selective labeling of eDHFR by the luminescent trimethoprim-terbium complex could be imaged by time-gated microscopy. Semiconductor quantum dots (QDs) are luminescent nanocrystals that offer an alternative for bioimaging and biosensing due to their unique photophysical and physicochemical properties, such as, broad absorption spectra, narrow and tunable photoluminescence (PL), large extinction coefficients, high emission quantum yields, improved resistance against photobleaching, and long fluorescence lifetimes.[94]

QDs are not intrinsically cell permeable, as a result, they are delivered to the cytosol by either of the following modalities. *Passive QD* delivery utilizes the inherent physical properties of the QD material such as surface coating and charge, to enable uptake. *Facilitated QD* delivery relies on the decoration of the QD surface with a polymer or biological (e.g., peptide, protein), to drive initial interactions of the QD with plasma membrane and ultimately its internalization, mostly by endocytosis. *Active QD delivery* which involves the direct, physical manipulation of the cell (e.g., microinjection) to introduce the QD to the cellular environment. [32] Intracellular delivery of QDs by microinjection has proved fruitful in our research group for example, by actively delivering properly functionalized QDs, it was possible to exploit Tb-to-QD FRET for biomolecular

imaging in live-cell studies[95], to develop an hypoxia[96] and a H_2S sensor[97] respectively. Although invasive and to some extent cell damaging, active delivery of QDs is still convenient as it circumvents endocytosis.[98] A well-established approach to facilitate QD delivery utilizes a cell penetrating peptide (CPP) with high arginine content, derived from the HIV-1 Tat protein.[99] The peptide can easily be bioconjugated to the QD surface via non-covalent metal affinity coordination between a polyhistidine tag on either end of the peptide and the Zn^{2+} atoms on the QD surface. This assembly strategy is facile and convenient since it takes minutes, and it allows for control on the number of peptides assembled to the QD surface by controlling QD: peptide molar ratios.[33]

We and others, [99-108] have observed that upon incubation at 37 ^{o}C in ~1 h, live cells readily internalize QD-polyarginine or QD-TAT assemblies, however, almost all QD materials are taken in by endocytosis and consequently, remain trapped in the endosomes. A few others have reported the successful facilitated delivery of QDs to the cytosol either by employing peptides found in screening studies[109-113] or by using lytic peptides derived from viral proteins.[114-119]

From microscopy and colocalization studies, we found a clear difference between the facilitated intracellular delivery and apparent escape ability of QD:CPP versus QD:CPP:EE. The results are shown and discussed in the following sections.

While both, the wild type HA2 viral protein[66] and the Aurein 1.2 peptide[120] have been studied for their endosomolytic activity, their ability to promote the endosomal escape of QD-CPP complexes has not been reported.

2.2 Results and Discussion

2.2.1 Formation of QD-Biomolecule Assemblies

QD bioconjugates were formed by mixing the $(His)_6$- biomolecule with CL4 capped QDs for at least 30 min prior to use. This allows the ligands to self-assemble onto the QD surface via metal affinity coordination between Zn^{+2} on the ZnS QD surface and the nitrogen atoms on the imidazole ring of the polyhistidine tag. This bioconjugation method takes minutes and it is reliable since the dissociation constant of this interaction is estimated to be stronger than most antigen-antibody interactions (K_d> 10^{-9}M).[8] Additionally, the desired number of ligands per QD can easily be controlled by using the appropriate molar ratios of the ligand (polyhistidine-peptide or protein) and the QD stock solutions.[8] Self-assembled QD-bioconjugates were prepared by incubating stock solutions of 2 μM QD-CL4 with appropriate molar ratios of pure and desalted polyhistidine-peptide (or protein) in 1X PBS buffer (pH= 7.4) for 30 min to 1h.

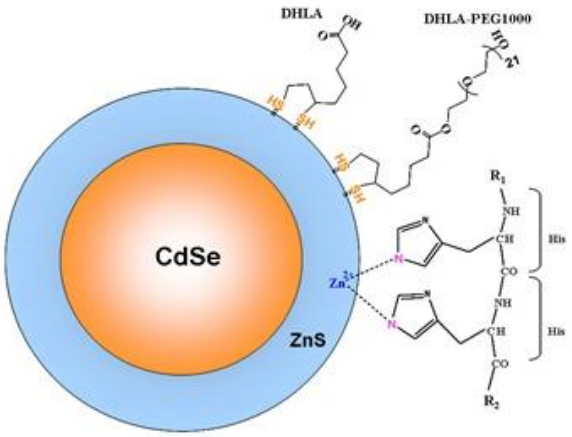

Figure 2.1. Bioconjugation via metal-affinity coordination.[8]

2.2.2 Titration of CPPs per quantum dot needed to facilitate intracellular delivery

To determine the efficiency of CPP-mediated internalization, HeLa cells were incubated with 550-nm QD-CPPs bioconjugates assembled at 1:5, 1:10, 1:15 and 1:20 ratios. The final QD concentration was 50 μM. Epifluorescence images (Figure 2.2) were recorded after a 2 h- incubation period at 37 ^{o}C.

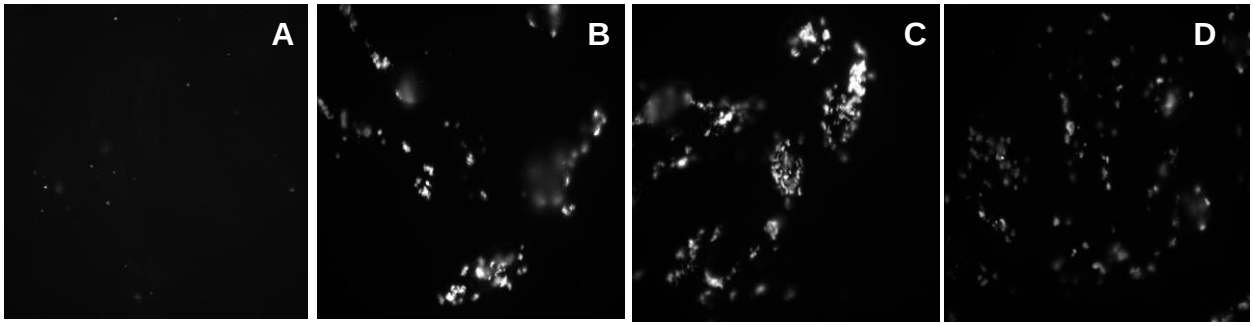

Figure 2.2. Cellular internalization of CL4 coated QD: CPP assemblies. HeLa cells were incubated with 550 nm QD:CPP assemblies at ratios of 1:5 (A), 1:10 (B), 1:15 (C), 1:20 (D) at QD concentrations of 50 nM. Images show the punctate QD fluorescence pattern indicative of endosomal entrapment.

The images clearly show that 1:10, 1:15 and 1:20 QD-CPP conjugates were internalized, in contrast, to the negligible uptake observed for QD-CPP assembled at a 1:5 ratio. Furthermore, as a control experiment, when unconjugated 550-nm QDs at the same concentration were incubated with Hela cells under the same conditions, no cellular uptake was observed (data not shown). Therefore, we conclude that a minimum ratio of QD-CPP of 1:10 is necessary for intracellular uptake. Consistent with reports by several other groups,[14, 98, 101, 121-123] and as Fig. 2.2 shows, we observed a punctate QD fluorescence pattern around the cell nuclei and throughout the cytoplasm, which frequently indicates the endosomal entrapment of the QD-bioconjugates.

2.2.3 Colocalization studies confirm endosomal entrapment

Next, we co-delivered green emitting QD-CPP bioconjugates at different ratios with Texas Red-transferrin (TR-Tf), a commonly used endosomal marker that readily enters cells by receptor-mediated endocytosis. After a 2 h-incubation period with HeLa cells at 37 ºC, we recorded epifluorescence/phase contrast images. Figure 2.3 shows a representative merged micrograph of our results, in which a punctate QD fluorescent pattern (green channel) was observed around the nuclei and throughout the cytoplasm. When the endosomal marker staining pattern (red channel) was merged with the QD fluorescence pattern it became clear that most of the internalized QD-CPP bioconjugates were colocalized within endosomes (yellow pattern).

QD: CPP (1: 15)

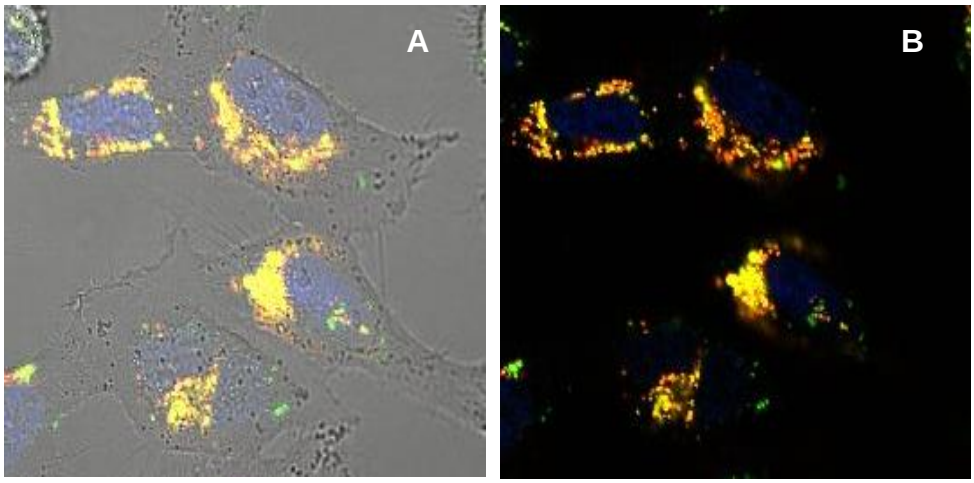

Figure 2.3. Cellular internalization and colocalization of CL4 coated QD:CPP (1:15 ratio) assemblies within the endosomes. HeLa cells were coincubated with green 550-nm QD:CPP assemblies and 40 μg/mL of endosome marker Texas red-Tf. for 1.5 h at 37 ºC. Cells were stained with DAPI as well. After washing 3 times with 1X PBS (pH = 7.4), cells were replenished with fresh medium (with FBS), re-incubated at 37 ºC for 24 h and imaged. A) Overlay of phase contrast, QD fluorescence (green), Texas red-Tf (red) DAPI (blue), colocalization (yellow). B) Overlay QD fluorescence (green), Texas red-Tf (red), DAPI (blue), colocalization (yellow).

The high degree of colocalization observed indicate that the cellular uptake of our QD-CPP bioconjugates is mostly driven by endocytosis. Studies using live-cell imaging and FACS analysis have found that arginine-rich CPPs and their conjugated cargos are internalized by endocytosis.[124-126] Moreover, our results (Figure 2.3 are not unexpected and agree with reports by other groups[14, 98, 101, 121-123] on the endosomal entrapment of QDs delivered by CPPs.

2.2.4 Assessment of a membrane-active peptide to mediate endosomal enhancement of QD-CPP bioconjugates.

Aurein 1.2 is an antimicrobial peptide (AMP) that belongs to a class of membrane-active peptides. Interestingly, Aurein 1.2 was recently found from a screen of short sequences known to disrupt microbial membranes without mammalian cell toxicity.[120] In this study, Liu's group demonstrated that Aurein 1.2, a 13-amino-acid peptide, efficiently enhances the endosomal escape of proteins fused to super positively charged GFP (+36 GFP) in vitro and in vivo. Motivated by the relatively simple synthetic work to generate this peptide, I designed, synthesized, purified and characterized the peptide in Figure 2.4.

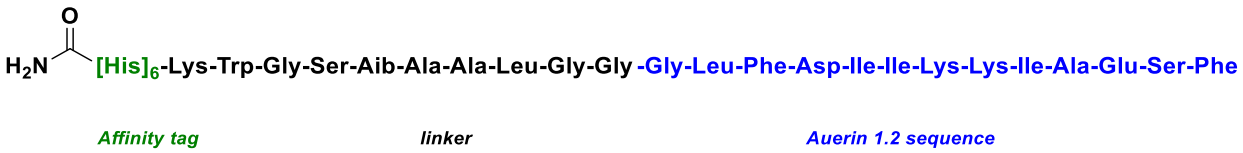

Figure 2.4. Designed Aurein 1.2 peptide ligand to test for endosomolytic activity. $CONH_2$ (*C*-terminus), $[His]_6$ (affinity tag), KWGS(Aib)AALGG (spacer/linker), GLFDIIKKIAESF (Auerin 1.2 sequence at *N*-terminus).

This peptide is equipped with an hexahistidine sequence as an affinity tag for self-assembly to QDs, a KWGS(Aib)AALGG that serves as a spacer and a linker between the membrane-active peptide Auerin 1.2 and the polyhistidine tag.

The KWGS(Aib)AALGG peptide linker was originally developed and continuously improved by the Medintz group with a tryptophan for quantitation, an Aib residue to provide rigidity and position the ligand away from the QD surface, and a Gly-Gly sequence to provide some flexibility. Our previous results indicated that QD-bioconjugates displaying 10 to 25 CPPs per QD, were intracellularly delivered, mostly by endocytosis. Building upon these results, the possible endosomolytic activity of the Aurein 1.2 peptide was investigated. This time we tested red (emission= 625 nm) -CL4 coated QDs.

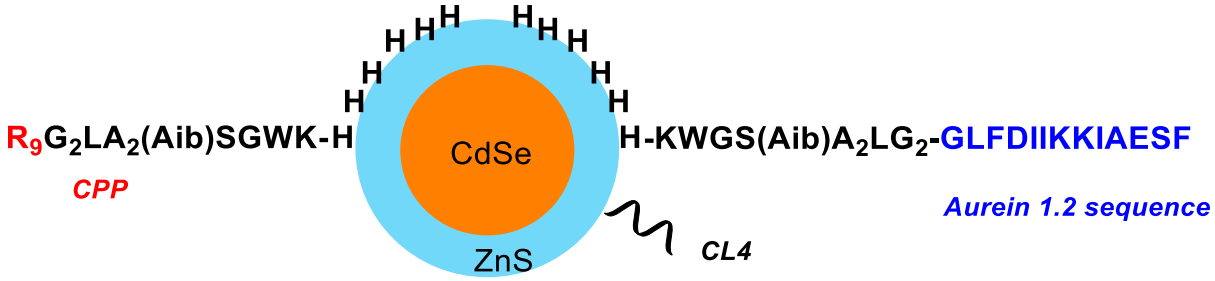

Figure 2.5. General structure of QD- bioconjugates employed in this study. QDs core CdSe, Shell ZnS. Red (620 nm). CL4 is a zwitterionic ligand that confers stability to QDs under acidic environments. The His_6-linker-CPP ligand was conjugated for intracellular delivery. The His_6-linker-Auerin 1.2 ligand was conjugated to test for endosomolytic activity. The spacer/linker sequence is KWGS(Aib)AALGG (spacer/linker). The CPP sequence is $(Arg)_9$, the Auerin 1.2 peptide sequence is GLFDIIKKIAESF. All peptide sequences start from the *C*-terminus and end at the *N*-terminus.

Initially we incubated HeLa cells with 25 nM QD:CPP: Auerin peptide conjugates at a 1:17:13, 1:22:13 and 1:22:17 ratios at 37 ^{o}C for 2 h for CPP-mediated cellular uptake. Subsequently, cells were washed three times with 1X PBS (pH = 7.4), replenished with fresh cell medium and re-incubated at 37 ^{o}C to allow the internalized QD-bioconjugates time to escape the endosomes. After 17 h cells were washed three more times with 1X PBS (pH = 7.4), replenished with fresh cell medium and stained with patent blue prior to microscopic examination. Representative results are shown in micrographs A-C (Figure 2.6). We found that even after 17 h of incubation cells were healthy and undergoing cell division.

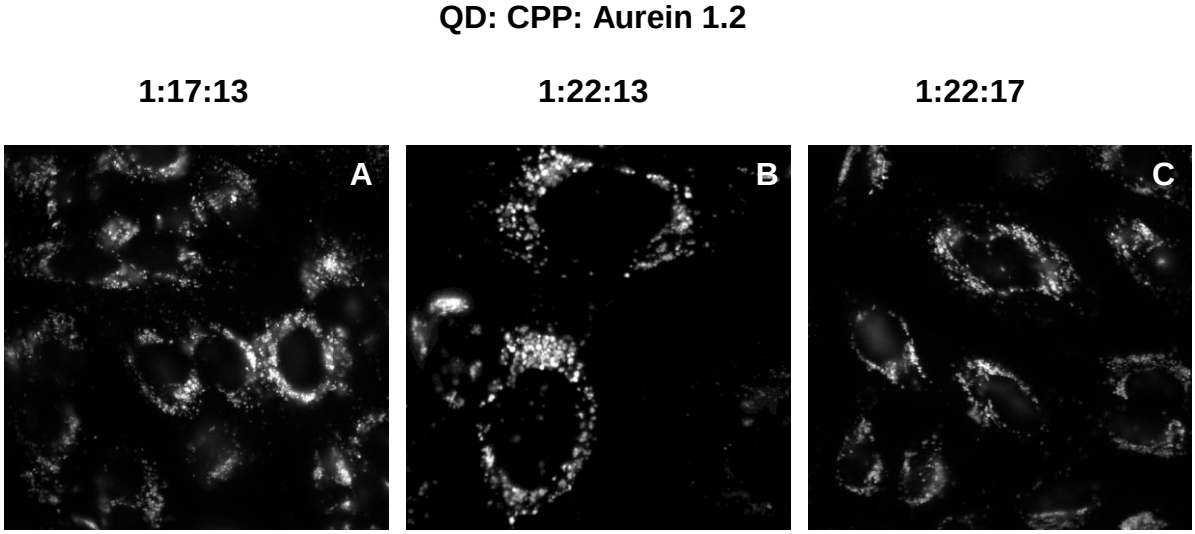

Figure 2.6. Cellular internalization of QD: CPP: Aurein 1.2 assemblies. HeLa cells were incubated for 2 h at 37 ^{o}C with CL4 coated 620 nm (red) QD-CPP-Aurein 1.2 assemblies at ratios of 1:17:13 (A), 1:22:13 (B), 1:22:17 (C) at QD concentrations of 25 nM. After washing 3 times with 1X PBS (pH = 7.4), cells were replenished with fresh medium (with FBS), stained with patent blue and imaged with an epifluorescence microscope equipped with a Zeiss camera. Excitation: 535/30 nm, emission: 605/15 nm.

A shown in Figure 2.6, the intracellular QD-bioconjugate fluorescence profile was punctate occupying the entire cell volume except for nuclei in all experiments, which might be an indication of endosomal entrapment. QD-bioconjugate aggregation is unlikely since we used CL4-coated QDs which stay soluble and resist acidic pH environments.
We were expecting to detect a more diffuse or homogenous fluorescent pattern as a sign of endosomal escape, rather than the observed punctate pattern.

2.2.5 Results from Confocal microscopy studies

To qualitatively evaluate the amount of delivered QD-nano assemblies that reach the cytosol from those that stay trapped inside the endosomes, we coincubated green QD:CPP: Aurein peptide complexes (539 nm emission) with Texas red-transferrin (endosomal marker) and HeLa Cells for 2 h at 37 ^{o}C.

After washing with 1X PBS and refilling with fresh medium, cells were further incubated for 24 h, washed and imaged by confocal microscopy as it offers improved resolution and eliminates out-of -focus fluorescence.

We tested the ability of the reported Aurein 1.2 peptide to mediate the endosomal escape of our nanoassemblies. QD: CPP: Aurein peptide ratios were 1:12:15 and 1:12:30 at a 100 nM QD final concentration.

Qd : CPP (1:15)

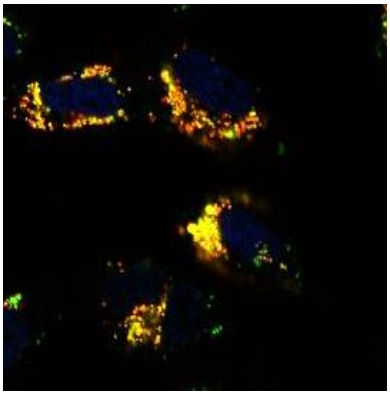

Qd: CPP: Aurein 1.2 1:12:15, qd [100nM]

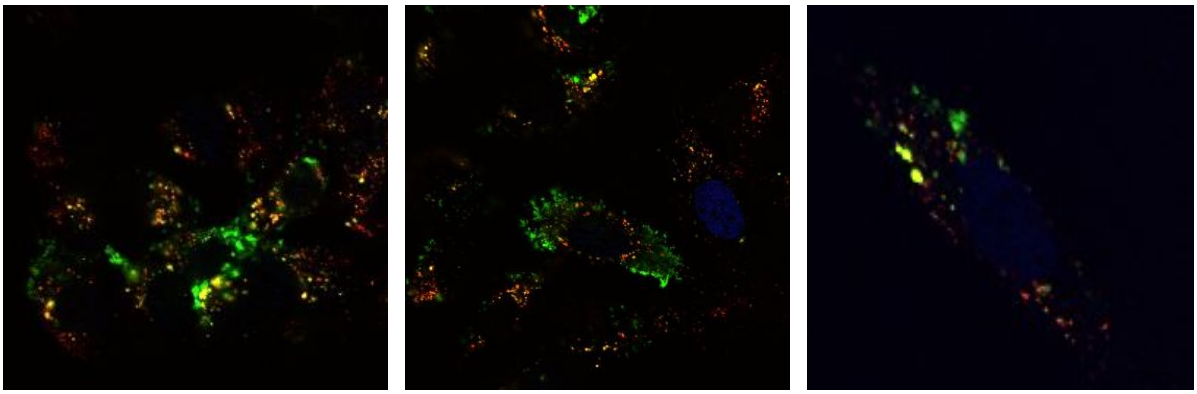

Figure 2.7. Cellular internalization and colocalization of QD: CPP: Aurein 1.2 assemblies within the endosomes (1:12:15 ratio). Top panel: HeLa cells were coincubated with 539-nm (green) CL4 QD:CPP assemblies (1:15 ratio) and 40 μg/mL of endosome marker Texas red-Tf. for 1.5 h at 37 ^{o}C. Bottom panel: HeLa cells were coincubated with 539-nm (green) CL4 QD: CPP:Aurein 1.2 conjugates. Cells were stained with DAPI as well. After washing 3 times with 1X PBS (pH = 7.4), cells were replenished with fresh medium (with FBS), re-incubated at 37 ^{o}C for 24 h and imaged with an Olympus FV3000 Confocal Laser Scanning Microscope. Texas red-Tf: excitation 561 nm, detection 600-635 nm; green QD: excitation 405 nm, detection 520-560 nm; DAPI: excitation 405 nm, 440-480 nm.

Qd: CPP: Aurein 1.2 1:12:30, qd [100nM]

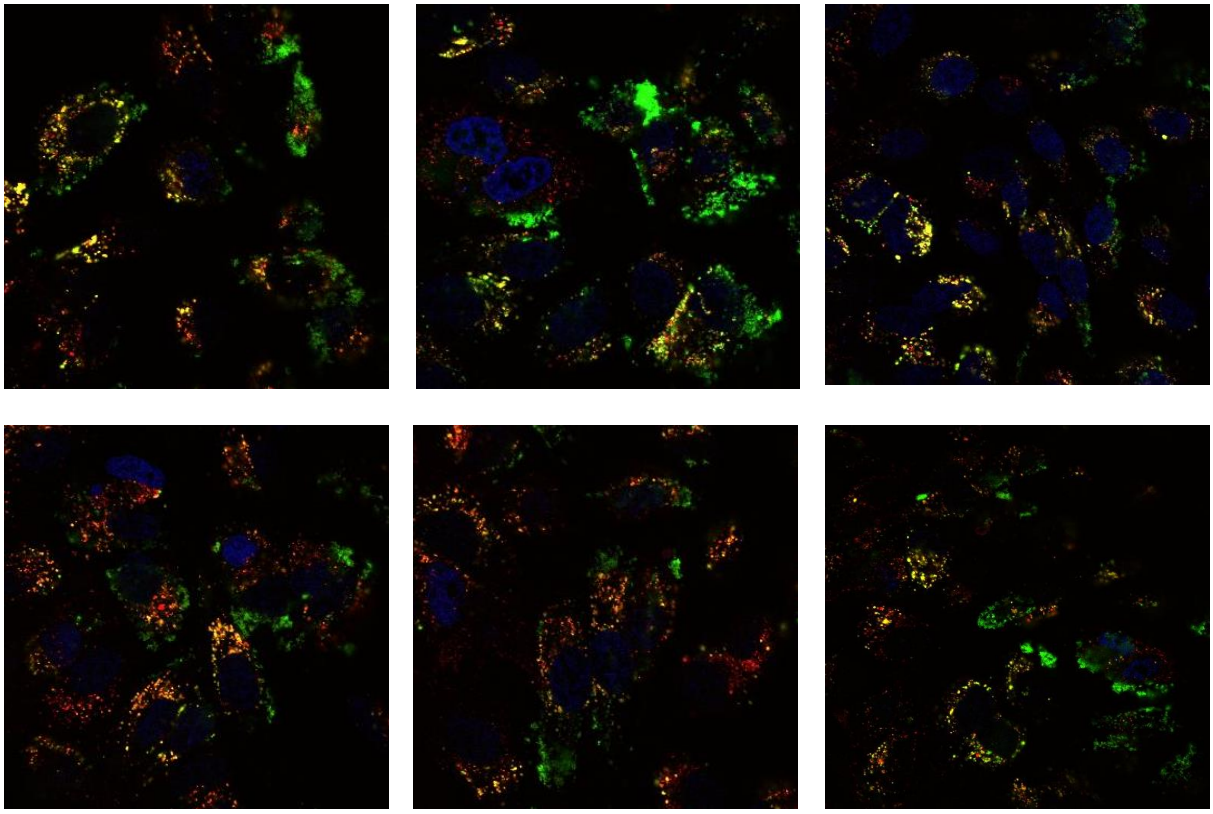

Figure 2.8. Cellular internalization and colocalization of QD: CPP: Aurein 1.2 assemblies within the endosomes (1:12:30 ratio). HeLa cells were coincubated with 539-nm (green) CL4 QD: CPP: Aurein 1.2 conjugates and 40 μg/mL of endosome marker Texas red-Tf. for 1.5 h at 37 ^{o}C. Cells were stained with DAPI as well. After washing 3 times with 1X PBS (pH = 7.4), cells were replenished with fresh medium (with FBS), re-incubated at 37 ^{o}C for 24 h and imaged with an Olympus FV3000 Confocal Laser Scanning Microscope. Texas red-Tf: excitation 561 nm, detection 600-635 nm; green QD: excitation 405 nm, detection 520-560 nm; DAPI: excitation 405 nm, 440-480 nm.

Qd : CPP (1:15)

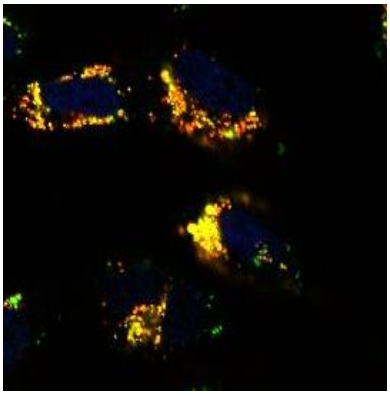

Qd: CPP: HA2 1:12:15, qd [100nM]

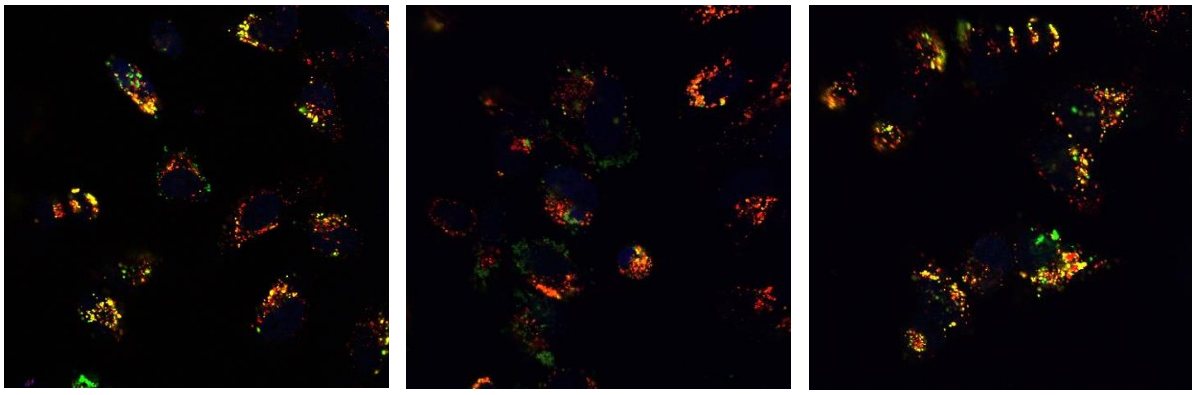

Figure 2.9. Cellular internalization and colocalization of QD: CPP: HA2 assemblies within the endosomes (1:12:15 ratio). Top panel: HeLa cells were coincubated with 539-nm (green) CL4 coated QD:CPP assemblies (1:15 ratio) and 40 μg/mL of endosome marker Texas red-Tf. for 1.5 h at 37 ^{o}C. Bottom panel: HeLa cells were coincubated with 539-nm (green) CL4 coated QD: CPP: HA2 conjugates. Cells were stained with DAPI as well. After washing 3 times with 1X PBS (pH = 7.4), cells were replenished with fresh medium (with FBS), re-incubated at 37 ^{o}C for 24 h and imaged with an Olympus FV3000 Confocal Laser Scanning Microscope. Texas red-Tf: excitation 561 nm, detection 600-635 nm; green QD: excitation 405 nm, detection 520-560 nm; DAPI: excitation 405 nm, 440-480 nm.

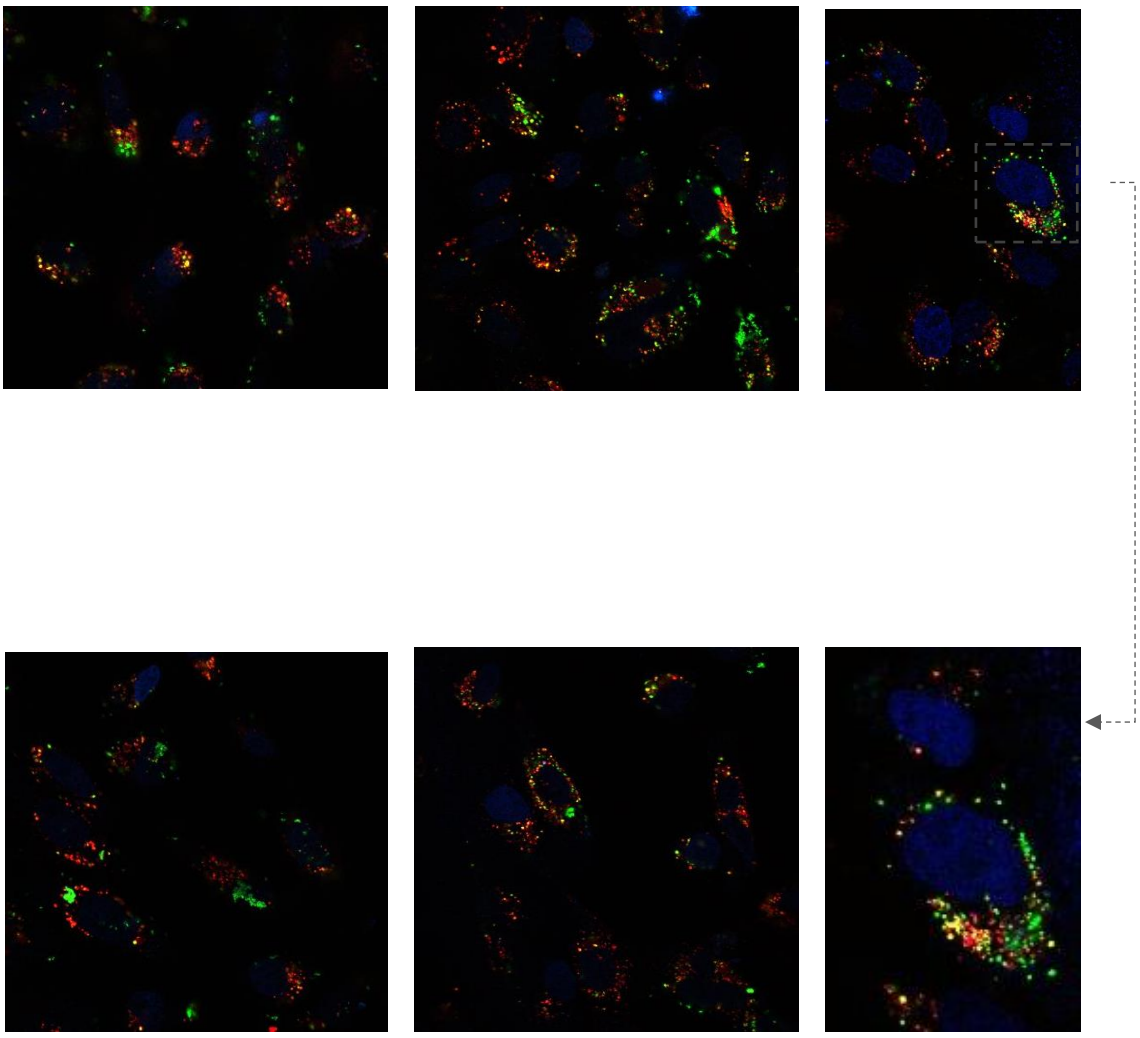

Figure 2.10. Cellular internalization and colocalization of QD: CPP: HA2 assemblies within the endosomes (1:12:30 ratio). HeLa cells were coincubated with 539-nm (green) CL4 coated QD: CPP: HA2 conjugates. Cells were stained with DAPI as well. After washing 3 times with 1X PBS (pH = 7.4), cells were replenished with fresh medium (with FBS), re-incubated at 37 ^{o}C for 24 h and imaged with an Olympus FV3000 Confocal Laser Scanning Microscope. Texas red-Tf: excitation 561 nm, detection 600-635 nm; green QD: excitation 405 nm, detection 520-560 nm; DAPI: excitation 405 nm, 440-480 nm.

2.2.6 Conclusion

Colocalization studies (Figures 2.7-2.10) showed that the intracellular delivery of our QD-Bioconjugates can be facilitated by a polyarginine CPP, however, upon coincubation of QD:CPP bioconjugates with an endosomal marker (Tf-red texas), we confirmed that all QD:CPP assemblies remained trapped inside endocytic vesicles by the colocalization of the green emission of QDs and the red emission of the endosomal marker Tf, which resulted in a merged yellow signal. The internalization of Tf into the cells begins with clathrin-mediated endocytosis, then Tf without distinction enters two populations of early endosomes, that subsequently proceed to the degradation pathway involving lysosomes,[55] therefore Tf is used as a general endosomal marker.

We also did a few preliminary live-cell studies in which we added an endosomolytic protein (HA2, Figures 2.9 and 2.10) and a peptide (Aurein 1.2, Figures 2.7-2.8) separately, to our QD:CPP bioconjugates to explore their potential abilities to mediate endosomal escape of our QD probe (QD:CPP: HA2 and QD:CPP:Aurein 1.2 respectively). After incubation with HeLa cells, we were expecting to observe a diffuse pattern of QD:CPP:HA2 (or Aurein1.2) conjugates as an indication of their endosomal escape, but instead, we still observed a punctate pattern.

However, when QD:CPP:HA2 (or Aurein 1.2) were coincubated with Tf-red Texas, we observed a distribution of green and red punctae, and a decrease in yellow colocalization signal (when green QD and red-Tf emissions were overlaid,), which suggests that protein HA2 and peptide Aurein 1.2 may facilitate the endosomal escape of our QD probes.

2.3 Experimental Methods

2.3.1 Materials and instrumentation. All solvents and chemicals were purchased from commercial sources and used without further purification: DMF (reagent grade) from Chem-impex, CH_2Cl_2, MeOH and diethyl ether from Sigma- Aldrich, TFA and CH_3CN (HPLC grade) from Fisher. Water was purified using a Millipore Milli-Q water purification system. DIEA (N,N-diisopropylethylamine), acetic anhydride, piperidine, ß-mercaptoethanol, 1,2-ethanedithiol, thioanisole, phenol, and anisole from Alfa Aesar. HBTU (O-(Benzotriazol-1-yl)-N,N,N',N'-tetramethyluronium hexafluorophosphate) , Oxyme (Ethyl Isonitrosocyanoacetate), palmitic acid, TIPS-H (triisopropylsilane), MALDI matrix HCCA (α-Cyano-4-hydroxycinnamic acid) and chloroquine phosphate from Sigma-Aldrich. Fmoc-protected natural and artificial amino acids Fmoc-L-Dap(Mtt)-OH (Dap = diaminopropionic), Fmoc-L-Lys(Mtt)-OH, Fmoc-L-Aib(Mtt)-OH (Aib= alpha-aminoisobutyric acid), Fmoc-4-(2-aminoethyl)-1-carboxymethyl-piperazine dihydrochloride, Fmoc-L-Lys(Fmoc)-OH and tetra-Boc-spermine-5-carboxylic acid from Chem-impex international. Rink amide resin AM Resin LL, 100-200 mesh (substitution = 0.35 mmol/g) from Novabiochem. Desalting buffer TEAA (triethylammonium acetate) 2.0 M pH = 7.0 from Glen Research. All peptides were synthesized manually by using a bench-top shaker. 20-mL and 3-mL polypropylene fritted syringes (with a plunger) as reaction vessels along with their respective polypropylene caps from Torviq.

Peptides were purified by reverse phase preparative HPLC in a Shimadzu LC-20 AT equipped with a UV-Vis dual detector model SPD-20A and a semi-prep Aeris column (10 µm, 90 Å, 250 × 10 mm) at a flow rate of 5 mL/min employing Acetonitrile / Water with 0.1% TFA as a mobile phase. Injections were simultaneously monitored at 220 and 254

nm. Peptides were desalted with Oligonucleotide Purification Cartridge (OPC, Applied Biosystems) before conjugation to QDs, freeze-dried (Labconco) and stored as a pellet at -20 °C. Peptide masses were obtained by MALDI-TOF 4700 Proteomics Analyzer (Applied Biosystems). Small molecules masses were obtained by electrospray ionization on a LC/MS APCI quadrupole ion trap LC mass spectrometer (Thermo Finnigan LCQ) and their chemical structures were confirmed by NMR recorded on a Bruker Avance DRX 400 or 500 MHz NMR spectrometer. UV/vis absorbance spectra were measured using a Varian Cary 300 Bio UV/vis spectrophotometer.

HeLa cells (CCL-2) were purchased from American Type Culture Collection. Dulbecco's modified eagle medium (DMEM, 10-014 CV) and 0.25% trypsin/2.21 mM EDTA were purchased from Corning Cellgro® Micropipette preparation glass bottom culture dishes (P50G-1.5-14-F) were purchased from Matek Corporation (Ashlan, MA). Fluorescence images were acquired using an epi-fluorescence microscope (Axiovert 200, equipped with AxioCam MRm CCD camera and Axiovision software (V 4.6.2.0), Carl Zeiss, inc) modified with a UV LED emitting at 365 nm (UV-LED-365, Prizmatix, Ltd). All images were obtained with a 63x/1.25 N.A. EC Plan Neofluar oil-immersion objective (Carl Zeiss, Inc) and G365 excitation filter.

2.3.2 Quantum Dots. CdSe–ZnS core–shell QDs with emission maxima centered at 539 nm (CL4 coated) and 566 nm (DHLA coated) were synthesized by Snee's group[97] and made hydrophilic by exchanging the native trioctylphosphine/trioctylphosphine oxide (TOP/TOPO) capping shell with either DHLA (dihydrolipoic acid) or CL4 zwitterionic ligands as described in section 2.3.4. These are subsequently referred to herein as DHLA

or CL4 ligands. In general, CL4-QDs are preferred as they provide superior intracellular solubility and pH stability under acidic conditions, similar to the acidic environment inside endosomes; 539 nm QDs capped with CL4 ligands were used for CPP-mediated delivery. 566 nm QDs capped with DHLA ligands were used for spectroscopic studies.

2.3.3 Synthesis of zwitterionic ligand CL4. Procedure adapted from Medintz publication.[127]

Synthesis of compound 2. Carbonyldiimidazole (2.59 g,16 mmol) and thioctic acid **1** (3 g, 14.5 mmol) were added to a 100-mL round-bottom flask filled with argon and equipped with a stir bar. 30 mL of dry $CHCl_3$ were added by syringe and argon was bubbled through. The reaction was left to run at room temperature for 1 h with an argon balloon. The reaction solution was transferred to a dried addition funnel flushed with argon, and added dropwise over 1 h and with vigorous stirring to minimize polymerization to a round-bottomed flask containing a solution of ethylenediamine (8 mL, 120 mmol) dissolved in $CHCl_3$ (30 mL) at room temperature, under argon, in a two-neck round bottom flask equipped with a stir bar.

The reaction was stirred overnight at room temp. and transferred to a separatory funnel followed by addition of 100 mL of water. The organic layer was separated, and the aqueous layer was washed three more times with $CHCl_3$. Organic layers were combined, and concentrated to about 15 mL and this crude was loaded into a silica gel packed column and purified using and isocratic gradient of 8% MeOH/ 92% $CHCl_3$ as the eluent.

KMnO4 was used as the TLC stain. Pure fractions containing product **2** were collected and concentrated to get a yellow and thick oil. ^{1}H and ^{13}C NMR were as reported.[127]

Synthesis of compound 3. Compound **2** was dissolved in 70 mL of MeOH and argon was bubbled through in a 250-mL round-bottom flask. After 5- 10 min, methyl acrylate (110 mmol, 10 mL) was added dropwise and the reaction was further stirred for 2 days at room temperature under argon. After that time, the reaction mixture was rotovaped. The residue was purified by flash chromatography on silica using 3 % MeOH/$CHCl_3$ as the eluent. ^{1}H and ^{13}C NMR were as reported.[127] Low resolution found ESI-MS m/z: 419.3 $(M+H)^{1+}$.

Synthesis of compounds 4 and 5 (CL4). Compound **3** (80 mg, 1.9 mmol) was dissolved in 5 mL of ethanol and transferred into a 25-mL round-bottom flask equipped with a stir bar. A solution of LiOH (103.8 mg, 4.33 mmol) dissolved in 2.47 mL of water, was added dropwise and the reaction was stirred at room temperature. Ester hydrolysis takes about 1-2 h and can be monitored by TLC with 15% MeOH/ $CHCl_3$ as the mobile phase.

After 2 h, compound **4** was the only product, and it was used without any further treatment for the following reaction. First the pH of the crude reaction was adjusted to ~ 8.0 by dropwise addition of a 4 M aq. HCl solution and stirring, then $NaBH_4$ (2.84 mmol, 107 mg) was added carefully in powder form by using the wide end of a Pasteur pipette. Upon addition of $NaBH_4$ bubbles due to H_2 release, and the solution turned clear. After stirring briefly, argon was flushed through and the reaction was stirred for 1.5 h at room temperature with an argon balloon. A 3 M aq.HCl solution was added dropwise to adjust pH~ 7-8 (this step is very important). Ethanol was evaporated, and remaining solution

was filtered to removed precipitated salts (although it remained turbid). Argon was bubbled through the crude to avoid re-oxidation of thiol groups, and the crude was stored at - 20^{o}C until purification. Low resolution MS found ESI-MS m/z: 393.3 $(M+H)^{1+}$. In contrast to the original procedure reported,[127] CL4 was isolated by reverse phase HPLC, using a water/acetonitrile (with 0.1% TFA) gradient, to afford a light-yellow oil which was stored at 4 ^{o}C and blanketed with argon. The structure of compound CL4 was further confirmed by ^{1}H and ^{13}C NMR.

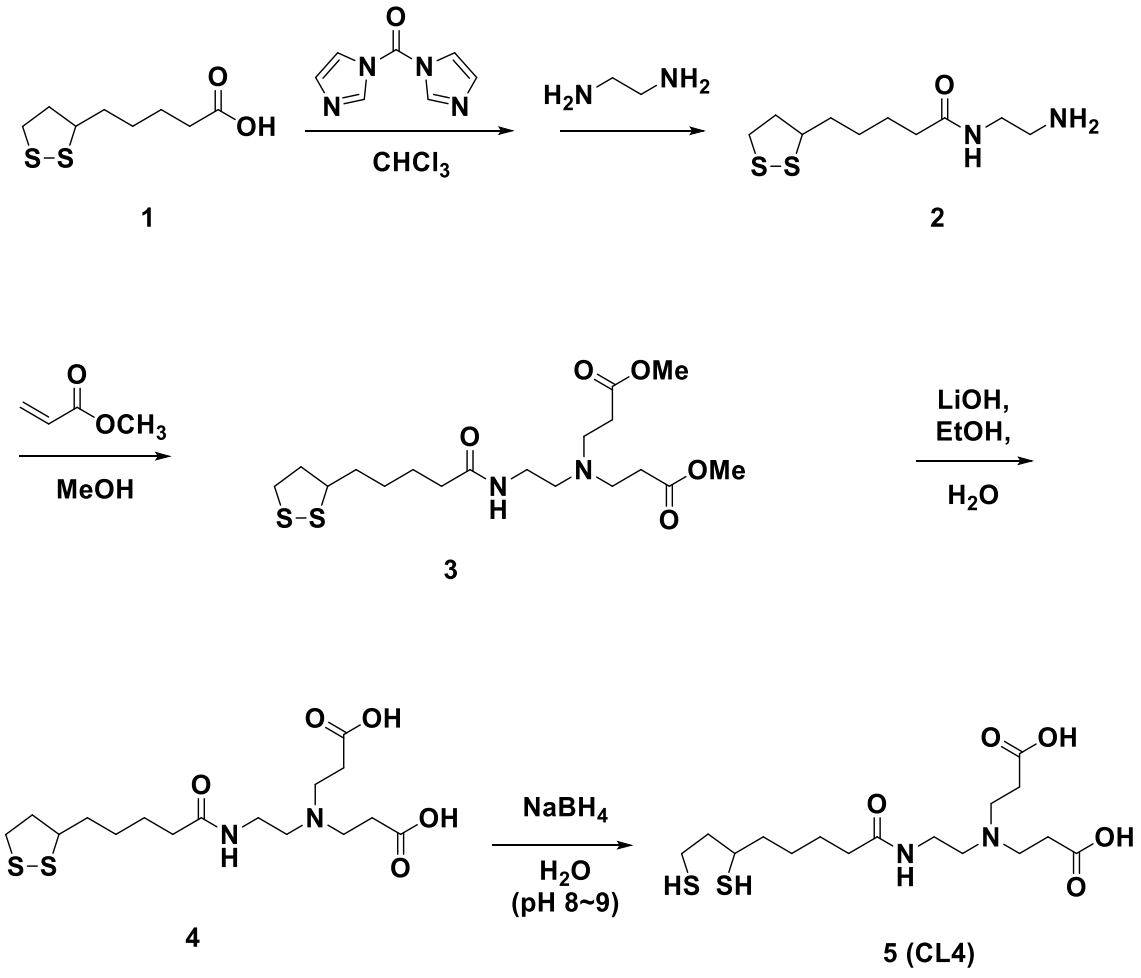

Scheme 2.1. Synthesis of CL4 ligand.[127]

2.3.4. Cap exchange of TOPO coated Qdots with zwitterionic CL4 ligand.

The CL4 ligand was prepared and purified by HPLC as described in section 2.3.3. One gram of TOPO-coated CdSe/ZnS QDs of a 4.9864×10^{-8} mol QDs/gram solution were weighed out in a 5-mL glass vial, and 1 mL of hexane was added followed by sonication. Additional hexane (1 mL) was added and the mixture was centrifuged at 3.5 x1000 rpm for 5 min. Isopropanol was added until the QD solution turned clear, then 1 mL of methanol was added (acetone or ethanol can be used as well) until the solution turned cloudy. The solution was centrifuged again at 3.5 x1000 rpm for 5 min and the supernatant was discarded. Methanol (1 mL) was added followed by centrifugation at 3.5 x1000 rpm for 5 min and supernatant disposal one more time. The vial containing precipitated quantum dots was left upside down on piece of paper towel to dry, then 4 mL of $CHCl_3$ were added to dissolve the TOPO-coated clean quantum dots. This solution was then transferred into a 50-mL round bottom flask equipped with a magnetic stir bar. In a 20-mL scintillation glass vial, 300 mg of CL4 ligand were weighed and completely dissolved with a minimum amount of water (~ 3-4 mL), followed by sonication. Since the resulting pH was acidic, a 0.1 M NaOH solution was added dropwise to reach a pH= ~8.0. The CL4 solution was added to the round bottom flask containing the TOPO coated QDs in $CHCl_3$.

The ligand exchange reaction was left overnight under N_2 atmosphere with vigorous stirring at room temperature. Over time, quantum dots migrate from the organic to the aqueous phase. The aqueous phase containing the water soluble CL4-coated QDs was collected and further purified by 5-6 cycles of dialysis through a centrifugal filter (100 kDa MW cutoff regenerated cellulose membrane, Millipore, centrifuge at 1.0 x 1000 rpm for 6

min each time) using molecular biology grade water (phosphate buffer pH=7 could be employed as well) until the flow through comes out with a neutral pH. Finally, the sample was purged through a 0.2 µm filter and diluted to a proper concentration for analysis.

2.3.5 General protocol for solid phase peptide synthesis. All peptides were manually synthesized using Fmoc-solid phase peptide synthesis (Fmoc-SPPS) on a 100 µmol scale on rink amide resin (AM Resin LL, 100-200 mesh, substitution = 0.35 mmol/ g) from Novabiochem. Couplings were performed using 300 µmol of amino acid (3.0 equiv), 300 µmol of Oxyme (3.0 equiv), 300 µmol of HBTU (3.0 equiv), dissolved in approx. 10 mL of DMF and 600 µmol of DIEA (6.0 equiv), for 30 min. Fmoc deprotection was carried out in the presence of a freshly prepared 20% piperidine in DMF solution for 15 minutes, twice. Following Fmoc removal, the resin was washed in the following order: 3X DMF, 3X DCM, 3X DMF. Pre-activation times were typically 5 minutes, and for cysteine containing amino acids 1 minute. Fmoc-Pro-OH was coupled twice. Mtt groups were removed with 1% TFA/ DCM solution for 10 minutes, 6 times. After Mtt group removal, the resin was washed in the following order: 2X/DCM, 2X/MeOH, 2X/DCM, 2X with 5% DIEA in DMF solution (to neutralize the resin and the Mtt-deprotected amine of interest).

N-acetylation at the N-terminus: The acetylation reaction consisted of reaction of Fmoc-deprotected N- terminal amine with acetic anhydride (20 equiv) in the presence of DIEA (30 equiv) in dry DCM for 1h at rt*. Pre-cleavage treatment*: The resin was treated with a series of washes as follows: 3X DCM, 3X MeOH containing acetic acid (pH~5), 3X DCM, 3X MeOH and then high vacuumed overnight, with the objective of removing as much

DMF as possible. Peptides were then cleaved from the resin with TFA and the appropriate scavengers (described below for each peptide) for 2-4 hours at rt. The crude peptide was precipitated in cold ether. TFA was rotovaped completely in cases where no precipitation of crude peptide was achieved in the presence of ether.

2.3.6 Synthesis of a bioconjugatable CPP peptide 6.

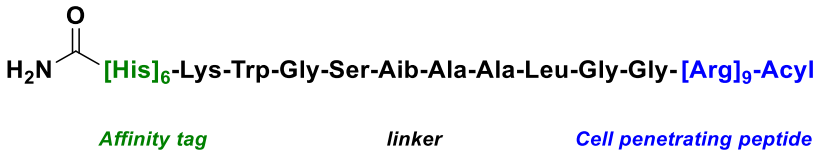

(6)

Peptide **6** was synthesized on rink amide resin and N-acetylated as described in **section 2.7.5** with a few modifications, for instance, double coupling was used for each amino acid residue after the nineteenth residue (Arg-19) to avoid the generation of truncation products and therefore a decrease in the overall yield of the target linear peptide.

Pre-cleavage treatment was performed as described in **section 2.7.5**.

After screening several cleavage conditions, we found that a combination of 80% TFA, 5% thioanisole, 5% anisole, 5% phenol, 5% water, was the best combination to cleave this peptide, for 4h at room temperature. Other cleavage conditions did not give the desired product.

Post-cleavage treatment: The crude cleavage mixture had a characteristic dark brown color. TFA was rotovaped to about 20% of the total volume, and added dropwise to a 50-mL centrifuge tube with 45 mL of cold ether in an ice bath. A white solid formed

immediately, and the brown color disappeared. This solution was centrifuged at 4000 rpm for 5 min, the ether layer was discarded, and the pellet was dried overnight in high vacuum. This peptide was purified by reverse phase HPLC using a water/acetonitrile (both solvents containing 0.1% TFA) gradient from 2% ACN/water to 47% ACN/water over 43 minutes, and then ramped to 100% ACN over 5 minutes by employing a semi-prep reverse phase column (Aeris, 10 mm diameter x 250 mm length) at a 5 mL/ min flow rate and monitoring with a dual detector (λ_1= 220 nm, λ_2= 254 nm). Fractions containing the desired peptide were lyophilized and desalted. Calculated m/z 3199.7823, found $[M+H]^{1+}$ = 3200.537 by MALDI-TOF (reflector positive mode).

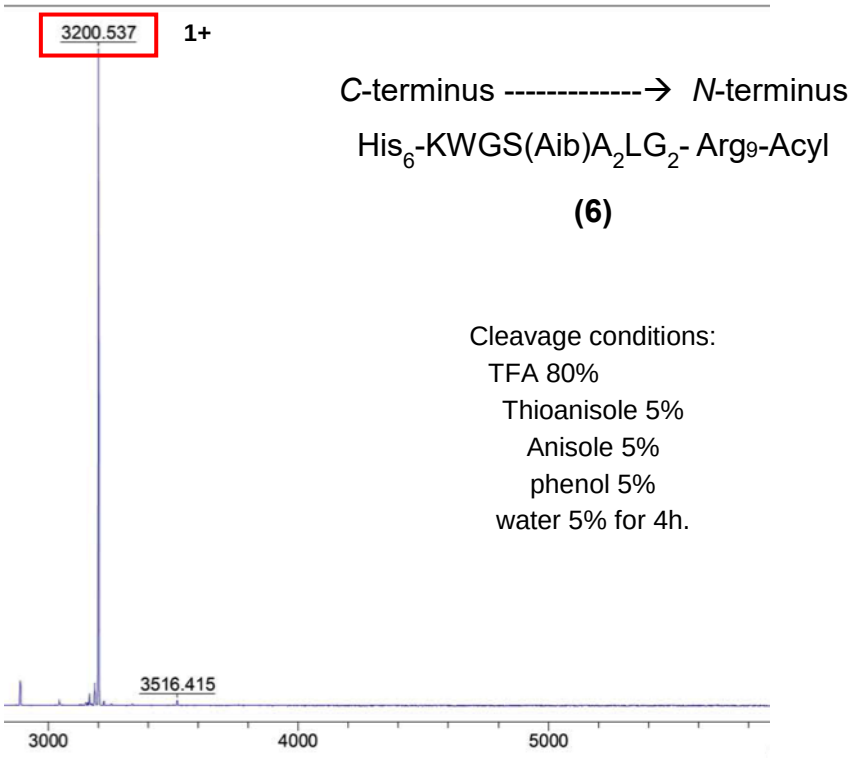

C-terminus ----------→ *N*-terminus

His_6-KWGS(Aib)A_2LG_2- Arg_9-Acyl

(6)

Cleavage conditions:
TFA 80%
Thioanisole 5%
Anisole 5%
phenol 5%
water 5% for 4h.

2.3.7 Synthesis of a bioconjugatable Aurein 1.2 peptide 7.

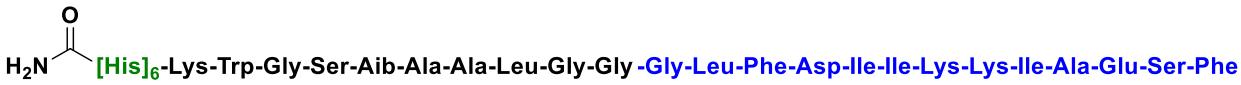

(7)

Peptide **7** was synthesized on rink amide resin as described in **section 2.7.5** with a few modifications, for instance, double coupling was used for each amino acid residue after the sixteenth residue (Gly-16) to avoid the generation of truncation products and therefore a decrease in the overall yield of the target linear peptide.

Pre-cleavage treatment was performed as described in **section 2.7.5.**

After screening a few cleavage conditions, we found that a combination of 90% TFA, 5% thioanisole, 2% anisole, 3% EDT, for 3h at room temperature was the best condition to cleave this peptide neatly. Another combination that also affords this peptide is: 80% TFA, 5% thioanisole, 5% anisole, 5% phenol, 5% water for 3-4 h at room temperature.

Post-cleavage treatment: TFA was rotovaped to about 20% of the total volume, and added dropwise to a 50-mL centrifuge tube with 40 mL of cold ether in an ice bath. A white solid formed immediately, which was further centrifuged at 4000 rpm for 5 min, the ether layer was discarded, and the pellet was dried overnight in high vacuum.

This peptide was purified by reverse phase HPLC using a water/acetonitrile (both solvents containing 0.1% TFA) gradient by employing a semi-prep reverse phase column (Aeris, 10 mm diameter x 250 mm length) at a 5 mL/ min flow rate and monitoring with a dual detector (λ_1= 220 nm, λ_2= 254 nm). Fractions containing the desired peptide were

lyophilized and desalted. Calculated m/z 3214.685, found $[M+H]^{1+}$ = 3215.534 by MALDI-TOF (reflector positive mode).

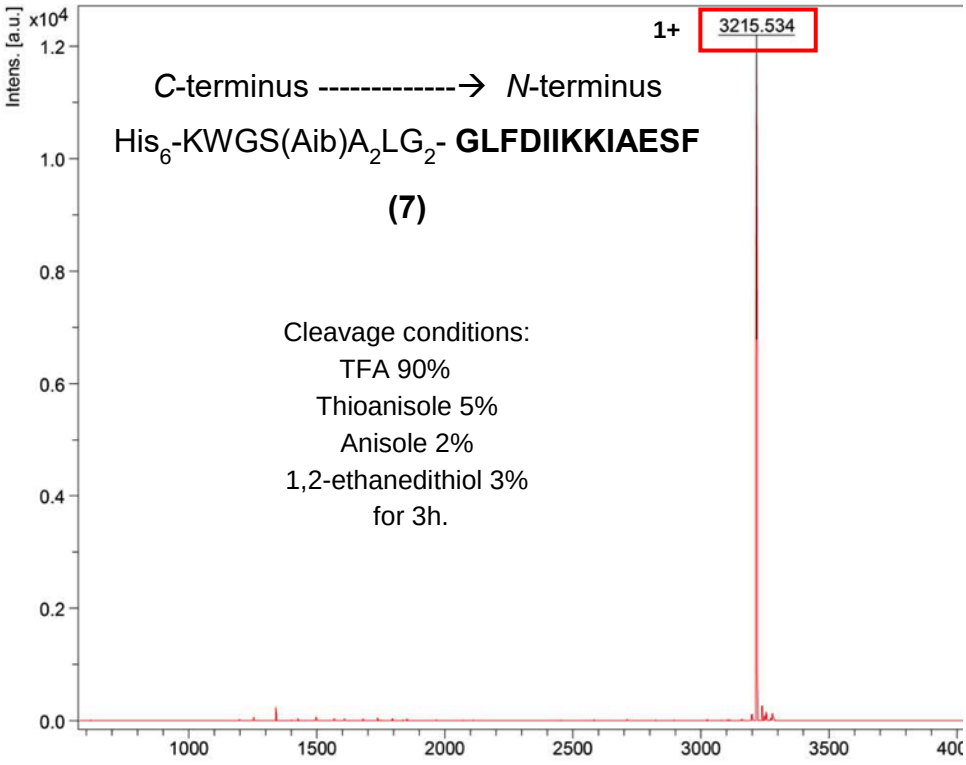

2.3.8 HAfp protein sequence (referred as HA2 in this thesis). The His_6-GB1-HAfp23-K_4D protein was provided by Sean Smrt in collaboration with Prof. Lorieau's group.[128] The sequence is as follows:

MGSS**HHHHHH**SSGMQYKLILNGKTLKGETTTEAVDAATAEKVFKQYANDNGVDGEW

TYDDATKTFTVTEGSSGIEGR-**GLFGAIAGFIEGGWTGMIDGWYGSG-** KKKKD

2.3.9 Peptide desalting. All peptides were desalted before being assembled to quantum dots. Briefly, about 1 mg of HPLC purified peptide was dissolved in 1-3 mL of molecular biology grade water or in 0.1 M TEAA buffer solution. An OPC cartridge (Applied Biosystems) was washed with 5 mL of HPLC grade acetonitrile, followed by 5 mL of 2.0 M TEAA buffer. Peptide solution was passed through OPC cartridge at a 1 drop/second rate. The eluate was collected and passed through a second time or more, to maximize the amount of peptide bound to the C18 stationary phase. The eluate was discarded, and 10 mL of molecular biology grade water were passed through the OPC cartridge to remove all salts.

Finally, desalted peptide was eluted from the OPC cartridge by slowly passing a 1 mL of a 50% Acetonitrile / water solution drop by drop (1 drop every 4 seconds). Eluate was collected and freeze-dried. Note: Do not exceed the loading capacity of the OPC cartridge.

2.2.10 Cell Culture. HeLa cells were maintained in DMEM (+) (DMEM supplemented with 10% FBS, 1X MEM non-essential amino acids and 15 mM HEPES) at 37 °C and 5% CO_2. The cells were passaged with 0.25% trypsin/2.21 mM EDTA.

2.3.11 Polylysine coating of plates. 8-well plates (400 μL volume each well) were exposed to UV irradiation for about 20 minutes, then coated with 200 μL of polylysine solution for 5 minutes at room temperature, the polylysine solution was removed and the wells were washed with molecular biology grade water (400 μL, 3 times). Subsequently, polylysine coated plates were left to dry under laminar flow for 2h.

2.3.12 Cell seeding into polylysine plates. 400 mL of fresh media were transferred into each well, then, 15 mL of HeLa containing DMEM medium were transferred into each well, and mixed gently. The 8-well plate was covered with a lid and put back inside a cell incubator at 37 ^{o}C and 5% CO_2 overnight.

Once HeLa cells reached a 50%, media was removed, and wells were washed 3 times with warm (37 ^{o}C) PBS 1X (pH = 7.4) , and reconstituted with 100 μL DMEM-HEPES (no FBS) before addition of QD-bioconjugates.

2.3.13. Assembly and Delivery of QD-CPP conjugates.

An example of an assembly and delivery of QD-CPP conjugates was performed as follows (see Table X as a reference):

1) To four 0.4 mL Eppendorf tubes (1:5, 1:10, 1:15, 1:20), add 10.5 μL of 10X PBS buffer.

2) To each tube, add the corresponding amount of water and mix.

3) To each tube, add the corresponding amount of CPP peptide stock solution, and gently mix. In this example, the CPP stock concentration is 15 μM.

4) To a separate set of four 0.4 mL Eppendorf tubes, add 5.2 μL of [2 μM] QD stock.

5) Transfer the prepared CPP peptide solution from steps 1-3 to the corresponding tubes containing QD solutions prepared in step 4, and gently pipette up and down (do not vortex, nor centrifuge). The final volume for each tube should be 105 μL. Incubate for 1 hour at room temperature and protect from light.

6) Take out from the 37 ^{o}C incubator, the 8-well polylysine coated plate seeded with HeLa cells grown in DMEM-HEPES (no FBS) medium at ~ 50% confluency. Remove the media from each seeded well and wash three times with 400 μL/well of warm (37 ^{o}C) 1X PBS buffer (pH = 7.4) right before addition of the QD- conjugates, and replenish each well with 100 μL of fresh DMEM-HEPES (no FBS) media.

7) Co-incubate cells with the corresponding QD-CPP conjugates by transferring 100 μL of each QD-CPP assembly reaction (1:5, 1:10, 1:15, 1:20) prepared in step 6 to their respective wells and mix gently. In this example, the final concentration of QD-conjugate is 50 nM after mixing with cell media. Incubate at 37 ^{o}C for 1.5-2 h.

8) Remove media from each well and wash three times with 400 μL of warm (37 ^{o}C) DPBS buffer and replenish each well with fresh DMEM-HEPES (no FBS) media (400 μL/well). Put plate back into incubator while setting up the microscope.

Desired QD/CPP ratio				
	1: 5	**1: 10**	**1: 15**	**1: 20**
Volume QD [2 μM]	5.2	5.2	5.2	5.2
Volume 10X PBS (μL)	10.5	10.5	10.5	10.5
Volume CPP [15 μM]	3.5	7.0	10.5	14
Volume water (μL)	85.8	82.3	78.8	75.3
Total volume (μL)	105	105	105	105
Final QD conc. (nM)	100 nM	100 nM	100 nM	100 nM
Final CPP conc. (μM)	0.5 μM	1 μM	1.5 μM	2 μM

Table 2.1. Reagent volumes utilized for QD- CPP peptide self-assembly

3 FRET- based strategies to detect and quantify endosomal escape in live cells

3.1 Introduction

Our primary goal was to investigate the endosomal escape ability of three peptides and a protein (HA2) with potential endosomal escape ability, except for the expressed HA2 protein, we utilized SPPS methods to synthesize a palmitoyl (**23**), polyamine (**31**) and Aurein 1.2 (**7**) peptides on rink amide resin.

Upon their CPP facilitated delivery, very often the fate of fluorescent nanoparticles is followed mostly by two methods; intracellular fluorescence pattern (IFP) and colocalization studies.[90] In IFP, the efficiency of endosomal escape is assessed based on whether the cytosolic pattern observed is diffuse (good escape), medium or punctate (poor escape). Colocalization studies in which QDs are simultaneously delivered with a differently colored fluorescent endosomal marker, provide valuable information, for example by using confocal microscopy it is possible to distinguish QDs sequestered in endosomes (QD and endosomal marker distinct emissions overlap) versus QDs diffused in the cytoplasm (only the QD emission is observed).

Both methods to assess the efficacy of endosomal escape, IFP and colocalization studies, are informative and necessary but they both remain qualitative. Because of the lack of methods to quantify endosomal escape of QDs, we decided to develop a FRET-based strategy capable of measuring the endosomal escape abilities of the selected protein/peptides in live-cells.

Moreover, a FRET-based strategy was our choice for intracellular detection of endosomal escape for several reasons,[129] for instance; 1) It is distance-dependent, 2) the FRET signal can be triggered when the probe meets a specific setting such as the reductive cytosolic environment, 3) Sensitivity is improved by background reduction, 4) There are many FRET-pair choices that make possible employing donors with low energy excitation wavelengths, to avoid harming live-cells during microscopy studies, 5) The freedom to design FRET probes wherein the FRET acceptor can be either a non-emissive dark quencher or an emissive fluorescent dye, 6) FRET generates a luminescent or ratiometric signal, which can be measured even in the non-homogenous intracellular environment . Briefly, these last features are highly sought after in live-cell studies.

In this chapter, I discuss the synthesis, and characterization of several FRET acceptor peptides, as well as their respective spectroscopy studies. Then, I show results (obtained in collaboration with Dr. Hamid Samareh Afsari and Ha Pham) from colocalization studies in live cells that prove the CPP-facilitated intracellular delivery of QDs and the qualitative assessment on the endosomal escape abilities of a viral protein (HA2), a reported endosomolytic peptide **23** (palmitoyl), a bacterial membrane active peptide **7** (Aurein 1.2) and a polyamine peptide **31**, which I designed.

After that, ratiometric-FRET quantitative evaluations on endosomal escape ability of HA2, Aurein 1.2 and polyamine are provided along with a discussion. Ratiometric maps were developed by Dr. Hamid Samareh Afsari.

3.2 FRET-acceptor peptide design

Peptides were designed with 1) *C*-terminal polyhistidine tag to facilitate self- assembly on CL4-coated QDs; 2) The sequence S-L-G-A-A-A-G-S-G (from *C*-terminus to *N*-terminus) reported by the Medintz group[130] contains a GAAAG spacer/linker containing three consecutive alanine residues to provide rigidity, flanked by two glycine residues. The Ser and Leu residues provide some rotational flexibility and the amine group on the *N*-terminal glycine is used for further conjugation or continuation of the peptide synthesis; 3) A disulfide linker with a terminal amino group for conjugation with the FRET acceptor and 4) The FRET acceptor dye.

The SLGAAAGSG linker allows tight self-assembly on the QD surface, provides some rigidity (by the row of alanine residues) so it does not fold back onto the QD, and possesses appropriate length to allow the QD and N-terminal dye to engage in FRET.

The FRET acceptor dye can be a dark quencher, a chromophore that can absorb photons from a FRET donor to reach higher electronic states and then relax to the ground state by non-radiative mechanisms.[131] instead dark quenchers dissipate the absorbed energy in molecular vibrations or heat while remaining dark.

Alternatively, the FRET acceptor can be a fluorescent dye. In such case, the dye absorbs the non-radiative energy transferred from a QD FRET donor, as a result the acceptor becomes excited and relaxes back to the ground state by fluorescence emission. Regardless whether the FRET acceptor is a dark quencher (non- emissive) or an emissive fluorescent dye, the QD donor fluorescence is quenched as a result of this energy transfer.

3.3 General synthesis of FRET quenching peptides

Because of their absorbance profile, we selected BHQ-2, QSY-7 and QSY-21 terminated peptides. The detailed protocol is described in the experimental section, the general solid phase synthesis is shown in Scheme 3.1 and MALDI characterization data in Figure 3.1.

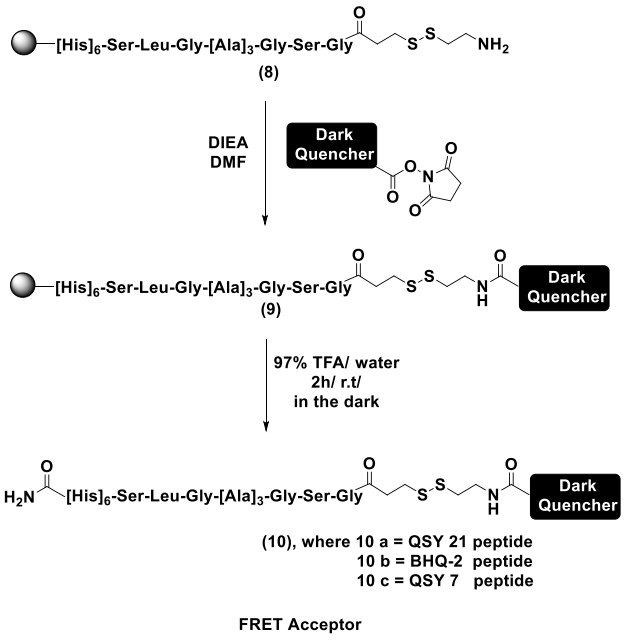

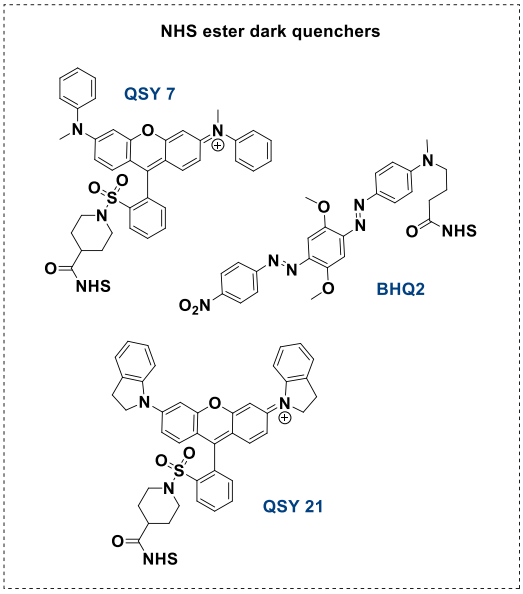

Scheme 3.1. Solid phase peptide synthesis of dark quencher peptides.

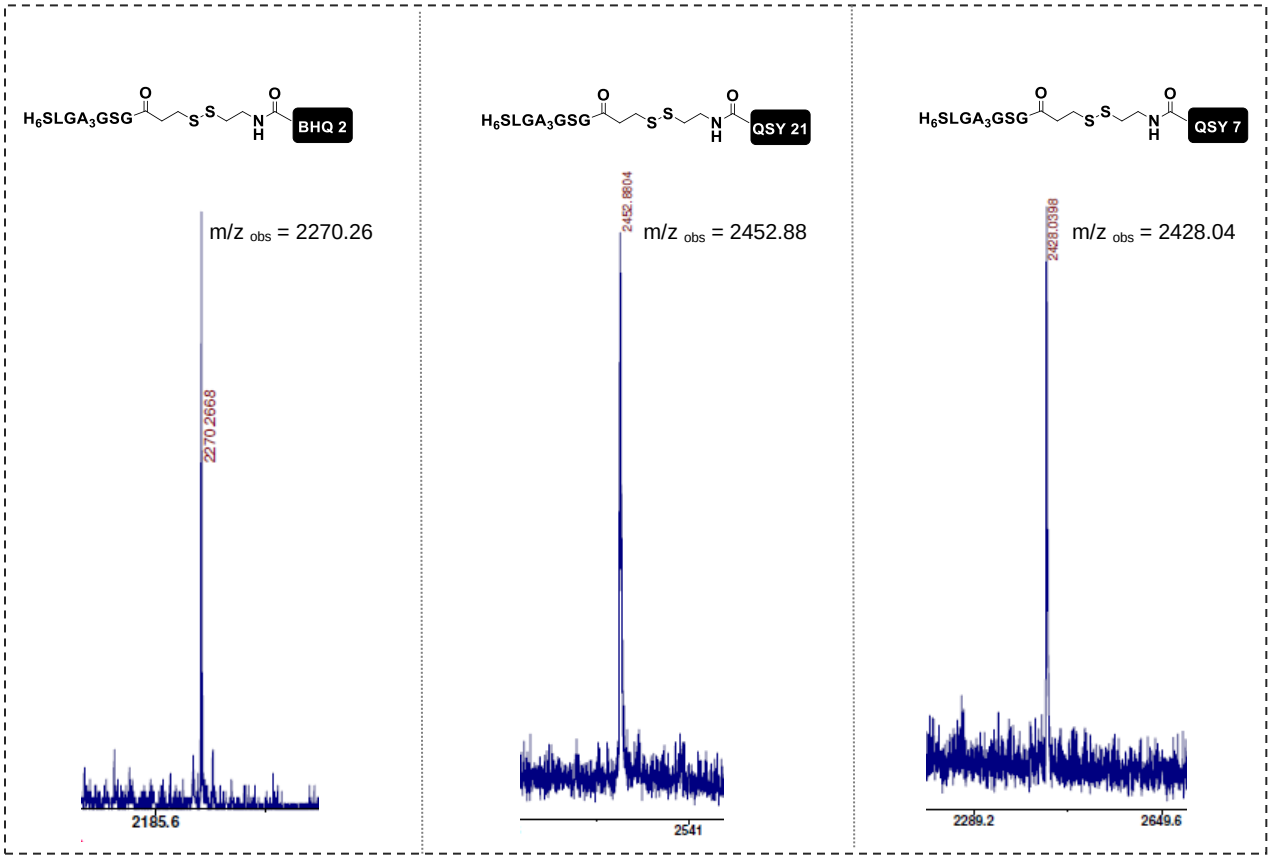

Figure 3.1. MALDI characterization of dark quencher peptides

3.4 Structures of disulfide linked dark quencher peptide ligands.

QSY-21 (10 a), BHQ-2 (10 b) and QSY-7 (10 c) structures

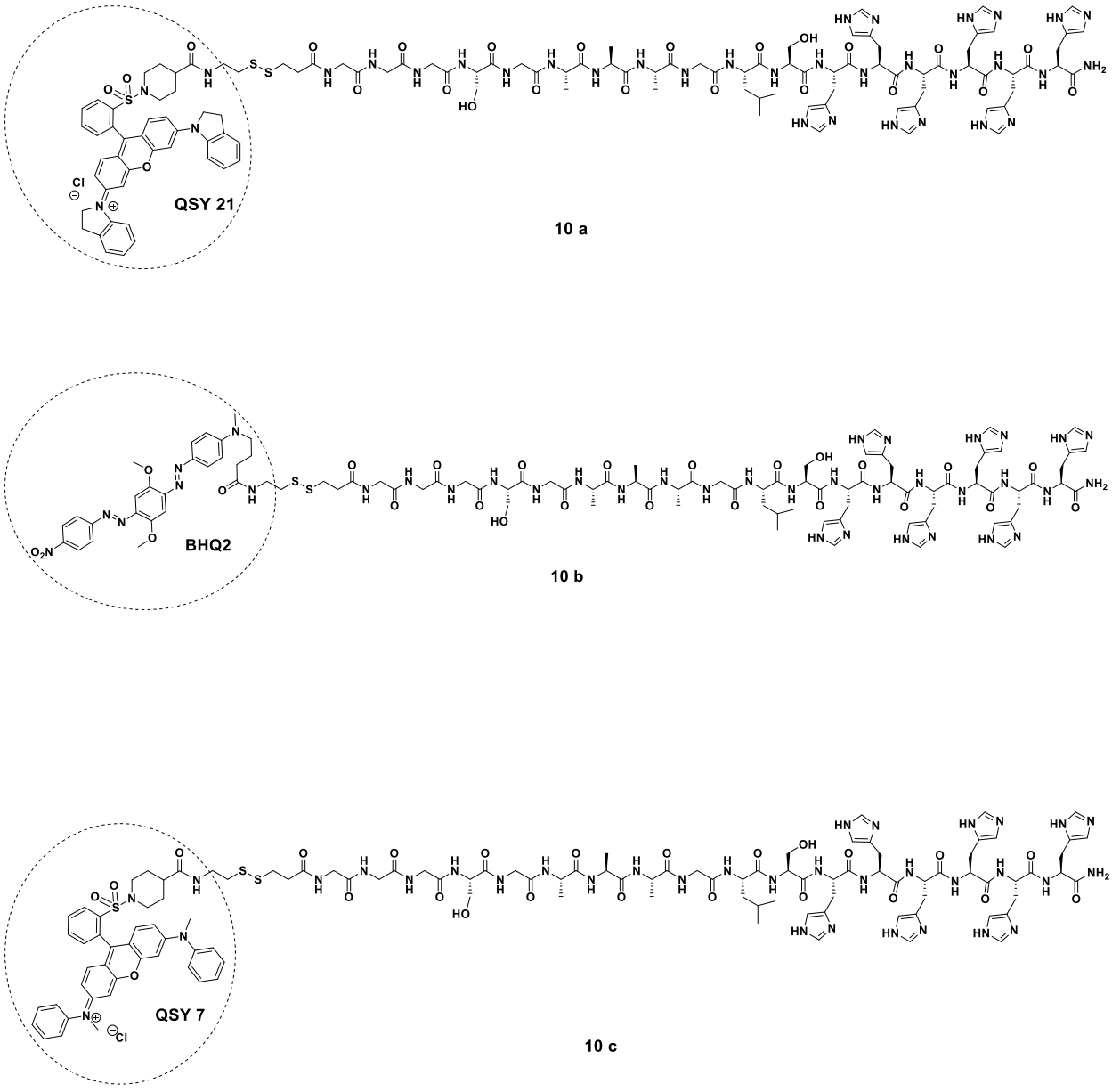

Figure 3.2: Structures of QSY-21 (**10 a**), BHQ-2 (**10 b**) and QSY-7 (**10 c**) quencher terminal peptides.

3.5 QD donor - dye acceptor spectra overlap and FRET quenching experiment results

3.5.1 Red QD (donor) and QSY-21 peptide acceptor 10 a.

QSY-21 peptide 10 a structure is represented in Figure 3.2.

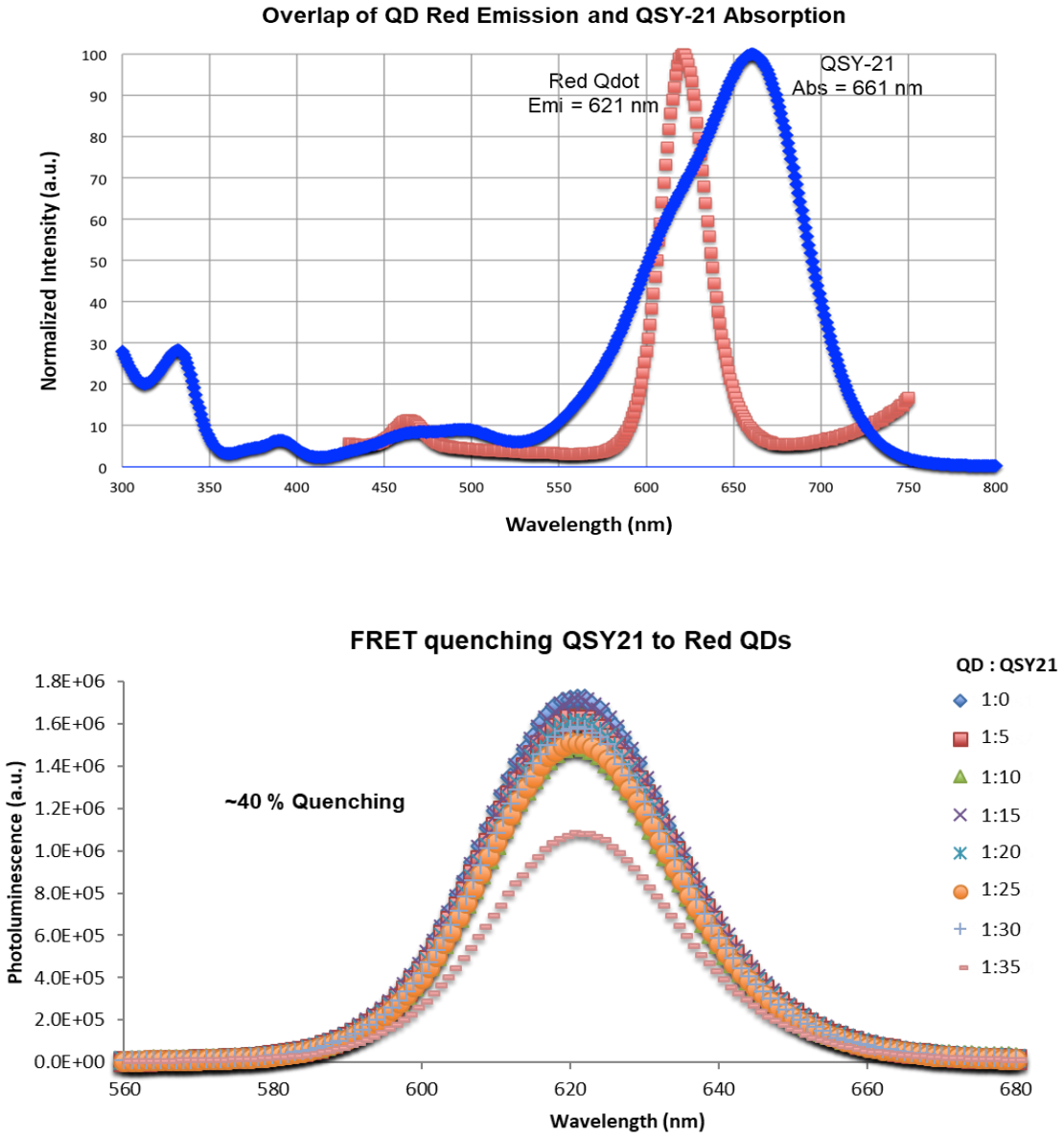

Figure 3.3: Overlap of red QD donor emission and QSY-21 absorption spectra overlap (Top), titration of QSY-21 peptides **10 a** per red QD and photoluminescence quenching (Bottom).

3.5.2 Red QD (donor) and BHQ-2 peptide acceptor 10 b.

BHQ-2 peptide **10 b** structure is represented in Figure 3.2.

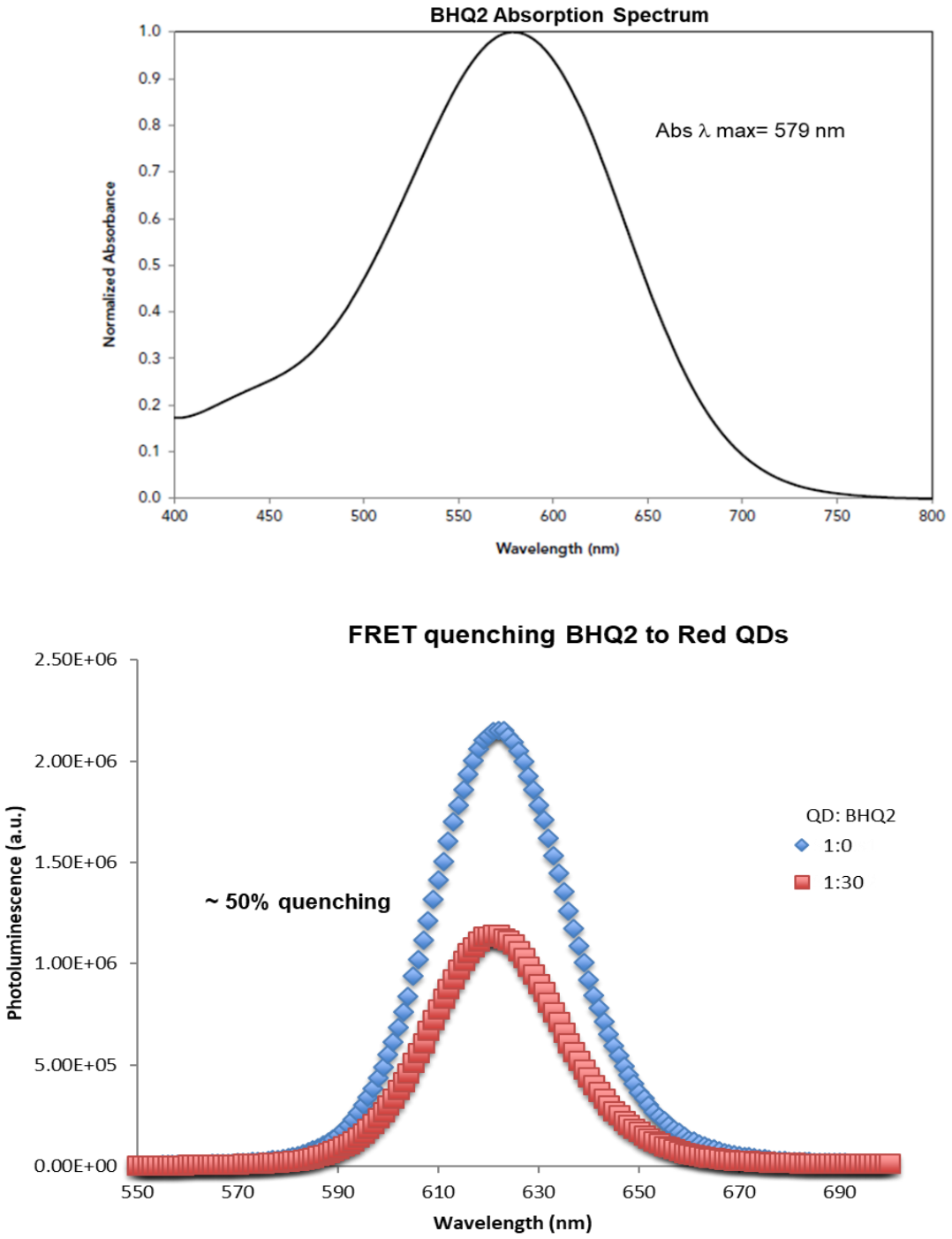

Figure 3.4: BHQ-2 absorption spectra reported by the vendor (Top**),** a couple of experiments that show ability of BHQ-2 peptide **10 b** to quench red QD photoluminescence quenching (Bottom)

3.5.3 Green QD (donor) and BHQ-2 peptide acceptor 10 b.

BHQ-2 peptide **10 b** structure is represented in Figure 3.2.

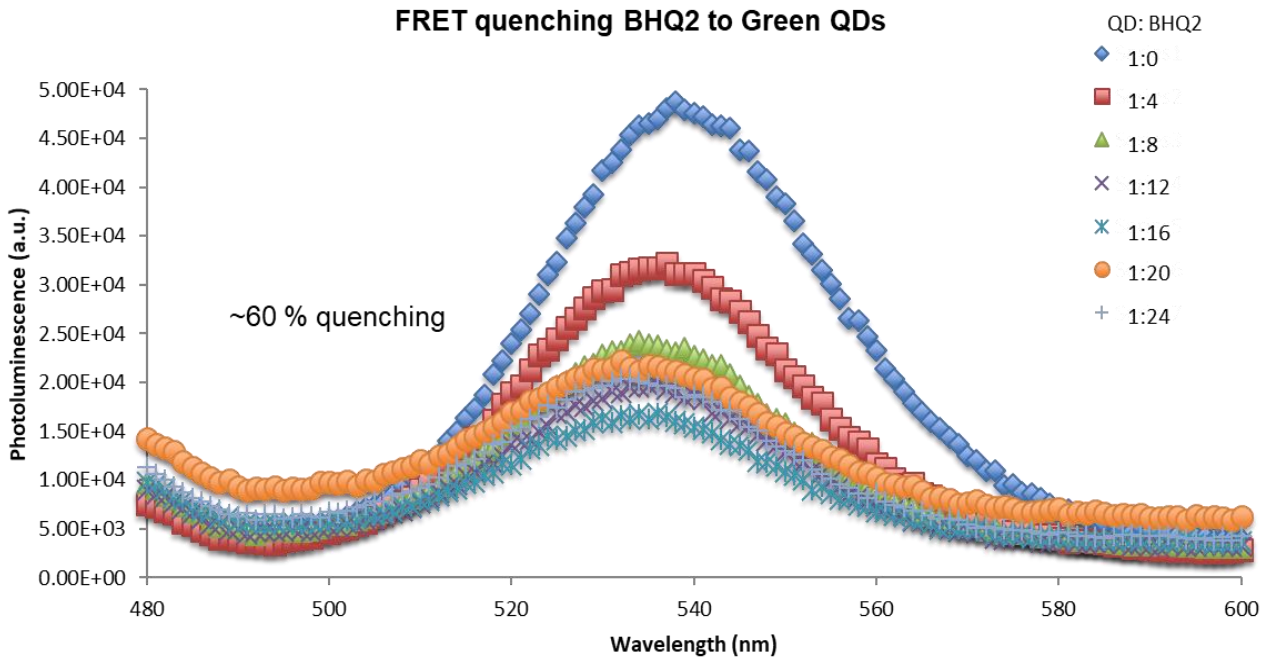

Figure 3.5: Titration of BHQ-2 peptides **10 b** per green QD and photoluminescence quenching.

3.5.4 Green QD (donor) and QSY-7 peptide (10 c) acceptor

QSY-7 peptide (**10 c**) structure is represented in Figure 3.2.

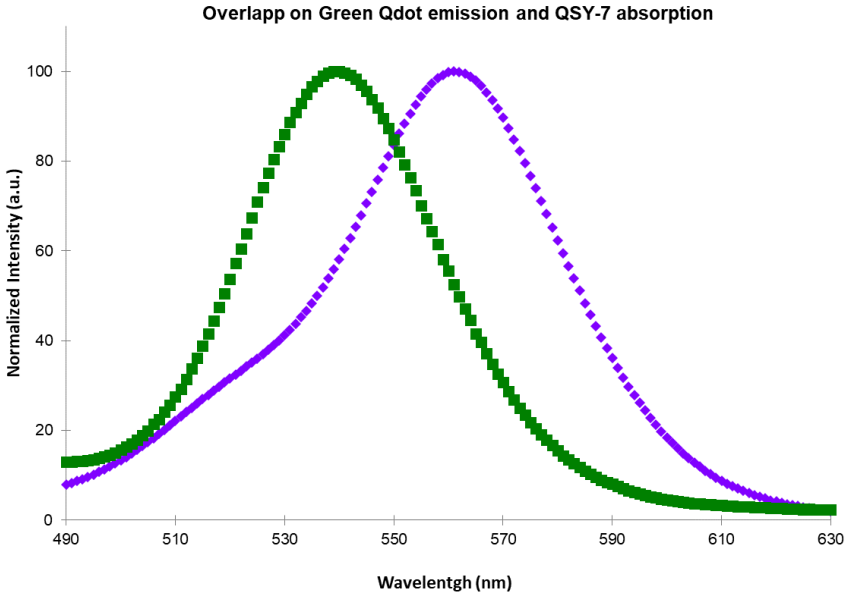

Figure 3.6: Overlap of green QD donor emission and QSY-7 absorption spectra overlap.

3.5.5 Conclusion

The three peptides I synthesized, QSY 21 (**10 a**), BHQ2 (**10 b**) and QSY-21 (**10 c**), showed quenching activity. We were expecting to observe a high quenching of red QDs photoluminescence (PL) since QSY-21 absorption almost completely the emission of red QDs at 621 nm (Figure 3.3, Top), however, this was not the case. Instead, QD luminescence was only quenched by 40% when loading the QD with 35 dark quencher ligands (Figure 3.3, bottom). A similar scenario was observed with the QSY-7 quencher peptide **10 c**. As the spectra overlap of green QD donor emission and QSY-7 absorption shows (Figure 3.6), the quenching efficiency should be highly efficient. In the last case,

we could not perform any quenching titrations due to very poor dye solubility. We noticed that QDs aggregated when mixed with the QSY-7 peptide. The solubility of QSY-21 peptide **10 a** was also poor, so we added DMSO (up to 20%) to coordinate the peptide to the QD surface, which is probably the reason why we found a very poor quenching ability (40%). Structure of the QSY dyes are quite hydrophobic (Figure 3.2), which means that for FRET quenching experiments they would have to be optimized for water solubility and incubation with QDs.

Interestingly, the BHQ2 peptide **10 b** could partially quench both, green and red emitting CL4 QDs, which can be explained by the dye broad absorption profile (Figure 3.4 top). BHQ2 quenched 50% of red QD luminescence (621 nm) when we conjugated 30 ligands per QD (Figure 3.4), and it also quenched 60% of green QD luminescence (539 nm) when 24 peptide ligands were assembled per QD. Again, we observed that this peptide had very poor water solubility, which was improved by adding DMSO, however, this adding organic polar solvents to QDs is not ideal.

To exploit the dark quenchers tested in this study for their full potential, the solubility must be improved first, for example by adding arginines, glutamic or aspartic acids, or peg linkers. Also, the length of the peptide should be considered to not compromise its fret quenching capacity. Another issue with these quenchers is their high cost, which limits the scale of the peptide synthesis and preferably should be conjugated during the last step to improve percent yields. In terms of scalability and practicality, these quenchers are not ideal. In terms of their FRET quenching capacity, BHQ2 and QSY-21 exhibited a

40-60 % quenching capacity, which might be sufficient for in vitro studies, but not enough for live-cell studies. Therefore, we turned our attention to another kind of FRET acceptors such as rhodamine B discussed in the following sections.

3.6 Selection of a suitable emissive FRET acceptor dye

From literature search and considering the emission spectra of our green emissive QDs, rhodamine B was selected for its absorption overlap with our CL4 coated QDs, (539 nm, Figure 3.7) and green DHLA coated 566 nm QDs (experimental section).

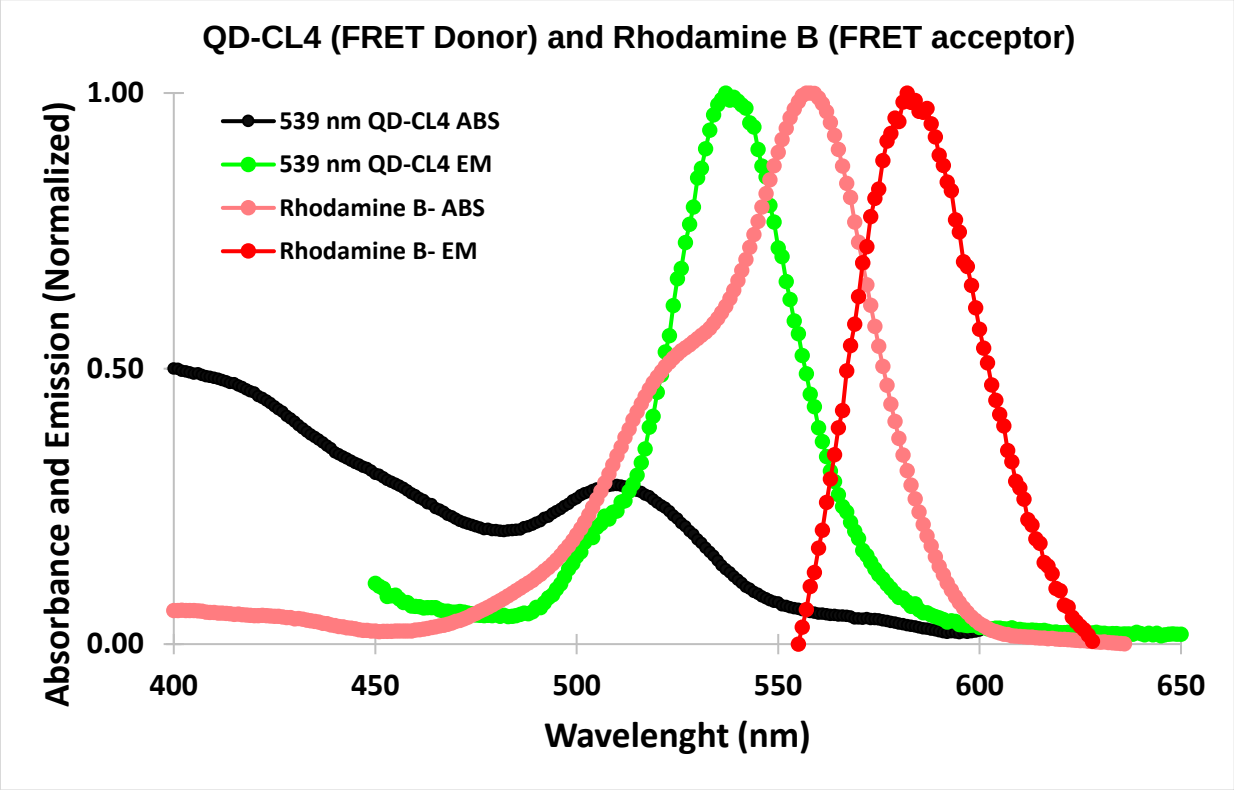

Figure 3.7. Normalized absorption and PL emission spectra of the QD -rhodamine B FRET pair and rhodamine B by itself (Excitation = 430 nm). Note the minimum in the absorbance of rhodamine B at 430 nm and the overlap between the QD emission and dye absorption.

The next step was the incorporation of rhodamine B to the amino-N terminal of our peptide ligand. We explored several synthetic routes and failed several times (one example is shown in Chapter 4). In section 3.7, we show the successful synthetic route found after several rounds of optimization and peptide design.

In section 3.8 we test the ability of a reducing agent (mercaptoethanol) to cleave the disulfide bond in our rhodamine FRET acceptor peptide

3.7 Synthesis of a rhodamine FRET acceptor peptide 18.

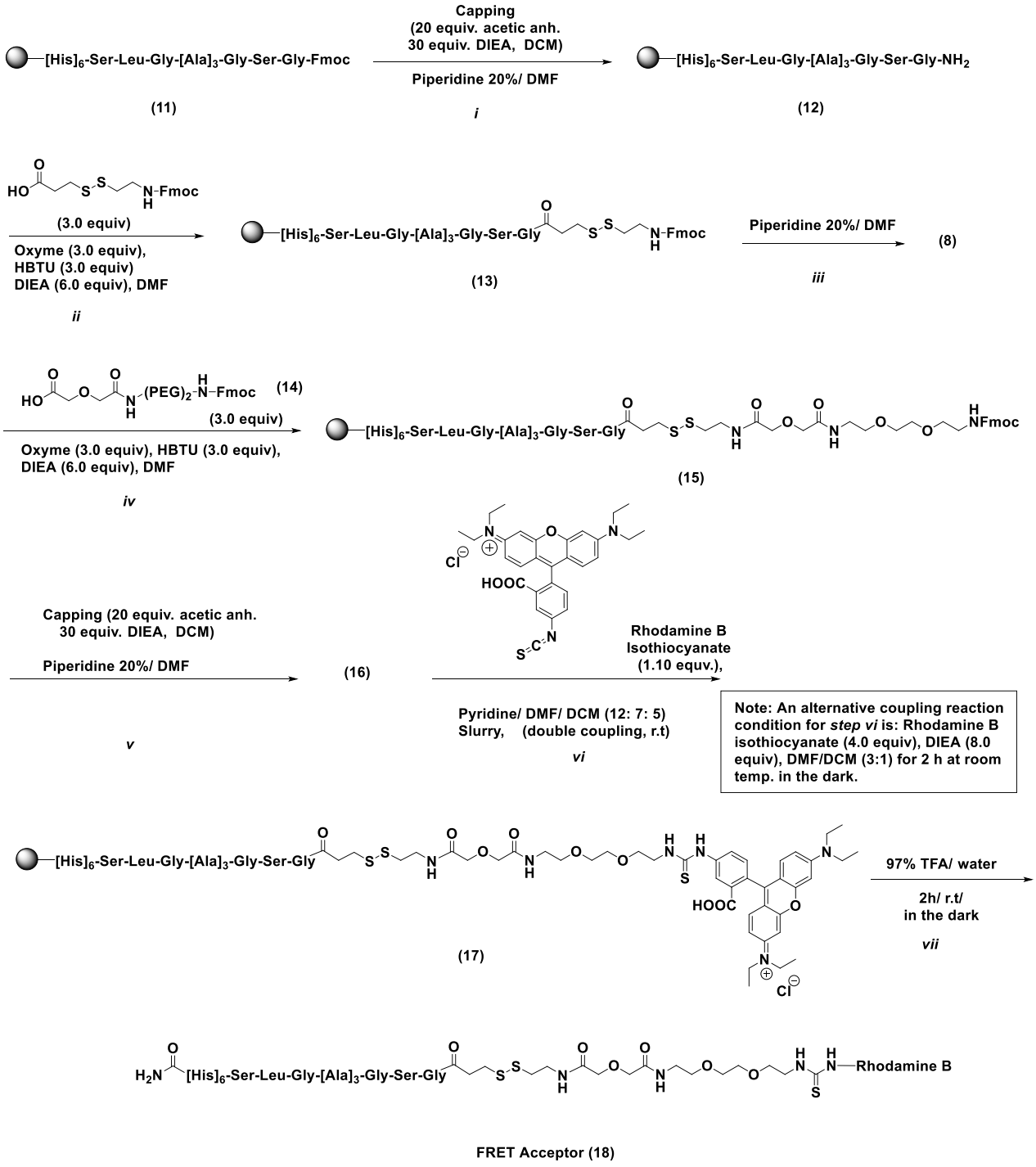

Scheme 3.2. Successful route that afforded rhodamine FRET acceptor peptide **18** by solid phase peptide synthesis.

3.8 Recovery of green signal upon disulfide bond cleavage by mercaptoethanol

Reduction of disulfide bond mercaptoethanol test. From titration experiments using green QD-DHLA (566 nm) it was determined that for an efficient FRET from QD-DHLA to Rhodamine B dye it is necessary to have at least six rhodamine peptides per QD (By Dr. Hamid Samareh Afsari).

The self-assembly of rhodamine peptides onto QDs was set up as described in **section 3.11.7**. After 1 h at room temperature, we tested the recovery of green emission signal from QDs upon disulfide bond reduction of the appended rhodamine peptides by adding a reducing agent and monitoring the change of emission in a fluorometer, using 430 nm as the excitation wavelength.

Mercaptoethanol was the reducing agent tested in our system. Briefly, the QD-Rhodamine conjugate solution (1:6) was diluted to 50 nM as the final concentration. This solution was then transferred into a quartz cuvette equipped with a stir bar at 25 ^{o}C.

A 20-mM stock solution of the reducing agent being tested, was added increasingly to the quartz cuvette and the change of emission was recorded every 5 minutes after the addition using an excitation of 430 nm. The results show a shift to the QD emission wavelength (566 nm) from the initial 584 nm rhodamine emission. FRET termination is due to disulfide bond reduction between QD and Rhodamine.

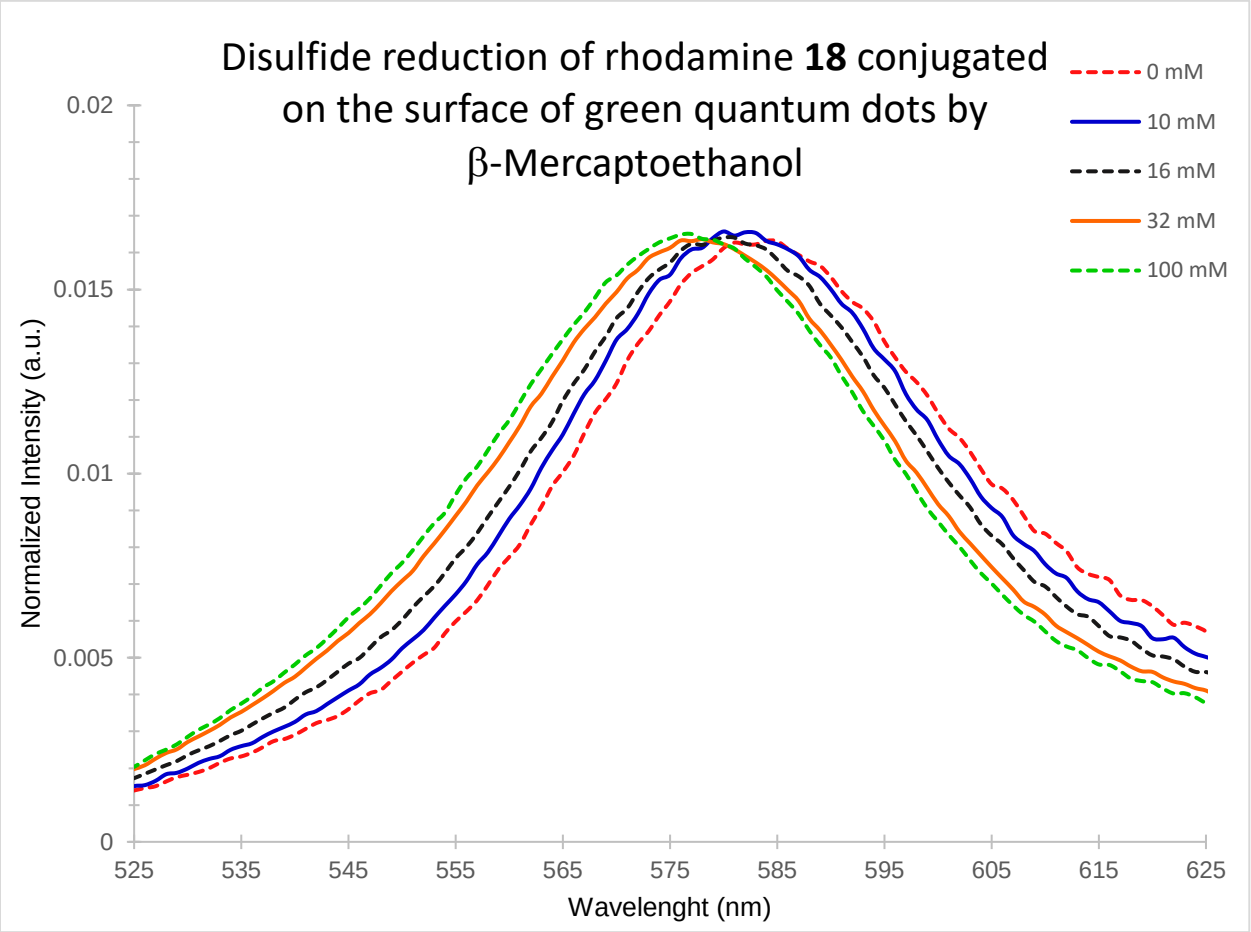

Figure 3.8. Shift of emission (from red to green) upon disulfide bond reduction of rhodamine B FRET acceptor peptide **18** by an increasing concentration of a reducing agent.

3.9 Synthesis of potential endosomal escape peptides

3.9.1 Solid phase peptide synthesis of palmitoyl peptide 23.

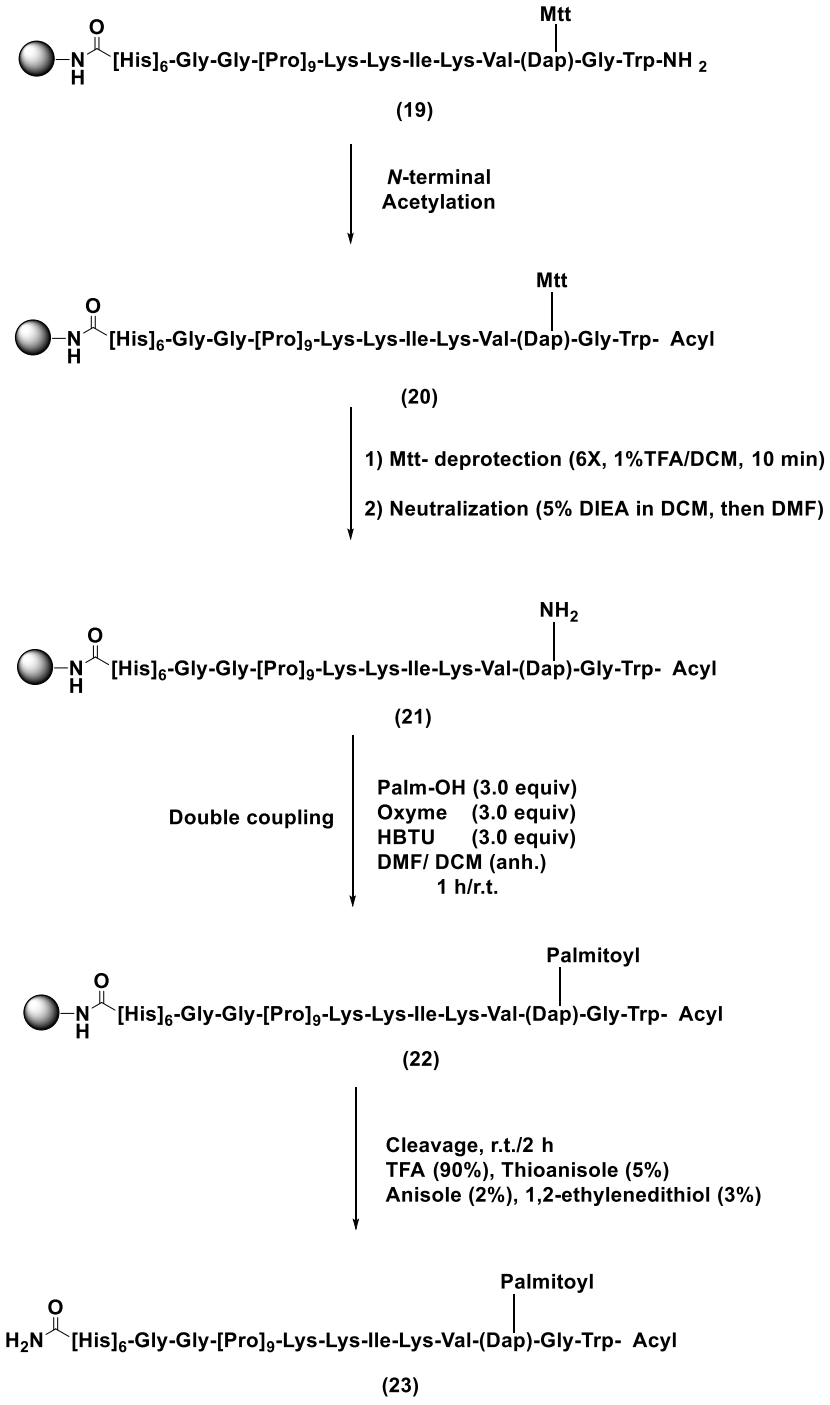

Scheme 3.3. Solid phase peptide synthesis of a palmitoyl peptide **23**.

3.9.2 Solid phase peptide synthesis of polyamine peptide 31.

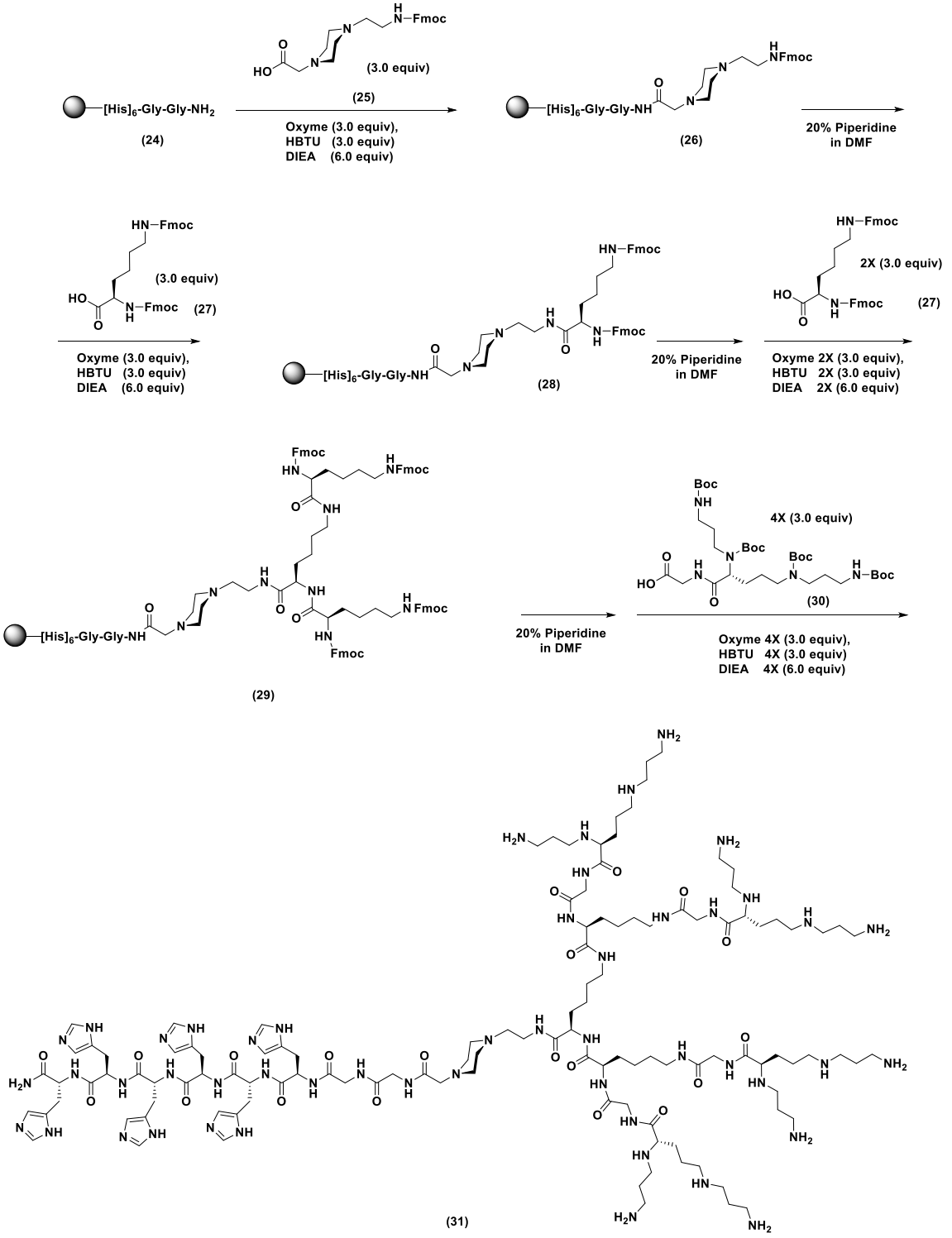

Scheme 3.4. Solid phase peptide synthesis of a polyamine peptide **31**.

3.10 Motivation to do colocalization studies and results

In Chapter 2, we showed that the intracellular delivery of our QD-Bioconjugates can be facilitated by a polyarginine CPP, however, upon coincubation of QD:CPP bioconjugates with an endosomal marker (Tf-red texas), we confirmed that all QD:CPP assemblies remained trapped inside endocytic vesicles by the colocalization of the green emission of QDs and the red emission of the endosomal marker Tf, which resulted in a merged yellow signal (Colocalization studies, Section 2.2.3).

The internalization of Tf into the cells begins with clathrin-mediated endocytosis, then Tf without distinction enters two populations of early endosomes, that subsequently proceed to the degradation pathway involving lysosomes,[55] therefore Tf is used as a general endosomal marker.

We also did a few preliminary live-cell studies in which we added an endosomolytic protein (HA2) and peptide (Aurein 1.2) separately, to our QD:CPP bioconjugates to explore their potential abilities to mediate endosomal escape of our QD probe (QD:CPP: HA2 and QD:CPP:Aurein 1.2 respectively). After incubation with HeLa cells, we were expecting to observe a diffuse pattern of QD:CPP:HA2 (or Aurein1.2) conjugates as an indication of their endosomal escape, but instead, we still observed a punctate pattern.

However, when QD:CPP:HA2 (or Aurein 1.2) were coincubated with Tf-red Texas, we observed a distribution of green and red punctae, and a decrease in yellow colocalization signal (when green QD and red-Tf emissions were overlaid, Section 2.2.5, which suggests that protein HA2 and peptide Aurein 1.2 may facilitate the endosomal escape of our QD probes. Encouraged by these promising results, we extended our investigation

by adding a polyamine peptide, which we designed to act as a proton sponge and a palmitoyl peptide[110] recently reported to deliver of QD complexes into the cytosol by facilitating both functions, their intracellular delivery and endosomal escape.

As a side note, from this section on, QD:CPP:EE (where EE = endosomal escape ligand) will be used to refer to either QD:CPP: HA2, QD:CPP: Aurein 1.2, or QD:CPP: polyamine.

In this section, we describe the cellular internalization of the QD:CPP (1:10) as a control run side by side with the respective QD:CPP: EE (in 1:10:20 ratios) assemblies under the same conditions. Thus, HeLa cells were incubated in DMEM at 37 ^{o}C with Tf marker and QD:CPP:EE conjugates (at a 50 μM final concentration) respectively to allow their respective internalization. After 1.5 h, DMEM was removed, cells were washed three times with PBS and reconstituted with fresh media to continue their incubation at 12 and 36 h.

At 12 h, media was removed, cells were washed and reconstituted with DMEM before being imaged. Confocal fluorescence imaging showed that all but the QD: Palmitoyl conjugate, were internalized under our delivery conditions (data not shown).

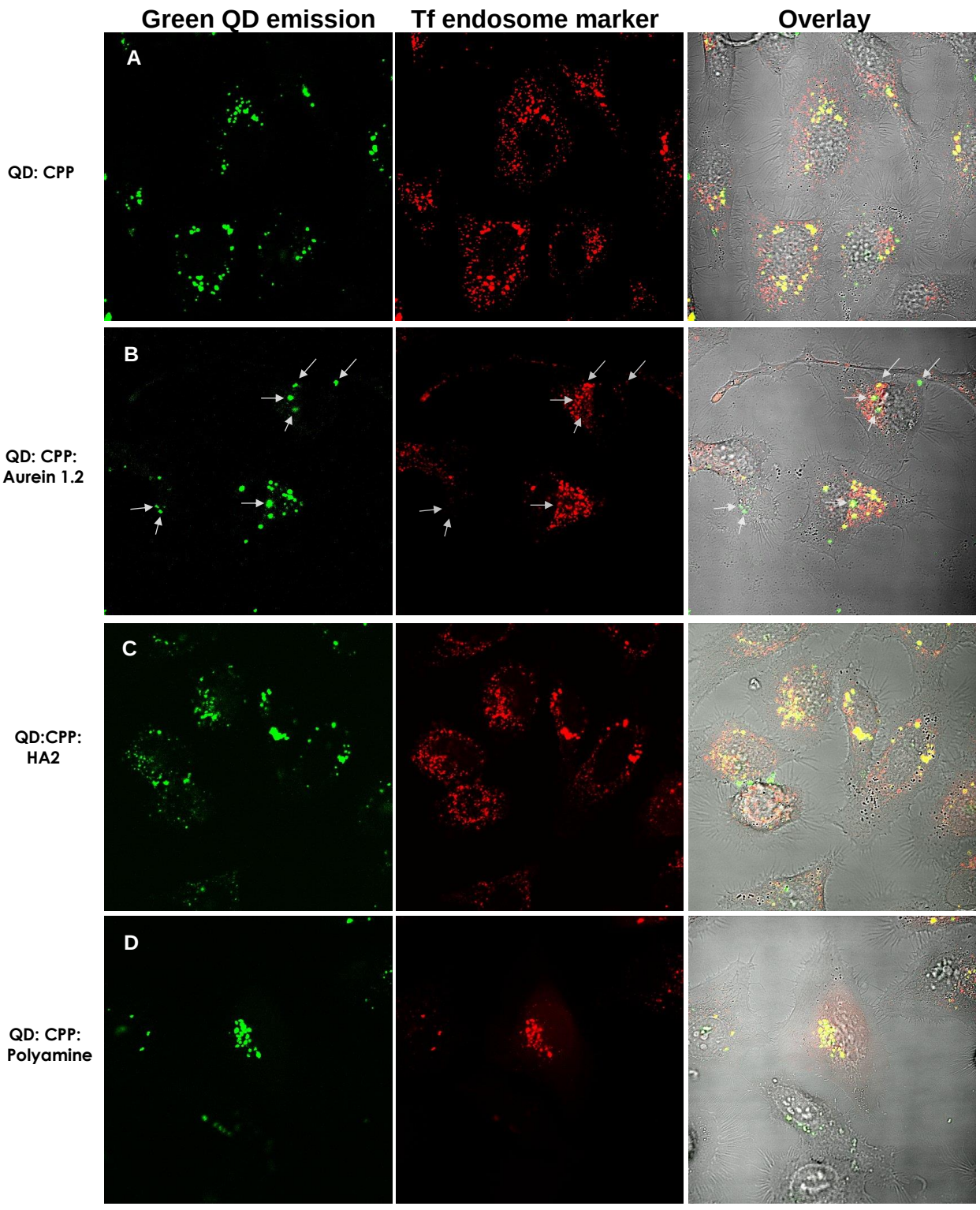

Figure 3.9. Cellular internalization of CL4 coated green QD:CPP: EE assemblies and colocalization at 12 h within endosomes.

Figure 3.9. **(continuation of description).** HeLa cells were incubated for 1.5 h at 37 ºC with 539 nm (green emission) QD:CPP (1:10) and QD:CPP:EE (1:10:20) assemblies at final QD concentrations of 50 nM and co-incubated with 25 μg/mL of endosome marker Texas red-Tf. for 1.5 h at 37ºC. After washing three times with 1X PBS (pH = 7.4), cells were replenished with fresh medium (with FBS), and imaged with a Zeiss LSM 710 Confocal microscope.
Endosome marker Texas red-Tf: excitation 561 nm, detection 580-620 nm; green QD: excitation 405 nm, detection 510-560 nm. **Panel A**, QD:CPP (1:10); **Panel B**, QD:CPP: Aurein 1.2 (1:10:20); **Panel C**, QD:CPP: HA2 (1:10:20); **Panel D**, QD:CPP: polyamine (1:10:20). White arrows in **Panel B** indicate areas of endosomal escape. **Left**: QD fluorescence (green), **Middle**: Texas-red-Tf (red), **Right**: Overlay of phase contrast DIC image (gray), QD fluorescence (green), Texas-red-Tf (red) and colocalization (yellow).

Figure 3.9, Panel A, shows the expected intracellular delivery (green emission) and endosomal entrapment (red emission) of QD:CPP conjugates (1:10). The merged image in **panel A**, shows almost complete colocalization (yellow signal) of QD:CPP and the presence of more endosomes (red punctae) than trapped QD probes. QD:CPP: HA2 (**Panel C**) and QD:CPP: Polyamine (**Panel D**) showed a similar degree of internalization and colocalization with endosomes, although with different punctate distribution.

In contrast, at 12 h, QD:CPP: Aurein 1.2 conjugates (**Panel B**) showed that although there was a high degree of colocalization (yellow signal) not all the internalized conjugates (green channel) were trapped inside endocytic vesicles (red channel). The pointed arrows indicate the location of internalized QD:CPP: Aurein 1.2 complexes that are not trapped inside endosomes, which might be an indication of endosomal escape, or a simultaneous clathrin-independent endocytic mechanism.

Unfortunately, we could not follow the progress of this experiment with the Aurein 1.2 peptide at 36 h incubation due to contamination.

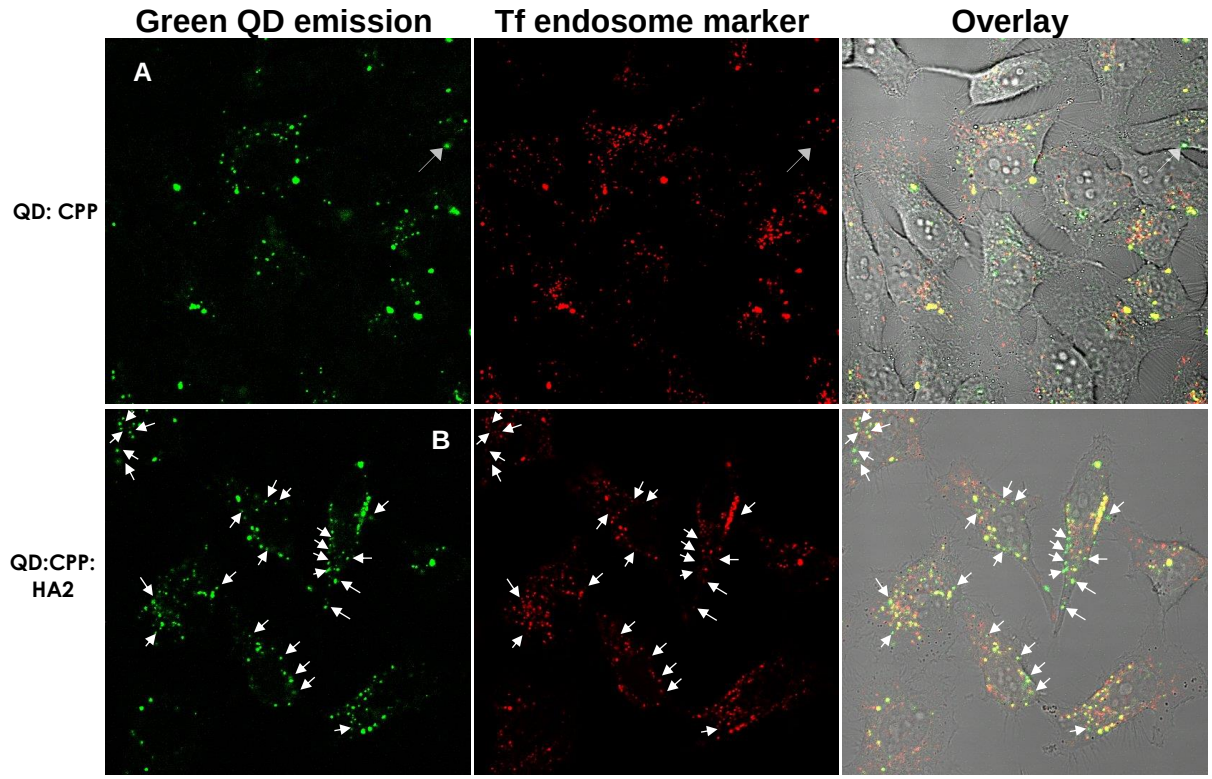

Figure 3.10. Cellular internalization of CL4 coated green QD:CPP: HA2 assemblies and colocalization at 36 h within endosomes. HeLa cells were incubated for 1.5 h at 37 ºC with 539 nm (green emission) QD:CPP (1:10) and QD:CPP:HA2 (1:10:20) assemblies at final QD concentrations of 50 nM and co-incubated with 25 μg/mL of endosome marker Texas red-Tf. for 1.5 h at 37 ºC. After washing three times with 1X PBS (pH = 7.4), cells were replenished with fresh medium (with FBS), and imaged with a Zeiss LSM 710 Confocal microscope. Endosome marker Texas red-Tf: excitation 561 nm, detection 580-620 nm; green QD: excitation 405 nm, detection 510-560 nm. **Panel A**, QD:CPP (1:10); **Panel B**, QD:CPP: HA 2 (1:10:20). White arrows indicate areas of endosomal escape. **Left**: QD fluorescence (green), **Middle**: Texas-red-Tf (red), **Right**: Overlay of phase contrast DIC image (gray), QD fluorescence (green), Texas-red-Tf (red) and colocalization (yellow).

Figure 3.10 shows that at 36 h of incubation, most of QD:CPP (**Panel A**) are colocalized (yellow signal) within endosomes. Interestingly, QD:CPP: HA2 conjugates (**Panel B**) show a more disperse punctate distribution and lesser degree of colocalization as indicated by the pointed arrows. Panel A is shown for comparison. Notably, cells incubated with HA2 conjugates are healthy.

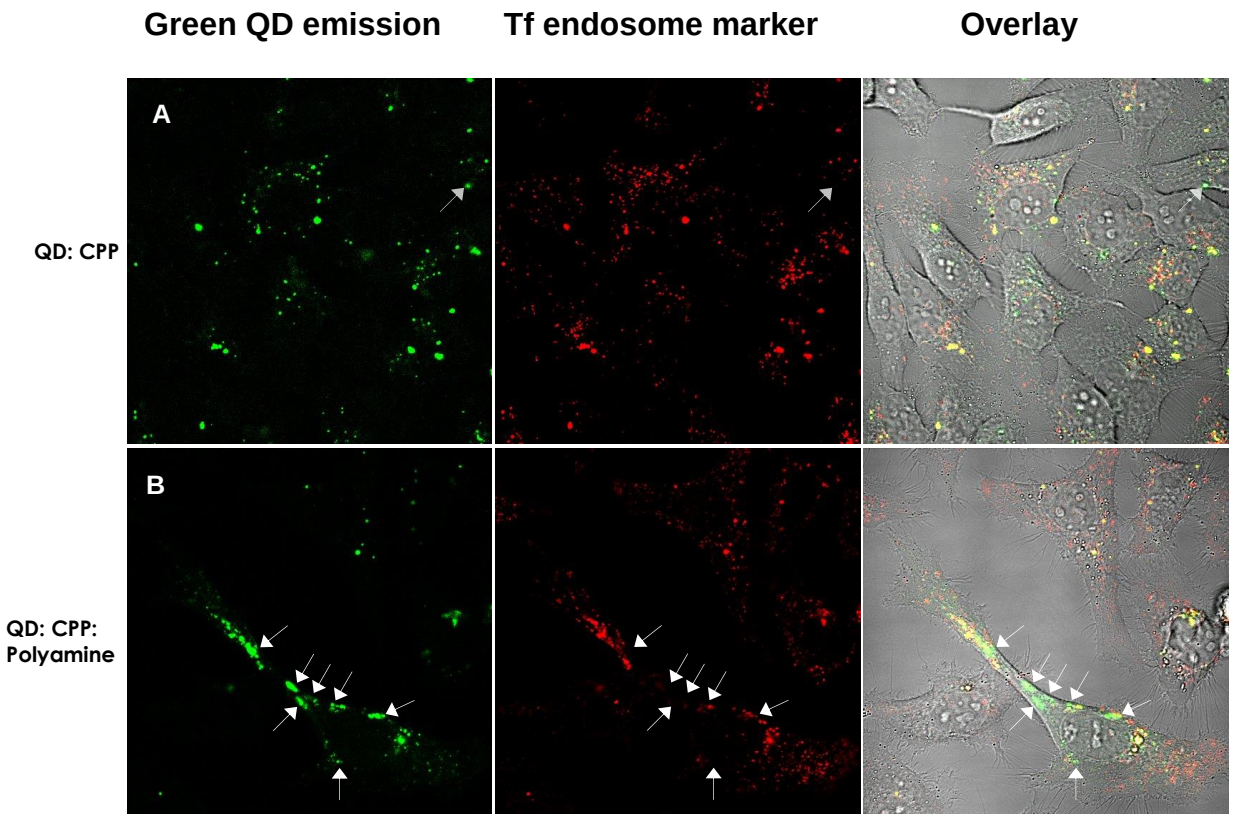

Figure 3.11. Cellular internalization of CL4 coated green QD:CPP: polyamine assemblies and colocalization at 36 h within endosomes. HeLa cells were incubated for 1.5 h at 37 ^{o}C with 539 nm (green emission) QD:CPP (1:10) and QD:CPP:EE (1:10:20) assemblies at final QD concentrations of 50 nM and co-incubated with 25 μg/mL of endosome marker Texas red-Tf. for 1.5 h at 37^{o}C. After washing three times with 1X PBS (pH = 7.4), cells were replenished with fresh medium (with FBS), and imaged with a Zeiss LSM 710 Confocal microscope. Endosome marker Texas red-Tf: excitation 561 nm, detection 580-620 nm; green QD: excitation 405 nm, detection 510-560 nm. **Panel A**, QD:CPP (1:10); **Panel B**, QD:CPP: polyamine (1:10:20). White arrows indicate areas of endosomal escape. **Left**: QD fluorescence (green), **Middle**: Texas-red-Tf (red), **Right**: Overlay of phase contrast DIC image (gray), QD fluorescence (green), Texas-red-Tf (red) and colocalization (yellow).

QD:CPP: Polyamine conjugates (Figure 3.11, Panel B) showed a more disperse punctate cytosolic distribution at 36 h incubation compared to 12 h. Also, micrographs in panel B clearly show that a high amount of QD conjugates (green channel) are not colocalized with endosomes (red channel) as indicated by the white arrows.

3.11 Conclusion on colocalization experiments.

In conclusion, we tested three different peptides and one protein for their potential endosomal escape abilities when conjugated to green QD:CPP complexes. These conjugates where QD:CPP: Aurein 1.2, QD:CPP: HA2, QD:CPP: polyamine, and QD: palmitoyl. As a control, we employed QD:CPP to have a baseline to compare with.

Upon co-incubation of green QD:CPP, QD: palmitoyl and QD:CPP: EE assemblies with Red-Tf, confocal microscopy studies showed that all complexes were cellularly internalized, except for QD: Palmitoyl under our conditions. The rest of the conjugates were internalized within 1.5 -2 h by live-cells and showed a punctate distribution throughout the cytoplasm at 12 and 36h. QD:CPP, QD:CPP: HA2 and QD:CPP:Polyamine were completely colocalized with endosomes at 12 hours, however QD:CPP:Aurein 1.2 complexes were not entirely trapped inside endosomes (Figure 3.9, Panel B).

At 36 h there was a significant decrease of colocalization of conjugates QD:CPP: HA2 and QD:CPP: Polyamine (green) with Tf-endosome marker (red) as showed in Figures 3.10 and 3.11 respectively, while most of the QD:CPP conjugates (control) remained trapped (yellow spots).

The above results suggest that QD:CPP:Aurein 1.2 may begin to escape the endosomes at less than 12 h, while it may take longer for QD:CPP:HA2 and QD:CPP:Polyamine to begin to escape the endocytic vesicles.

We cannot assure if the complexes that reached the cytosol (green punctae at 12 h with Aurein 1.2 and 36 h with HA2 and polyamine) remained punctate rather than diffuse, due to a slow diffusion rate, adhesion to ruptured endosome membranes, aggregation on the cytoskeleton actin tubule system, or due to further re-entrapment in a secondary type of vesicles (autophagosomes). Precipitation is less likely to be the cause of the observed punctate pattern as our QD conjugates are coated with a zwitterionic ligand that keeps their solubility at endosomal and cytosolic pH.

Although colocalization experiments provide useful data on the internalization path of nanoparticles, the information remains qualitative, which makes it ideal for preliminary studies, hence the need to have a more reliable method to detect and quantify the amount of QD conjugates that reach the cytosol. Correspondingly, in the next section we describe our results on a ratiometric FRET strategy to study the escape ability of Aurein 1.2, HA2 and polyamine peptide – QD conjugates in live cells.

3.12 Ratiometric FRET studies to detect and quantify cytosolic delivery of QD:CPP: endosomal escape bioconjugates (QD:CPP:EE).

As depicted in Figure 3.12 (below), to be able to detect and measure the amount of endocytosed QD:CPP:EE conjugates that reaches the cytosol, we added a rhodamine FRET acceptor ligand capable of absorbing at the emission wavelength of our green QD donor. The disulfide bond cleavage of the rhodamine acceptor from the QD surface is caused by the reductive cytosolic environment, which can only be reached after endosomal escape of our ratiometric probe.

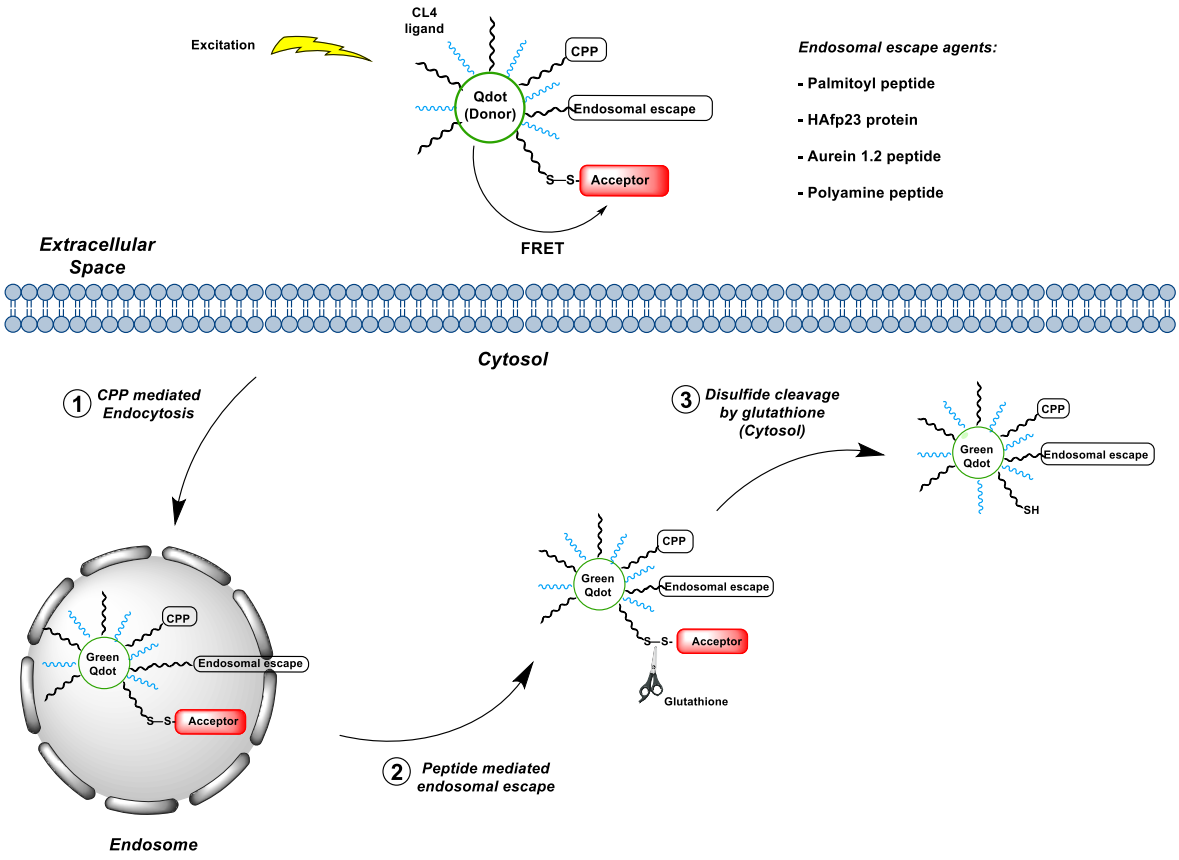

Figure 3.12. Aim and scope of this work.

Also, in FRET-based experiments there was no need to coincubate with the endosomal marker (transferrin) anymore, as our colocalization experiments (in section 3.10) indicated that most internalized conjugates are entrapped inside endosomes first.

3.13 Intracellular delivery of QD:CPP: Rhodamine- ratiometric map

Thus, live cells were incubated with QD:CPP:EE: rhodamine assemblies. After delivery optimization conditions, 1:12:25:12 at a 50μM final concentration, was the optimal ratio found to: 1) Facilitate intracellular deliver by using 12 CPPs per QD, 2) to microscopically detect and measure a change of red rhodamine/green QD emission ratios upon dissociation of the rhodamine FRET acceptor from the QD:CPP:EE: rhodamine bioconjugate.

Because our green QDs were partly quenched by the FRET to acceptor ligands (12 rhodamines per QD), we can monitor the attenuated green QD emission, thus, in a control experiment (Figure 3.13), after a 36-h incubation period with HeLa cells, confocal images showed that QD:CPP: rhodamine conjugates (1:12:12 ratio), were intracellularly delivered (donor channel). A laser energy of 405 nm was used to selectively excite green QDs but not the rhodamine acceptor, therefore, any red emission is due to excitation of rhodamine by the energy transferred from the QD donor.

The CPP-facilitated delivery of these complexes took place after 1.5 – 2.0 h incubation time at 37 ^{o}C the red channel in Figure 3.13, shows the red emission of the rhodamine FRET acceptor as a result of energy transfer from the QD donor.

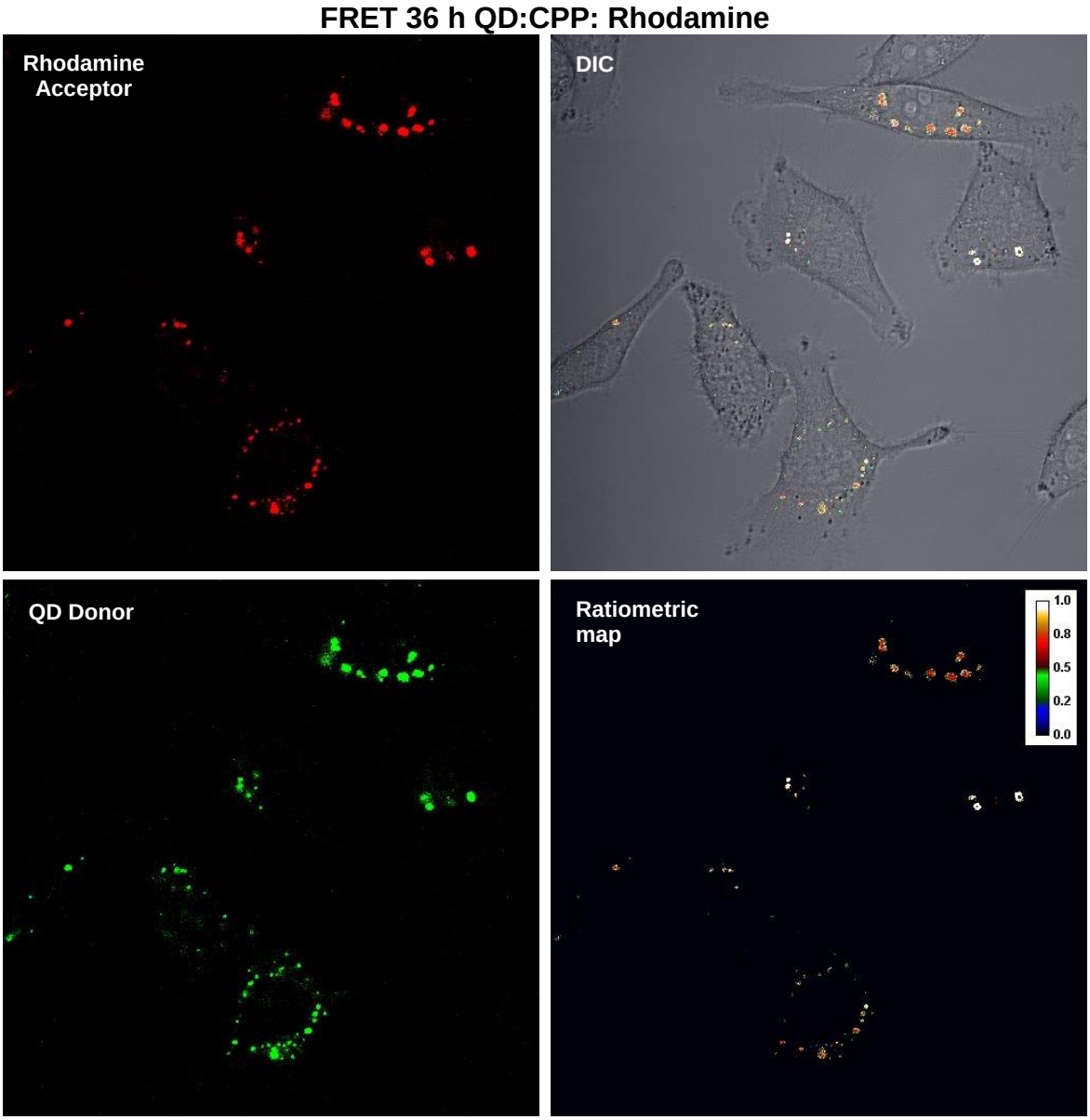

Figure 3.13 Cellular internalization of CL4 coated green QD:CPP: rhodamine assemblies at 36 h. HeLa cells were incubated for 1.5 h at 37ºC with QD:CPP: rhodamine (1:12:12) assemblies at final QD concentrations of 50 nM. After washing three times with 1X PBS (pH = 7.4), cells were replenished with fresh medium (with FBS), and imaged with a Zeiss LSM 710. Confocal Microscope. Rhodamine: excitation 405 nm, detection 570-640 nm; green QD: excitation 405 nm, detection 500-545 nm. **Top left**: Rhodamine FRET acceptor emission (red), **Top right**: Overlay of phase contrast DIC and ratiometric map (gray), **Bottom left**: QD FRET-donor fluorescence (green), **Bottom right**: Ratiometric map exhibits calculated intensity numbers (red/green) fitted into a scale ranging from 0.0 to 1.0. Endosomal regions (white, yellow and red areas) exhibit red/green ratios close to 1.0. Areas corresponding to QDs that could reach the cytosol (upon endosomal escape) exhibit a red/green ratio close to 0.0 (green and blue areas).

A ratiometric scale (red/green) (from 0.0 to 1.0) was generated with a software. The red/green signal for the unsaturated part of each cell (in a population of at least 10 cells) was quantified to give the corresponding intensity numbers, which were changed with a program to fit in a scale that goes from 0.0 (blue) to 0.2 (green), to 0.8 (red) to 1.0 (white). Changing calculated intensity numbers (red/green) into ratiometric maps on live-cell images, would allow to quantify and assign endosomal regions with different ratio than regions where QDs had escaped.

The observed punctate pattern of the cellularly internalized QD:CPP: rhodamine probes, and the calculated red/green ratios (from 0.8 to 1.0) depicted in the ratiometric map by artificially colored red and white areas, correlates well with the observation from qualitative colocalization studies, that most of the QD:CPP complexes are engulfed in endocytic vesicles and remain trapped at 36 h (Figure 3.13), because a measured red/green ratio in the 0.8-1.0 range, is an indication that most of the red rhodamine FRET acceptors are still associated through a disulfide bond to their green QD fret donor and no disulfide bond has been cleaved by cytosolic glutathione.

Finally, the differential interference contrast (DIC) image shows the overlay of the analyzed HeLa cells with their ratiometric map. DIC also shows the integrity of the HeLa cells.

3.14 FRET studies QD:CPP: Aurein 1.2: rhodamine-ratiometric map

Bioconjugates in a 1:12:25:12 ratio was incubated with HeLa cells for 1.5- 2 h to allow their cellular uptake. Cells were treated as described in section 2.3.10 to 2.3.13. Confocal images taken at 36 h exhibit that the QD:CPP: Aurein1.2: Rhodamine assemblies were efficiently internalized by HeLa cells (green channel).

Although the cytosolic pattern is punctate, it is more disperse throughout the cytosol when compared to the same QD conjugate without Aurein 1.2 (Figure 3.14). The acceptor channel shows the emission of the rhodamine ligands engaged in FRET.

The artificial colors of the ratiometric map show a mix of blue and green punctae, which means that the measured red/green ratios fall below 0.5 (green areas) and below 0.2 (blue areas). For red/green ratios to be below 0.5, means that the measured green intensity of the QD donor is larger than the red emission intensity of the rhodamine acceptor, which suggests that the Aurein 1.2 peptide may have caused the release of QD:CPP: Aurein1.2-Rhodamine bioconjugates from the endosomes to the cytosol. The increase in green QD luminescence (therefore the decrease in red/green ratio) indicates that several rhodamine ligands have disengaged from the QD surface because of disulfide bond reduction by cytosolic glutathione.

FRET 36 h QD:CPP: Aurein 1.2: Rhodamine

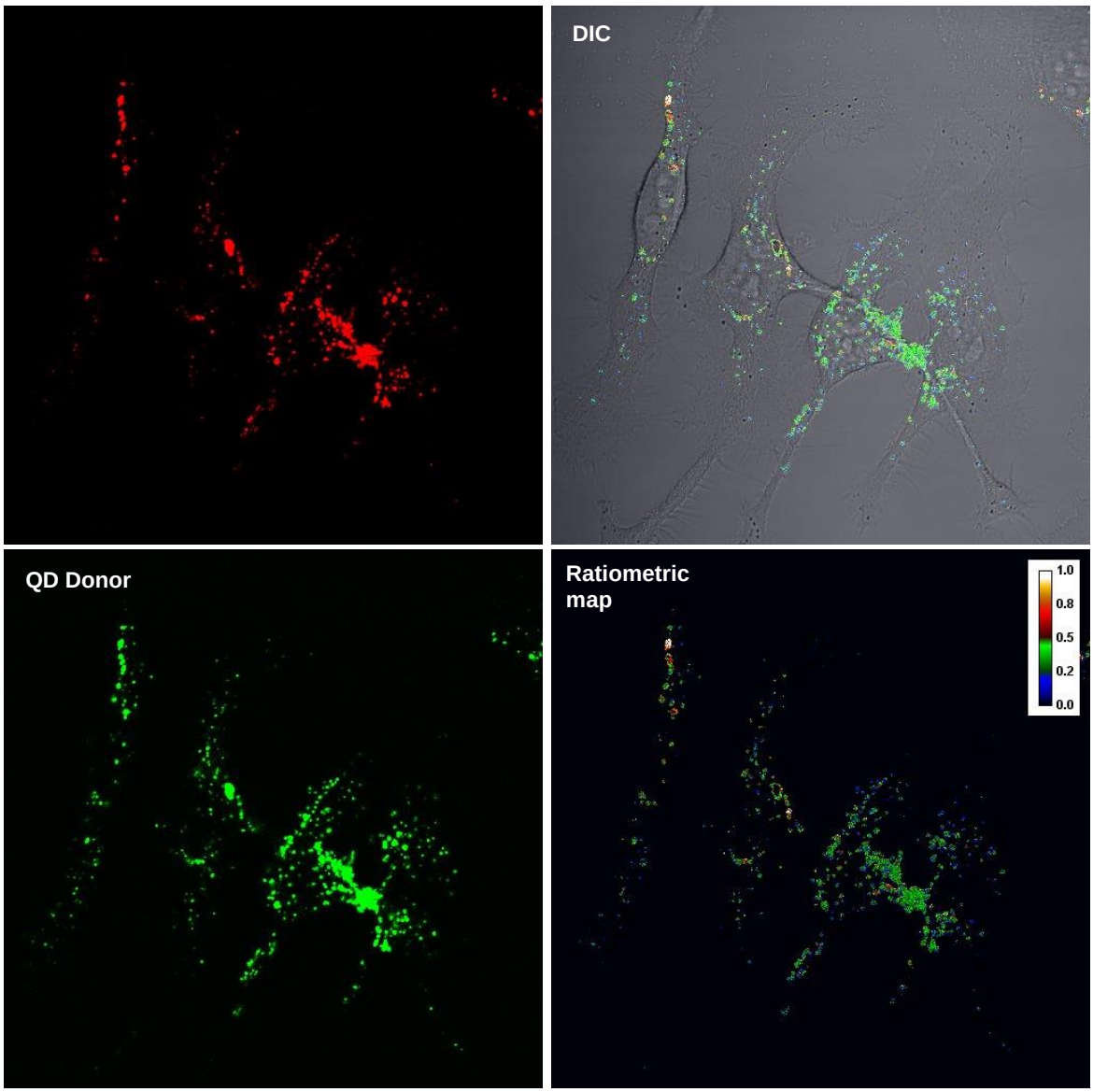

Figure 3.14. Cellular internalization of CL4 coated green QD:CPP: Rhodamine: Aurein 1.2 assemblies at 36 h. HeLa cells were incubated for 1.5 h at 37 ºC with QD:CPP: Rhodamine: Aurein 1.2 (1:12:25:12) assemblies at final QD concentrations of 50 nM. After washing three times with 1X PBS (pH = 7.4), cells were replenished with fresh medium (with FBS), and imaged with a Zeiss LSM 710. Confocal Microscope. Rhodamine: excitation 405 nm, detection 570-640 nm; green QD: excitation 405 nm, detection 500-545 nm. **Top left**: Rhodamine FRET acceptor emission (red), **Top right**: Overlay of phase contrast DIC and ratiometric map (gray), **Bottom left**: QD FRET-donor fluorescence (green), **Bottom right**: Ratiometric map exhibits calculated intensity numbers (red/green) fitted into a scale ranging from 0.0 to 1.0. Endosomal regions (white, yellow and red areas) exhibit red/green ratios close to 1.0. Areas corresponding to QDs that could reach the cytosol (upon endosomal escape) exhibit a red/green ratio close to 0.0 (green and blue areas).

3.15 FRET studies QD:CPP: HA2: Rhodamine- ratiometric map

Notably, QD:CPP: HA2: Rhodamine assemblies showed a very different punctate pattern, from the Aurein and polyamine conjugate analogs, upon their endocytosis by Hela cells. The micrographs in Figure 3.15, exhibit what appears to be a punctate pattern of minute endocytic vesicles. We have observed this several times for cellularly internalized QD conjugates loaded with the HA2 protein (see colocalization images in figures 2.10, 3.9 panel C, and 3.19 panel B).

The ratiometric map shows mostly a mix of blue and green punctate areas (red/green ratios from 0.5 to 0.0) and a few isolated red areas (red/green ratio ~0.8). These results suggest that some of the QD:CPP:HA2:rhodamine conjugates remain trapped (red punctae in ratiometric map). The mixture of red, green and blue area exhibited in the ratiometric map suggests that the HA2 protein facilitates endosomal escape, nevertheless, not as efficiently as the Aurein 1.2 peptide.

We were expecting this protein to be more endosomolytic as colocalization studies showed that at 36 h a large number of intracellularly delivered QD:CPP:HA2 conjugates were not colocalized with Tf-stained endosomes in Hela cells, making it appear as if they had reached the cytosol.

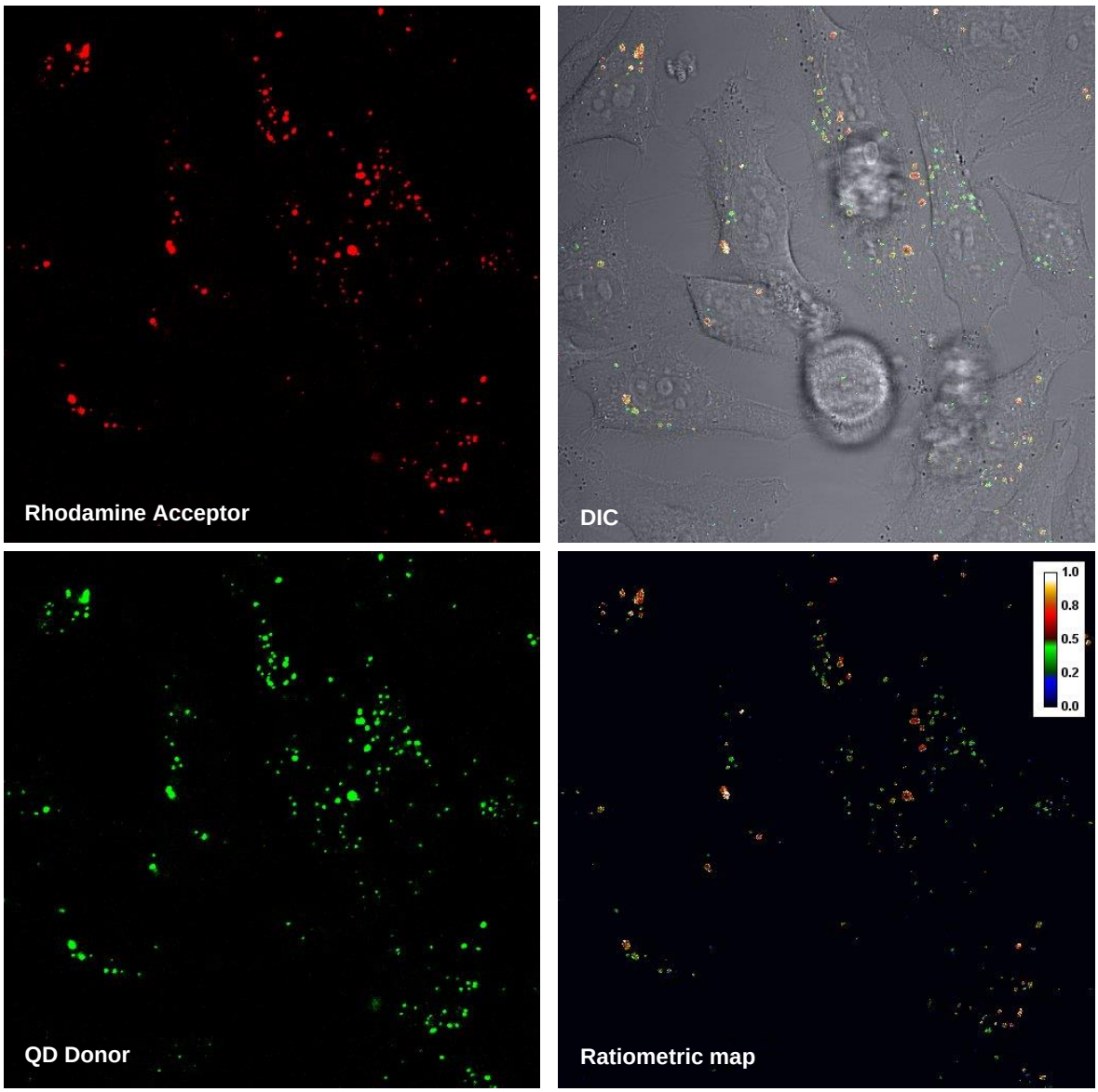

Figure 3.15. Cellular internalization of CL4 coated green QD:CPP: Rhodamine: HA2 assemblies at 36 h. HeLa cells were incubated for 1.5 h at 37 ºC with QD:CPP: Rhodamine: HA2 (1:12:25:12) assemblies at final QD concentrations of 50 nM. After washing three times with 1X PBS (pH = 7.4), cells were replenished with fresh medium (with FBS), and imaged with a Zeiss LSM 710

Figure 3.15 (continued description) Confocal Microscope. Rhodamine: excitation 405 nm, detection 570-640 nm; green QD: excitation 405 nm, detection 500-545 nm. **Top left**: Rhodamine FRET acceptor emission (red), **Top right**: Overlay of phase contrast DIC and ratiometric map (gray), **Bottom left**: QD FRET-donor fluorescence (green), **Bottom right**: Ratiometric map exhibits calculated intensity numbers (red/green) fitted into a scale ranging from 0.0 to 1.0. Endosomal regions (white, yellow and red areas) exhibit red/green ratios close to 1.0. Areas corresponding to QDs that could reach the cytosol (upon endosomal escape) exhibit a red/green ratio close to 0.0 (green and blue areas).

3.16 FRET studies QD:CPP: Polyamine: Rhodamine- ratiometric map

The ratiometric map of HeLa cells incubated with QD: CPP: polyamine:rhodamine conjugates at 36 h, shows a mixed blue and green punctate pattern, which points out areas where the measured red/green ratio ranks from 0.5 to 0.0.

This finding suggests that our polyamine peptide facilitates the endosomal escape of QD complexes. This outcome agrees with our qualitative colocalization experiments under the same culture conditions with QD: CPP: polyamine conjugates coincubated with red-Tf (figure xxx) where we observe a significant number of green punctae (due to probe emission) that was not colocalized with endosomes.

Markedly, cells remained healthy after the 36-h incubation period with polyamine as shown in the DIC micrograph (Figure 3.16).

FRET 36 h QD:CPP: Polyamine: Rhodamine

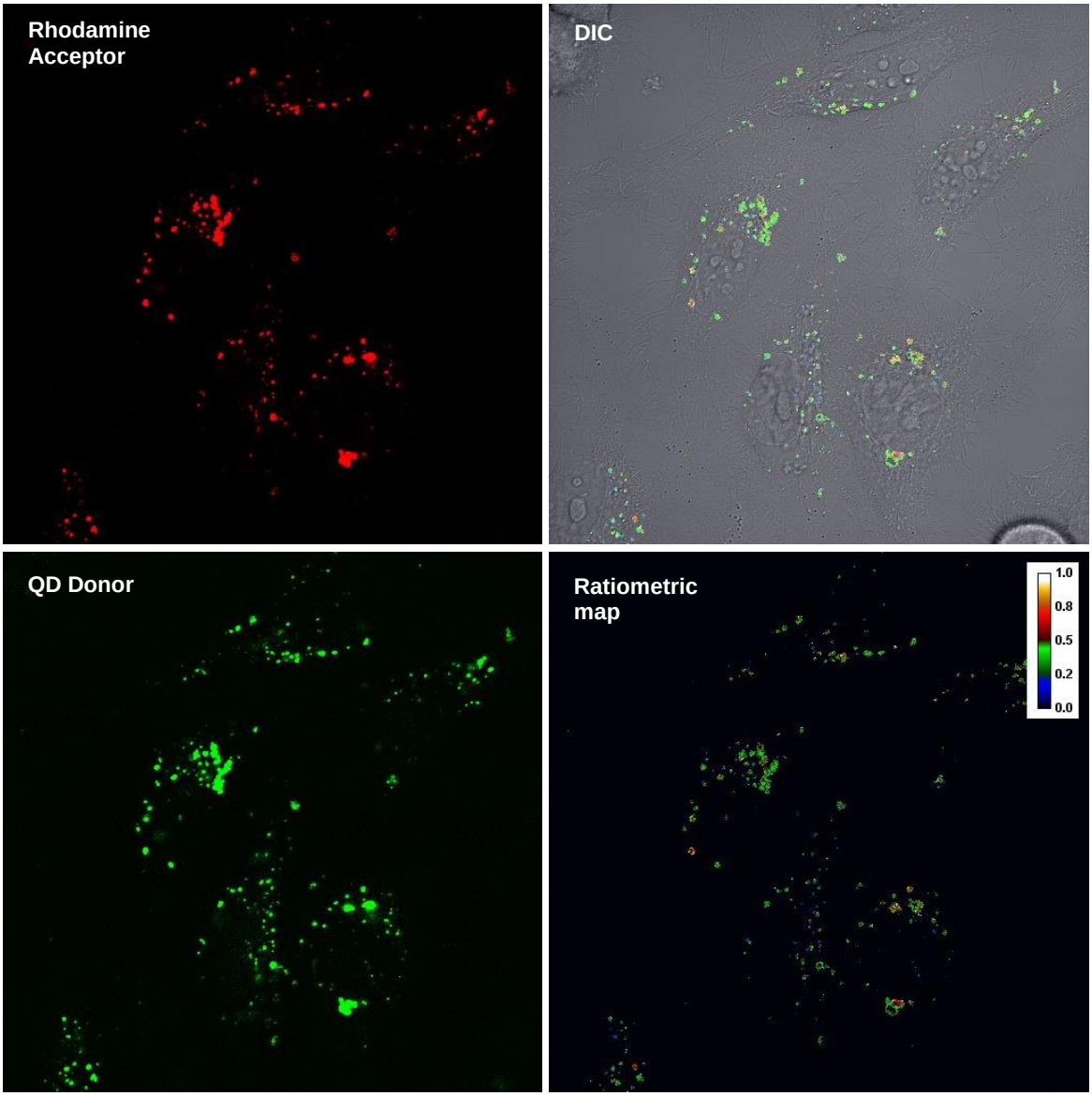

Figure 3.16. Cellular internalization of CL4 coated green QD:CPP: Rhodamine: polyamine assemblies at 36 h. HeLa cells were incubated for 1.5 h at 37ºC with QD:CPP: Rhodamine: polyamine (1:12:25:12) assemblies at final QD concentrations of 50 nM. After washing three times with 1X PBS (pH = 7.4), cells were replenished with fresh medium (with FBS), and imaged with a Zeiss LSM 710. Confocal Microscope. Rhodamine: excitation 405 nm, detection 570-640 nm; green QD: excitation 405 nm, detection 500-545 nm. **Top left**: Rhodamine FRET acceptor emission (red), **Top right**: Overlay of phase contrast DIC and ratiometric map (gray), **Bottom left**: QD FRET-donor fluorescence (green), **Bottom right**: Ratiometric map exhibits calculated intensity numbers (red/green) fitted into a scale ranging from 0.0 to 1.0. Endosomal regions (white, yellow and red areas) exhibit red/green ratios close to 1.0. Areas corresponding to QDs that could reach the cytosol (upon endosomal escape) exhibit a red/green ratio close to 0.0 (green and blue areas).

3.17 Whole cell average red/ green intensity ratiometric analysis

We also analyzed whole cell average red/ green intensity ratios for sets of at least ten cells (Figure 3.17).

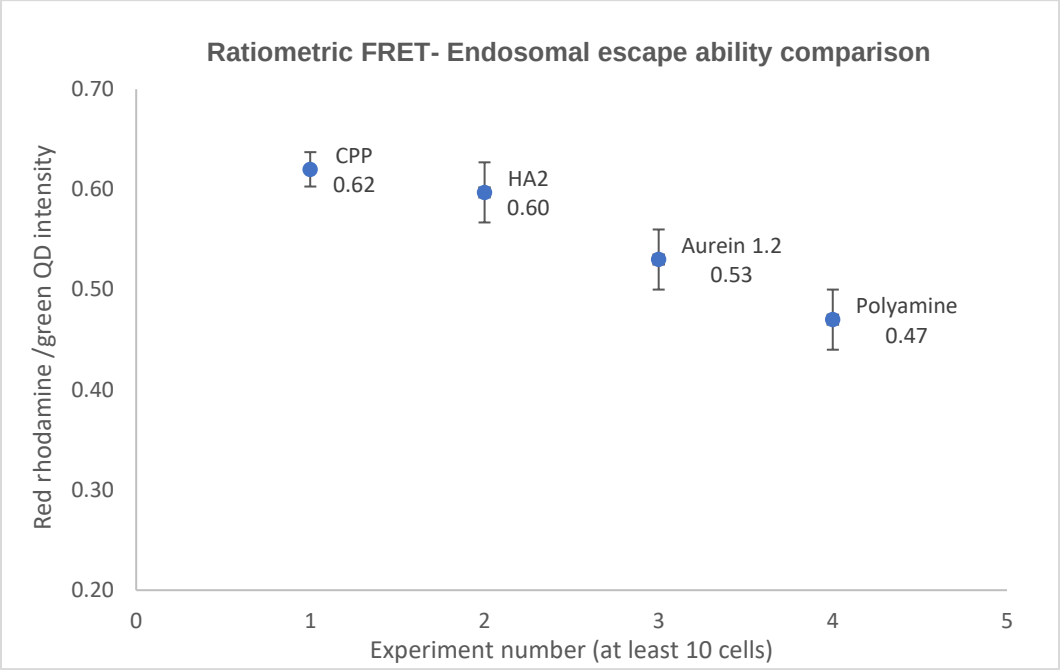

Figure 3.17. Whole cell averages of red/green intensity ratios after 12 hours of QD:CPP: rhodamine: EE cellular uptake. (≤10 cells, error bar: S.D.). From left to right, red/green ratios of internalized CL4 coated green QD:CPP: rhodamine (1:12:25) complex as the control, QD:CPP: rhodamine: HA2 (1:12:25:12), QD:CPP: rhodamine: Aurein 1.2 (1:12:25:12) and QD:CPP: rhodamine: polyamine (1:12:25:12) complexes. HeLa cells were incubated for 1.5 h at 37oC with the above complexes at final QD concentrations of 50 nM. After washing three times with 1X PBS (pH = 7.4), cells were replenished with fresh medium (with FBS), and imaged with a Zeiss LSM 710. Confocal Microscope. Rhodamine: excitation 405 nm, detection 570-640 nm; green QD: excitation 405 nm, detection 500-545 nm.

The QD: CPP: rhodamine complex red/green ratio (0.62) after intracellular uptake was used as the baseline. The graph above indicates that after 12 h, there is a very negligible 3% decrease in red/green ratio (0.60) for the QD:CPP: rhodamine: HA2, which indicated

that this complex remains trapped inside the endosomes and therefore, HA2 does not enhance escape after 12 h. The complex QD:CPP: rhodamine: Aurein 1.2 red/green ratio is equal to 0.53, therefore, 15% lower than the control QD:CPP: rhodamine, indicating that after 12 h there is some endosomal escape. Finally, the complex QD: CPP: rhodamine: polyamine red/green ratio is the lowest (0.47), and 24 % lower than the QD: CPP: rhodamine control, which indicates that our polyamine peptide has a better ability to cause endosomal escape after 12 h when compared to HA2, or Aurein 1.2.

The whole cell average ratios plotted in figure 3.17 show that Aurein 1.2 possess endosomolytic activity and that polyamine is better.

3.18 Conclusion

In the search for an endosomolytic peptide, and after extensive literature search, I learned that the Aurein 1.2 peptide had the ability to enhance endosomal escape of polycationic proteins (+36 GFP). Since Aurein 1.2 is a short peptide, I adapted its sequence to our needs, thus I synthesized a version of the Aurein 1.2 peptide that could be assembled on the surface of QDs via affinity coordination.

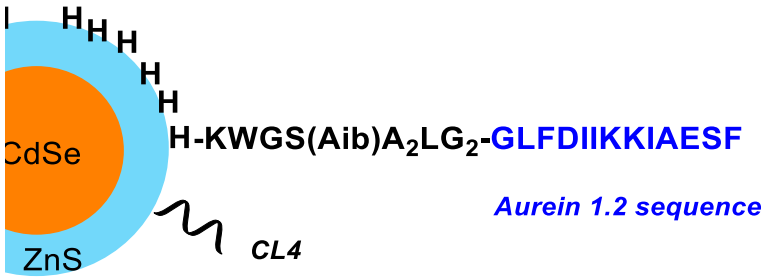

Figure 3.17. A reported Aurein 1.2 peptide was adapted to coordinate on the QD surface.

Hemagglutinin is a class I viral fusion protein that catalyzes the membrane fusion process during cellular entry and infection. Since the hemagglutinin fusion peptide (HAfp) plays a central role in the fusion of viral and endosomal membranes,[132] I decided to test it in our CPP-facilitated QD delivery system, with the hypothesis that by coordinating several proteins around a QD, we might be able to render endosomolytic QDs. This protein was provided with a polyhistidine tag by Lorieau's group.

It also known that certain polyeneimines possess high endosomolytic activity due to their high amine content. Therefore, I designed a peptide-based polyamine that could be easily synthesized by solid phase peptide synthesis, in the least number of steps, with the highest possible number of amine groups, a polyhistidine tag for non-covalent coordination to QDs, with a piperazine ring to provide some rigidity (and two tertiary amines), diglycines to provide a hinge, and four *N*-terminal spermine branches. This peptide was synthesized by Mona Hoseini Soflaee.

A palmitoyl peptide reported to facilitate the intracellular delivery and endosomal escape of QDs (ref) was also tested. Colocalization studies showed that cellularly internalized QD:CPP conjugates remained trapped inside the endosomes for 36 hours.

Because of the lack of methods to quantify endosomal escape, we worked on the development of a FRET-based strategy to microscopically determine whether QDs resided in the endosomes or the cytoplasm. We turned our attention to a QD FRET donor-Rhodamine FRET acceptor system to generate a ratiometric signal (red/green).

Both, colocalization studies and our FRET-based ratiometric method, support the idea that the polyamine and the Aurein 1.2 peptide respectively, enhance the endosomal

escape of QDs. Also, from colocalization studies, and from the intracellular fluorescence pattern, it seems that the HA2 protein possess some endosomolytic activity (when compared to CPP only) however, ratiometric analysis does not support this idea as strongly.

Also, we demonstrated the usefulness of ratiometric maps as they can detect areas of high escape activity (where red/green ratios are close to 0.0) and areas of endosomal entrapment (where red /green ratios are close to 1.0). This is useful, especially in cases were diffusion is not observed and punctate patterns are detected.

Overall, the ratiometric evidence (red/green ratios) from whole cell averages as well as ratiometric maps, along with colocalization experiments show that while the HA2 protein employed in this thesis (HAfp23, see sequence in section 2.3.8) has a poor ability to cause endosomal escape, the antimicrobial membrane peptide Aurein 1.2 and our designed polyamine peptide are more effective, with polyamine being the best.

3.19 Experimental methods.

3.19. 1 Materials and instrumentation. All solvents and chemicals were purchased from commercial sources and used without further purification: DMF (reagent grade) from Chem-impex, CH_2Cl_2, MeOH and diethyl ether from Sigma- Aldrich, TFA and CH_3CN (HPLC grade) from Fisher. Water was purified using a Millipore Milli-Q water purification system. DIEA (N,N-diisopropylethylamine), acetic anhydride, piperidine, ß-mercaptoethanol, 1,2- Ethanedithiol, thioanisole, phenol, and anisole from Alfa Aesar. 3- [(2-Aminoethyl)dithio]propionic acid was purchased from Toronto Research Chemicals. HBTU (O-(Benzotriazol-1-yl)-N,N,N',N'-tetramethyluronium hexafluorophosphate) , Oxyme (Ethyl Isonitrosocyanoacetate), palmitic acid, TIPS-H (triisopropylsilane), D-Biotin, TCEP (Tris-(carboxyethyl)phosphine hydrochloride, Glutathione and Rhodamine B isothiocyanate (mixture of 5 and 6 isomers) from Chem-impex international, MALDI matrix HCCA (α-Cyano-4-hydroxycinnamic acid) and chloroquine phosphate from Sigma-Aldrich. Fmoc-protected natural and artificial amino acids Fmoc-L-Dap(Mtt)-OH (Dap = diaminopropionic), Fmoc-L-Lys(Mtt)-OH, Fmoc-L-Aib(Mtt)-OH (Aib= alpha-aminoisobutyric acid), Fmoc-$(PEG)_2$-Suc-OH, Fmoc-$(PEG)_2$-DIG-OH and Chlorotrityl chloride resin from Chem-impex international. Rink amide resin AM Resin LL, 100-200 mesh (substitution = 0.35 mmol/g) from Novabiochem. Desalting buffer TEAA (triethylamine acetate) 2.0 M pH = 7.0 from Glen Research.

Peptides were purified by reverse phase preparative HPLC in a Shimadzu LC-20 AT equipped with a UV-Vis dual detector model SPD-20A and a semi-prep Aeris column (10 µm, 90 Å, 250 × 10 mm) at a flow rate of 5 mL/min employing Acetonitrile / Water with 0.1% TFA as a mobile phase. Injections were simultaneously monitored at 220 and 254

nm. Peptides were desalted with Oligonucleotide Purification Cartridge (OPC, Applied Biosystems) before conjugation to QDs, freeze-dried (Labconco) and stored as a pellet at -20 °C. Peptide masses were obtained by MALDI-TOF 4700 Proteomics Analyzer (Applied Biosystems). Small molecules masses were obtained by electrospray ionization on a LC/MS APCI quadrupole ion trap LC mass spectrometer (Thermo Finnigan LCQ) and their chemical structures were confirmed by NMR recorded on a Bruker Avance DRX 400 or 500 MHz NMR spectrometer. CdSe–ZnS core–shell QDs with emission maxima centered at 539 nm (CL4 coated) and 566 nm (DHLA coated) were synthesized by Snee's group. 539 nm QDs capped with CL4 ligands were used for CPP-mediated delivery. 566 nm QDs capped with DHLA ligands were used for spectroscopic studies.

UV/vis absorbance spectra were measured using a Varian Cary 300 Bio UV/vis spectrophotometer, and fluorescence emission spectra were obtained using a custom-designed Horiba Jobin Yvon FluoroLog spectrophotometer.

HeLa cells (CCL-2) were purchased from American Type Culture Collection. Dulbecco's modified eagle medium (DMEM, 10-014 CV) and 0.25% trypsin/2.21 mM EDTA were purchased from Corning Cellgro® Micropipette preparation glass bottom culture dishes (P50G-1.5-14-F) were purchased from Matek Corporation (Ashlan, MA). XenoworksTM Microinjection Systems, P-1000 pipette puller and borosilicate glass tubes (BF100-78-10) were used for microinjections (Sutter Instruments, Novato, CA). Fluorescence images were acquired using an epi-fluorescence microscope (Axiovert 200, equipped with AxioCam MRm CCD camera and Axiovision software (V 4.6.2.0), Carl Zeiss, inc) modified with a UV LED emitting at 365 nm (UV-LED-365, Prizmatix, Ltd). All images were obtained

with a 63x/1.25 N.A. EC Plan Neofluar oil-immersion objective (Carl Zeiss, Inc) and G365 excitation filter.

3.19.2 General protocol for solid phase peptide synthesis. As described in section 2.7.5.

3.19.3 Synthesis of Fmoc-aminoethyl-disulfide propanoic acid 34.

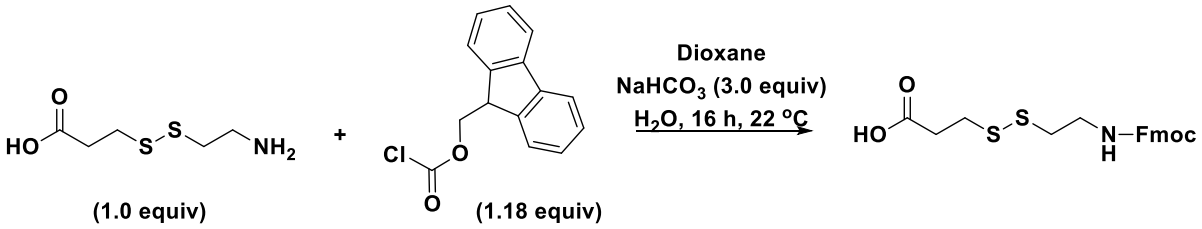

Procedure modified and adapted[133] as follows: 3-((2-aminoethyl) disulfaneyl) propanoic acid **32** (81.3 mg, 0.45 mmol, 1.0 equiv) was placed in an argon flushed 50 mL round bottom flask equipped with a spin bar. The round bottom flask was place in a water-ice Dewar bath to keep a cool temperature (~22 ^{o}C) then a solution of $NaHCO_3$ (135.2 mg, 1.35 mmol, 3.0 equiv) dissolved in 8 mL of water was added dropwise. Subsequently, a solution of Fmoc-chloride **33** (137.4 mg, 0.531 mmol, 1.18 equiv) dissolved in 4 mL of dioxane was added dropwise with stirring. The reaction mix was left stirring overnight in an ice-water bath, then 4 mL of dioxane were added to continue with a work-up. The reaction crude was acidified by addition of a 2 M HCL solution dropwise to bring the pH ~1.0, followed by extraction with ethyl acetate (4 times). The collected organic layers were washed with brine, dried over Na_2SO_4, filtered and rotovaped to afford an oily colorless

crude residue. Product was purified by silica gel flash chromatography with DCM followed by 3.3% Methanol/DCM as the mobile phase to afford the protected Fmoc-aminoethyl-disulfide propanoic acid **34** as a white solid in 80% isolated yield. This compound should be stored at -20 ^{o}C. Found m/z $[M+H]^{1+}$ = 438.1 by ESI. Compound structure was confirmed by 1H and 13C NMR as reported.[133]

3.19.4 Synthesis of Rhodamine B FRET acceptor peptide 18.

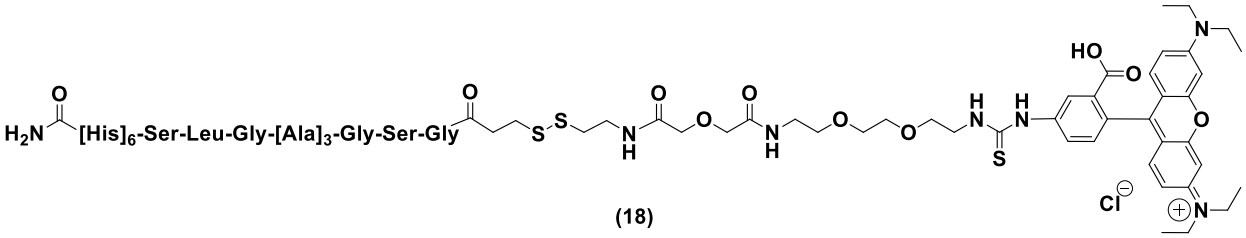

(18)

Peptide 11 (**scheme 3.2**) with sequence His_6-Ser-Leu-Gly-$(Ala)_3$-Gly-Ser-Gly-Fmoc (C→N-terminus) was synthesized on rink amide resin by following the general solid phase peptide synthesis protocol described in **section 2.3.5**. The synthesis was continued by capping any unreacted free amines by acetylation followed by Fmoc deprotection of terminal Glycine with 20% piperidine in DMF (*step i*). After washing the resin, Fmoc-aminoethyl-disulfide propanoic acid was pre-activated for 1 min and coupled for 2 h (*step ii*). After Fmoc deprotection (*step iii*) The synthesis was continued by preactivation (5 min) and coupling of the commercially available Fmoc-$(PEG)_2$-Suc-OH building block for 1 h (*step iv*). The resin was further treated with acetic anhydride (20 equiv) and DIEA (30 equiv) in DCM to cap (acylate) any unreacted free amines, followed by Fmoc-deprotection (*step v*). The coupling of Rhodamine B isothiocyanate was carried out as follows: A mass equivalent to 12.5 μmol of peptide on dry resin (estimated by the resin substitution) was

weighed out, then the resin was swollen with DCM for 30 min. Rhodamine B isothiocyanate (1.10 equiv, 13.75 μmol, 7.4 mg) was weighed out in a separate vial, and then 1 mL of a pyridine: DMF: DCM (12:7:5) solution was added and mixed to dissolve the rhodamine. This solution was then added to the resin and left to react with shaking overnight at room temperature (step vi). The reaction vessel was wrapped with aluminum foil to avoid photobleaching of the dye. *Step vi* was repeated next day for 2 h, since the coupling reaction did not go to completion the first time. *Step vi* can be repeated as many times as necessary. Finally, the resin was washed with DMF, followed by isopropanol, then by DCM as many times as needed to remove any uncoupled rhodamine. The resin was then treated with a pre-cleavage wash as follows: 3X DCM, 3X MeOH containing acetic acid (pH~5), 3X DCM, 3X MeOH and then high vacuumed overnight in the dark. Finally, the peptide was cleaved from the rink amide resin using 2 mL of a TFA 97%/ water mixture for 2 h at room temperature, in the dark. Rhodamine peptide **18** was purified by reverse phase HPLC using a water/acetonitrile (both solvents containing 0.1% TFA) gradient, followed by lyophilization and desalting. Calculated m/z for $C_{107}H_{147}N_{34}O_{26}S_3$ = 2420.04, found $[M+H]^{1+}$ = 2420.089 by MALDI-TOF (reflector positive mode).

3.19.5 Synthesis and characterization of palmitoyl peptide (23)

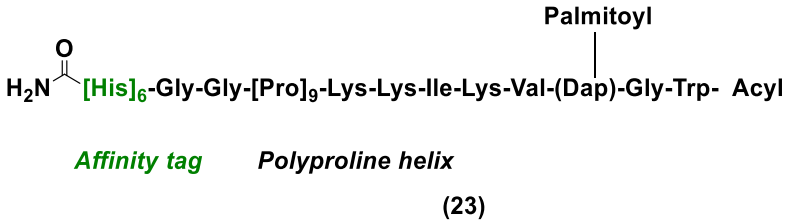

(23)

In contrast to the original solid phase peptide synthesis method reported by Medintz *et.al* [110] for the synthesis of this palmitoyl peptide **23**, we employed Fmoc chemistry as described in **section 2.3.5** with a few modifications, for instance, double coupling was used for each amino acid residue after the eighth residue (Gly-8) to avoid the generation of truncation products and therefore a decrease in the overall yield of the target linear peptide. As indicated in scheme 3.2, N-acetylation was carried out after assembly of the linear peptide **19** and Fmoc deprotection of terminal amine on tryptophan.

Lastly, selective Mtt deprotection of diaminopropionic acid was performed as described in **section 2.3.5**, followed by resin neutralization (by washing the resin three times with a solution of 5% DIEA in DCM and three times with DMF).

Palmitoylation of peptide **21** (scheme 3.2) was carried out with palmitic acid (3.0 equiv), oxyme (3.0 equiv.), HBTU (3.0 equiv.), in DCM/DMF 1:1 (anhydrous solvents), with a 5-minute pre-activation time, followed by an hour-long coupling time. *Pre-cleavage treatment* was performed as described in **section 2.3.5.** We found that a combination of 90% TFA, 5% thioanisole, 2% anisole, 3% 1,2-ethylenedithiol, for 2h at room temperature was the best condition to cleave this peptide.

Post-cleavage treatment: TFA was completely rotovaped and the crude peptide was dissolved in a 1:1 mixture of ACN: water. The crude peptide solution was passed through a 40-micron filter as we observed that an insoluble sticky white residue formed, possibly due to the cleaved protecting groups. Peptide **23** was purified by reverse phase HPLC using a water/acetonitrile/methanol gradient (all solvents containing 0.1% TFA) by employing a semi-prep reverse phase column (Aeris, 10 mm diameter x 250 mm length) at a 5 mL/ min flow rate and monitoring with a dual detector (λ_1= 220 nm, λ_2= 254 nm). Fractions containing the desired peptide were lyophilized and desalted.

3.19.6 Synthesis and characterization of polyamine peptide 31 (see scheme 3.4)

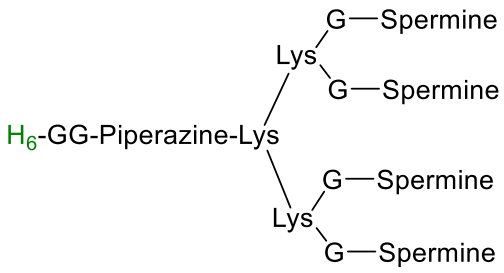

This peptide was manually synthesized by Mona Hoseini Soflaee. The first ten residues of polyamine peptide **29** was linearly assembled on rink amide resin as described in section 2.3.5. The synthesis was continued by coupling $BisLys_{11}$ (6.0 equiv. of Fmoc-L-Lys(Fmoc)-OH), with Oxyme (6.0 equiv), HBTU (6.0 equiv) and DIEA (12.0 equiv) in DMF for 1 h. After Fmoc deprotection, the synthesis was continued by coupling Gly_{12} (12.0 equiv. Fmoc-Gly-OH, 12.0 equiv Oxyme, 12.0 equiv. HBTU, 24.0 equiv DIEA in DMF) for 1 h. After a final Fmoc deprotection, the resin was washed, shrunk with MeOH and high

vacuumed overnight. Finally, the resin equivalent to 12 μmol of peptide (roughly estimated by resin substitution) was transferred into a 3 mL Torviq polypropylene vessel and swollen with DCM to continue the synthesis by coupling the spermine building block (12.0 equiv. tetra-Boc-spermine-5-carboxylic acid **30**, 12.0 equiv Oxyme, 12.0 equiv. HBTU, 24.0 equiv DIEA in DMF) for 1 h at r.t.

The pre-cleavage treatment of the residue was performed as described in section 2.3.5. The polyamine peptide was cleaved from the resin by using a 97% TFA/3% water cocktail for 2 h at room temperature. The crude peptide was purified by reverse phase HPLC with a water/acetonitrile (with 0.1% TFA) gradient, by employing a semi-prep reverse phase column (Aeris, 10 mm diameter x 250 mm length) at a 5 mL/ min flow rate and monitoring with a dual detector (λ_1= 220 nm, λ_2= 254 nm). Fractions containing the desired peptide **31** were lyophilized, desalted and analyzed by MALDI-TOF (reflector positive mode).

3.19.7 Table of sequences, cleavage conditions, time, [M+H] mass found

Peptide (*C*-terminus → *N*-terminus)		Cleavage conditions
H_6-KWGS(Aib)AALGG-R_9-Acyl	**(6)**	80% TFA, 5% thioanisole, 5% anisole, 5% phenol, 5% water, 4h/ r.t.
H_6-KWGS(Aib)AALGG-GLFDIIKKIAESF	**(7)**	90% TFA, 5% thioanisole, 2% anisole, 3% EDT, 3h/ r.t
H_6-GG-P_9-KKIKV-(Dap)palmitoyl-GW-Acyl	**(23)**	90% TFA, 5% thioanisole, 2% anisole, 3% EDT, 2h/ r.t
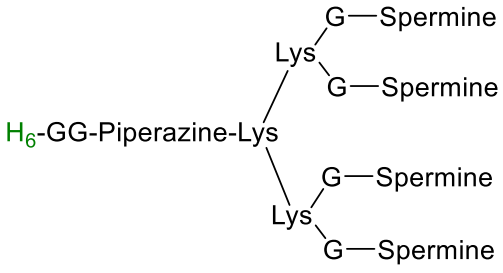	**(31)**	97% TFA/ 3% water

Table 3.1. Sequences cleavage conditions of endosomolytic peptides synthesized and tested.

3.19.8 Peptide desalting. As described in section 2.3.9

3.19.9 Selection of a QD-Dye FRET pair (Spectral properties of CL4-QDs and Rhodamine).

1) Prepare stock solution of QDs in molecular biology grade water or filtered 1X PBS pH=7.0 and measure the absorption spectra (black line in Fig.3.17) by UV-Vis to determine their concentration as described above.

2) From the QD stock solution, prepare 1 mL (or a volume equivalent to the quartz cuvette being used) of a 25- 50 nM QDs solution and transfer to a clean quartz cuvette.

3) In a fluorimeter, measure the photoluminescence spectrum of the QDs solution. An excitation wavelength of 400, 410 or 430 nm works well (Green dotted line, Fig. 3.17)

4) Follow the same steps 1-3 to measure absorption and emission of the FRET acceptor dye. Usually a solution in the low micromolar range yields good results.

Spectral properties of DHLA-QDs and Rhodamine B.

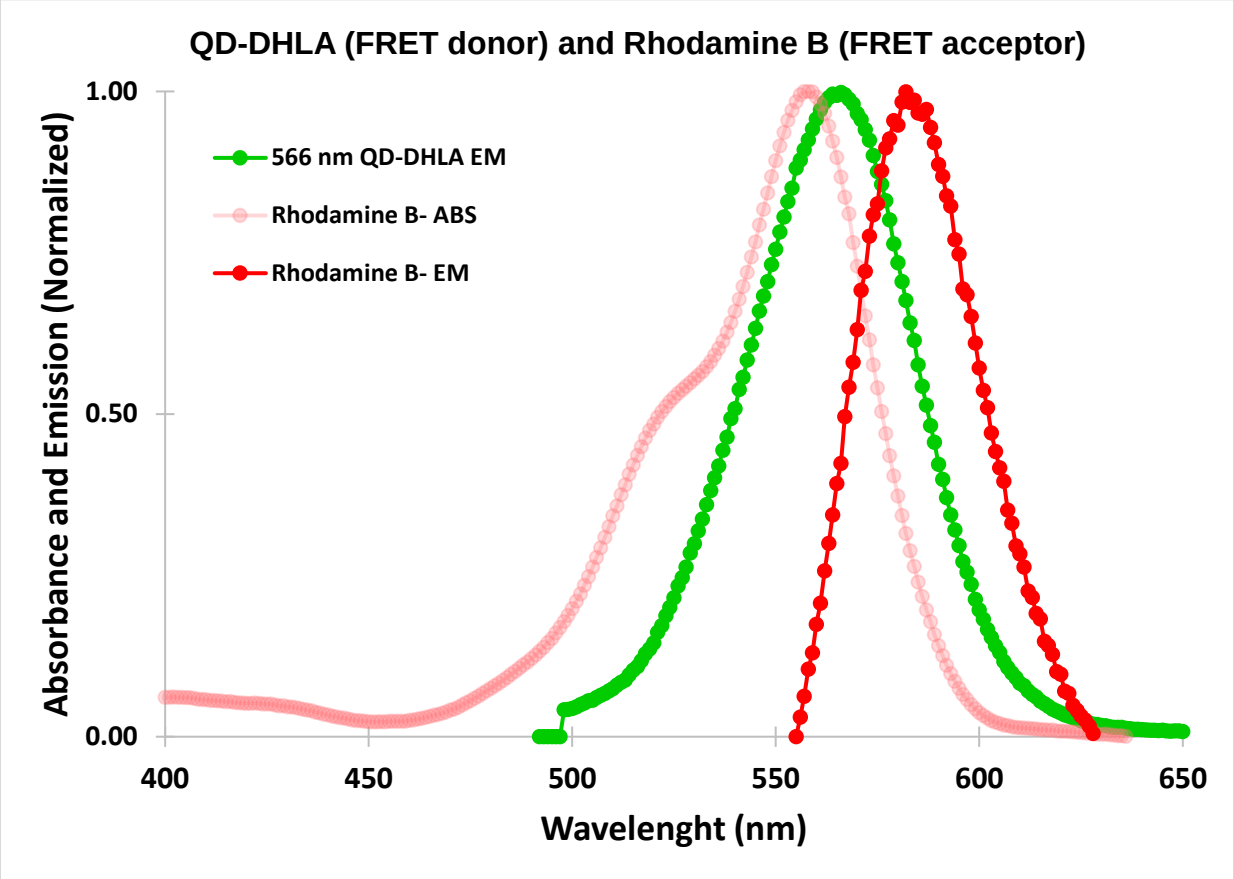

Figure 3.18. Normalized absorption and PL emission spectra for **a)** QD-CL4-Dye FRET pair and **b)** QD-DHLA-Dye FRET pair. An excitation wavelength of 430 nm was used for both FRET pairs. In both panels, note the minimum in the absorbance of the dye at 430 nm and the overlap between the QD emission and dye absorption.

3.19.10 Titration of Rhodamines needed per QD for FRET.[29]

Table 3.2, should be used as a reference for the experiment described below.

Example of an experiment set up for the self-assembly of Rhodamine B peptide to QDs:

1) When ready to use, dissolve the pure and desalted polyhistidine Rhodamine B peptide **18** in water yielding a final concentration of 50 μM.

2) Prepare a stock solution of QDs in molecular biology grade water or 1X PBS filtered buffer, and measure the final concentration by UV-Vis. In this example, the stock solution concentration is 2.38 μM.

3) To multiple 0.4 mL Eppendorf tubes, add 2.5 μL of 10X PBS buffer.

4) To each tube, add the corresponding amount of water (see Table below) and mix.

5) To each tube, add the corresponding amount of polyhistidine peptide stock solution (see Table below), and gently mix. In this example, the stock concentration is 50 μM.

6) To a separate set of multiple 0.4 mL Eppendorf tubes, add 6.3 μL of QD stock solution.

7) Add the prepared polyhistidine peptide solution from steps 3-5 to the corresponding tubes containing QD solutions prepared in step 6 and gently pipette up and down (do not vortex, nor centrifuge). The final volume for each tube should be 25 μL.

8) Incubate for 1-2 hours at room temperature and protect from light.

9) To each tube, add 275 μL of 1X PBS, and gently pipette up and down (do not vortex, nor centrifuge). The final volume for each tube should be 300 μL.

10) Transfer 300 μL of each reaction into a quartz cuvette and measure the respective emissions in a fluorimeter with an excitation at 430 nm.

Notes:

a) For peptides with poor solubility dmso can be added to a final 5- 10% DMSO /water (v/v) concentration.

b) 1X PBS buffer must be filtered through a 40-micron filter before use.

c) Reactions must be incubated in the dark to avoid dye photobleaching.

d) QD stock solution should be stored at 4 ^{o}C in the dark or with aluminum foil.

Desired ratio of peptide/ QD								
Reagent (μL)	**0**	**1**	**2**	**4**	**6**	**8**	**10**	**15**
QD (2.38 μM)	6.3	6.3	6.3	6.3	6.3	6.3	6.3	6.3
Peptide (50.0 μM)	---	0.3	0.6	1.2	1.8	2.4	3.0	4.5
10X PBS	2.5	2.5	2.5	2.5	2.5	2.5	2.5	2.5
H_2O	16.2	15.9	15.6	15.0	14.4	13.8	13.2	11.7
Total volume (μL)	25.0	25.0	25.0	25.0	25.0	25.0	25.0	25.0
1X PBS after 1 h incubation (μL)	275	275	275	275	275	275	275	275
Total volume (μL)	300	300	300	300	300	300	300	300
Final conc. QD (nM)	50	50	50	50	50	50	50	50
Final conc. Peptide (μM)	0	0.1	0.2	0.4	0.6	0.8	1.0	1.5

Table 3.2. Reagent volumes utilized for QD- Rhodamine peptide self-assembly

4 Synthesis of challenging peptides and potential alternative solutions

4.1 Motivation to synthesize NPyS-Cys-CPP-K-HA2 peptide 35.

Cell penetrating peptides (CPPs) such as polyarginine and the TAT sequence have been employed countless times as tools for the intracellular delivery of different cargoes, however, there is still a major problem to address, when CPPs are internalized through endocytosis, they along with their cargoes often remain trapped inside the endosomes and cannot reach the cytosol, which decreases their bioavailability.[134]

Several groups have developed tools to enhance the endosomal escape capacity of CPPs, for example, Dowdy., et al, reported that the efficiency to deliver an endocytosed TAT-Cre protein was significantly enhanced by co-incubation with a dTAT-HA2 fusogenic peptide.[124] Interestingly, a retro-inverso form of the fusogenic TAT- HA2 was used (**Figure 4.1 a**). Our group has also shown that conjugation to CPPs, mediates cytoplasmic delivery of otherwise membrane-impermeant Tb complexes, including TMP-Lumi4 (**Figure 4.1 b**) to selectively label an intracellular target.[93]

Conjugation to a CPP (R9) facilitated the Tb- probe delivery into the cytoplasm of various cell types at low micromolar concentrations, however, our group observed that endocytosis followed by endosomal entrapment took place when high concentrations of the Lumi4-Tb-TMP probe were employed. Encouraged by the endosomal escape reported abilities of the fusogenic peptide TAT-HA2[124] and the ability of TAT and R9 peptides to deliver Tb luminescent impermeable agents into living cells,[93] we started an

investigation aimed at the development of a modular peptide-based probe as a tool for cytosolic delivery, endosomal escape, and delivery of cargo in live-cells (**Figure 4.1 c**).

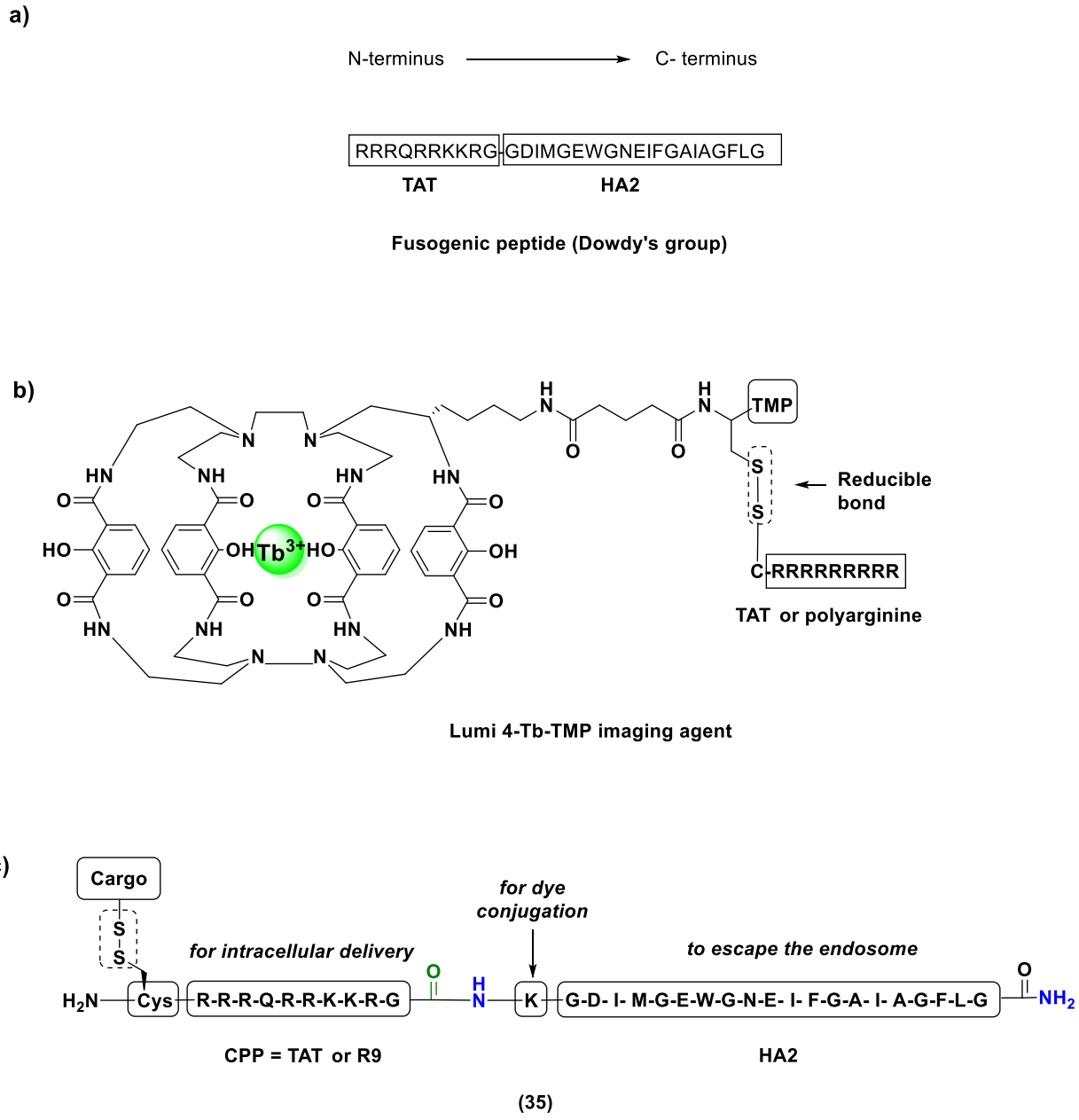

Figure 4.1 : a) Sequence of the TAT-HA2 peptide used by Dowdy et al, to enhance the endosomal escape of a TAT-Cre protein in live-cells.[124] b) A Lumi4-Tb-TMP probe equipped with a CPP for facilitated intracellular delivery.[93] c) Our synthetic target, NPyS-Cys-CPP-K-HA2 ,peptide **35**.

4.2 Retrosynthetic analysis

Peptide **35** is a relatively long sequence (33 amino acid residues), which means that the conventional stepwise solid phase peptide synthesis (SPPS) may afford minute quantities of the final product **35**. From experience, I have observed that SPPS is very useful for peptide sequences comprising up to 12 amino acids in average, after that length, chances are that yields will start to decrease dramatically with each amino acid added after twelve residues.

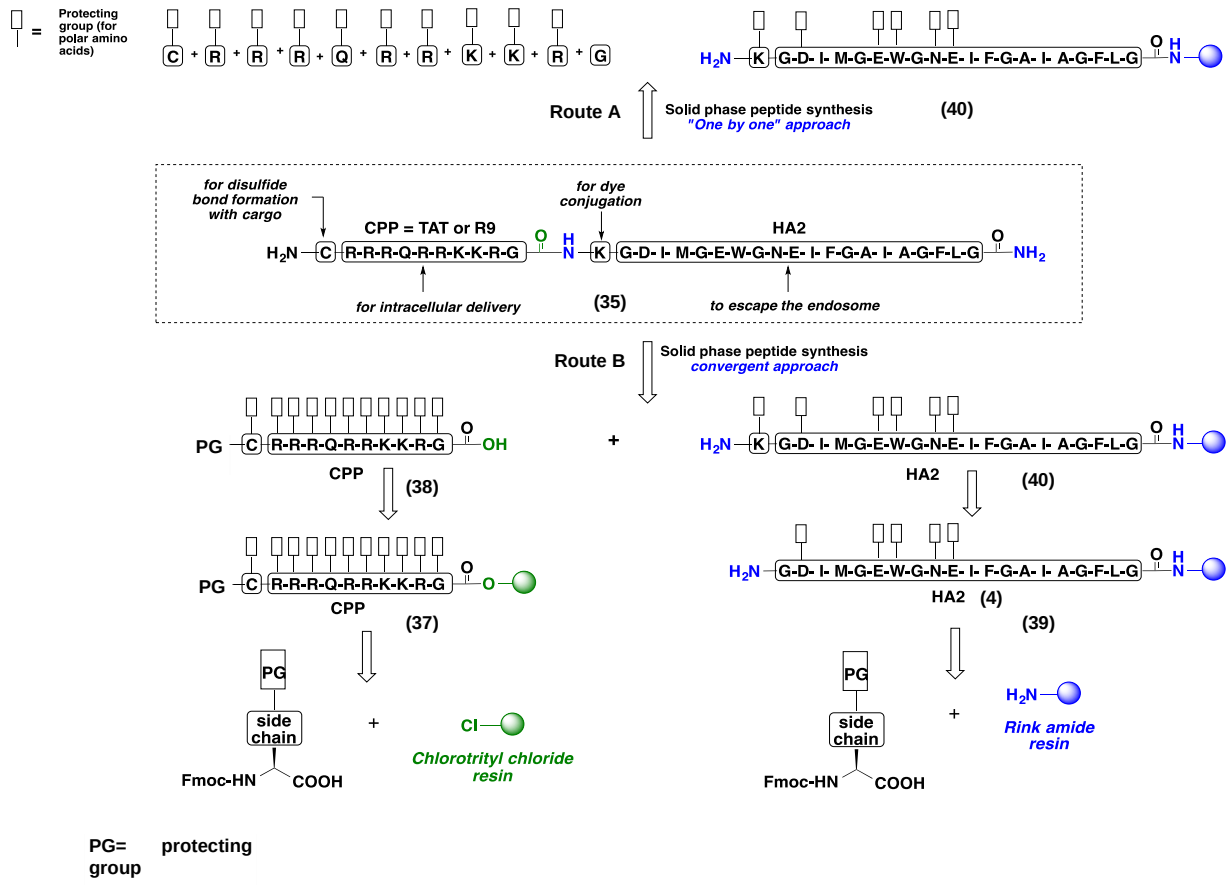

Scheme 4.1: Two alternative synthetic routes for the assembly of peptide **35**. Route A depicts the conventional stepwise solid phase peptide synthesis approach. Route B, entails a convergent approach wherein the key step is the condensation of fragments **38** and **40** on solid phase.

As depicted in **Scheme 4.1**, we initially considered two different synthetic approaches for the synthesis of **35**. Route **A**, comprises the conventional SPPS methodology where one amino acid is added at a time on solid support. In route **B**, we considered a convergent solid-phase approach, in which the key step would entitle the amide bond formation between the fully protected fragments **38** and **40**. We anticipated this convergent approach (route **B**) would afford **35** in much higher yield than route **A** would give, as we planned to use fully protected and purified fragment **38**, which theoretically, after only one subsequent coupling reaction with **40**, followed by Fmoc deprotection of the fusion peptide terminal amine, would give peptide **35** at once.

This approach has been employed for the synthesis of long peptides by several groups before.[135-138] I will discuss our results in detail on the following sections.

4.3 Convergent solid phase peptide synthesis

SPPS of fragment 40: Peptide **39** was synthesized on a low-level substitution rink amide resin (to avoid aggregation of long peptides on resin), by using commercially available *N*-terminal Fmoc protected amino acids and TFA labile side chain protecting groups.

The protocol for SPPS with Fmoc chemistry is described in more detail in the experimental section of chapter 3, however, the interested reader is encouraged to review the most recent and easy-to- follow protocols.[139]

As shown on the ESI-MS data of a crude sample, HA2 peptide **39** was successfully assembled (**Figure 4.2 a**). After Fmoc deprotection with 20% piperidine in DMF, the synthesis was continued by coupling Fmoc-Lysine (Mtt)-OH to afford the desired HA2 peptide **40 (Figure 4.2 b**).

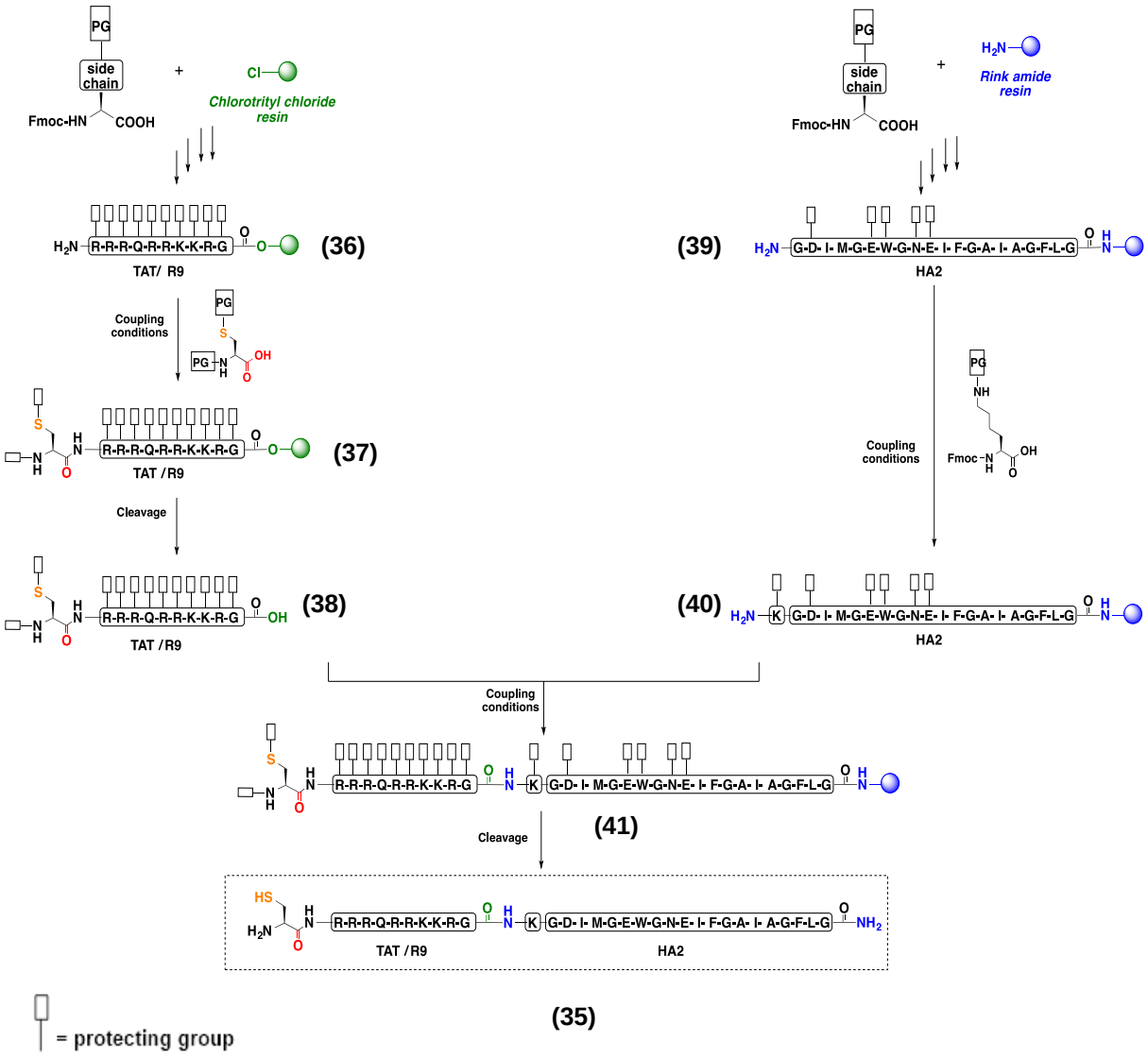

Scheme 4.2: Convergent solid phase peptide chemistry strategy in detail. (Route B).

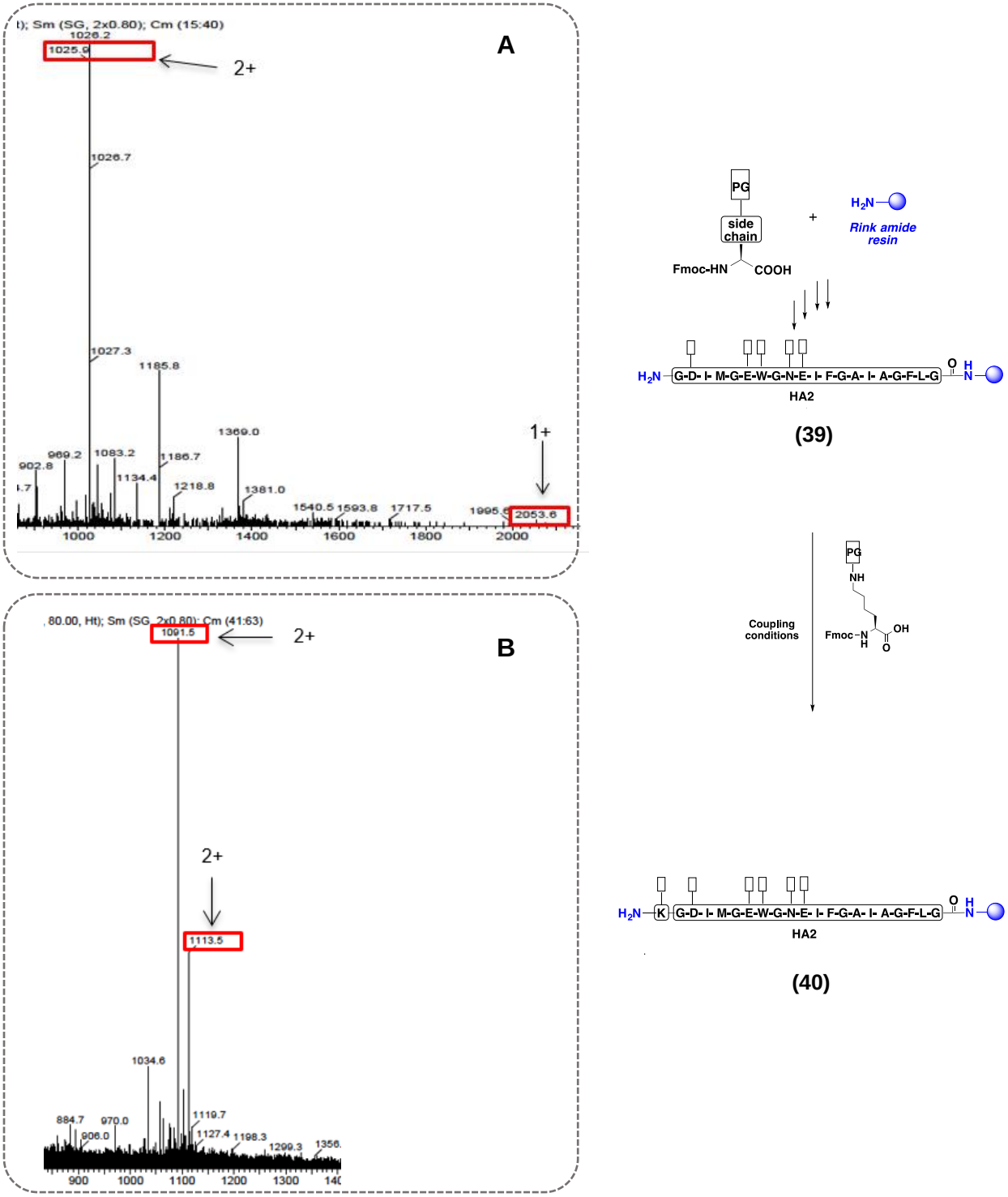

Figure 4.2: a) Crude MS analysis shows the corresponding mass of the HA2 peptide **39**, b) after coupling a lysine residue a cleavage test crude showed the correct mass for peptide **40**.

4.3.1 SPPS of fragment 37 (Scheme 4.3): Peptide **36** was assembled stepwise on CTC resin. Coupling of a cysteine residue at the *N*-terminus was the next intended step, however, as shown in **Scheme 4.3**, it was not a trivial task, in fact, protected cysteine residues **42**, **43** and **44** did not afford peptide **37**, and the only amino acid that coupled successfully was Boc-Cys(Trt)-OH, **45**. Cysteine residues **42**[140] and **43**[141] were synthesized by published procedures,[140-141] but they both proved to be quite unstable as they rapidly decomposed even though we fully characterized them. Cysteine derivative **44** is commercially available, but it seemed to have decomposed or rearranged under our reaction conditions (3 equiv amino acid, 3 equiv HBTU, 3 equiv oxyme, 6 equiv DIEA in DMF at r.t.).

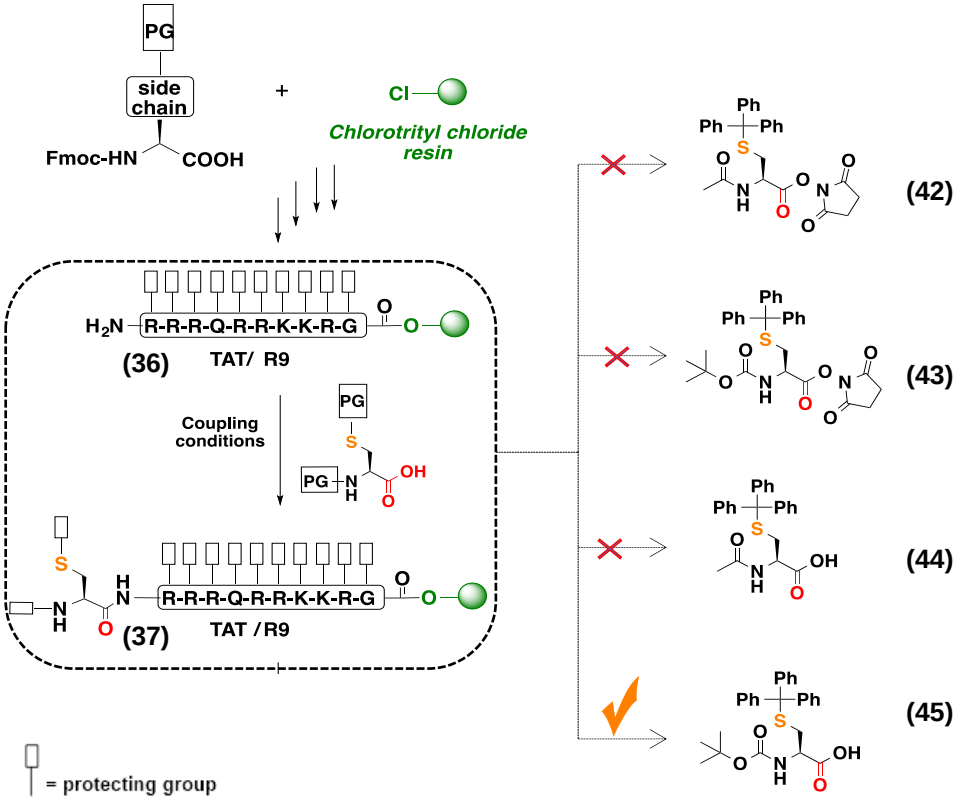

Scheme 4.3: Short screen of different protected cysteine residues wherein **42**, **43** and **44** failed to couple to the N-terminus amino group of **36**. Only Boc-Cys(Trt)-OH **45** coupled under our reaction conditions.

4.3.2 Coupling of a Boc-Cys(Trt)-OH residue to the *N*-terminus of peptide 36.

As described above Boc-Cys(Trt)-OH was the only residue that successfully coupled to the *N*-terminus of our CPP peptide on CTC resin to afford peptide **37,** irrespective of the parent peptide (fully protected TAT or polyarginine). MS analysis confirmed the assembly of peptide **37** (Figure 4.3).

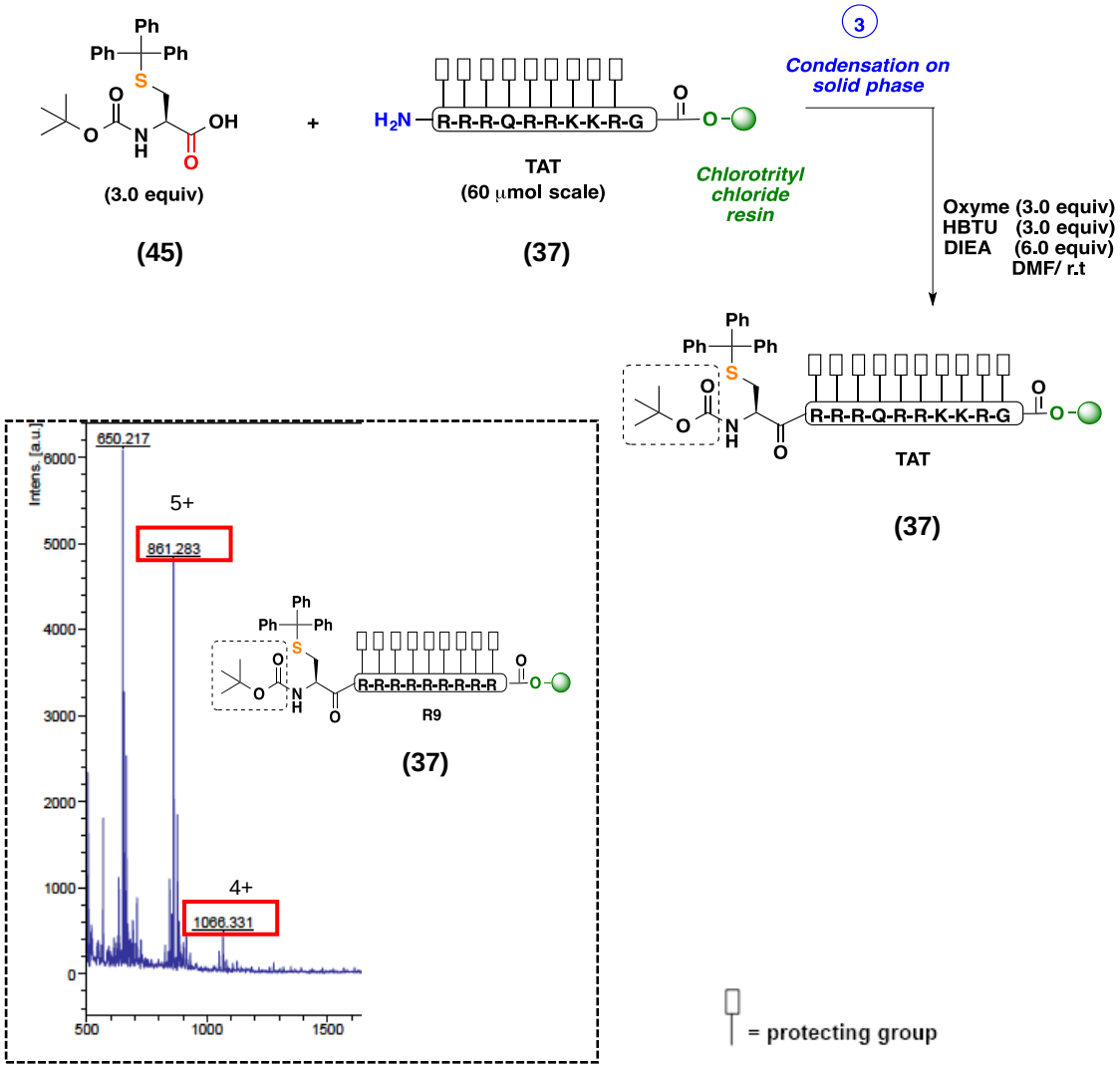

Figure 4.3. MS analysis confirms the expected mass for Boc-Cys-CPP peptide **37** (where CPP is either TAT or polyarginine).

4.3.3 SPPS of fragment 38 (Scheme 4.2): Peptide **38** was assembled on CTC resin with the intention to access the fully protected TAT and polyarginine peptides **38** with a COOH group (at the *C*-terminus) available for fragment condensation down the path. The CTC resin is very acid-labile, and it is highly employed because it allows to cleave fully protected peptides by using 1%TFA in DCM, alternatively, it also allows to cleave fully deprotected peptides if a high TFA percent is used instead (more than 80% TFA), while still affording a COOH group available for further chemical modifications. First, peptide **36** was synthesized on CTC resin. After Fmoc deprotection followed by coupling of Boc-Cys(Trt)-OH, peptide **37** was cleaved with 1% TFA in DCM solution to afford the fully protected peptide **38** (MS-ESI of a crude sample shown in **Figure 4.4**).

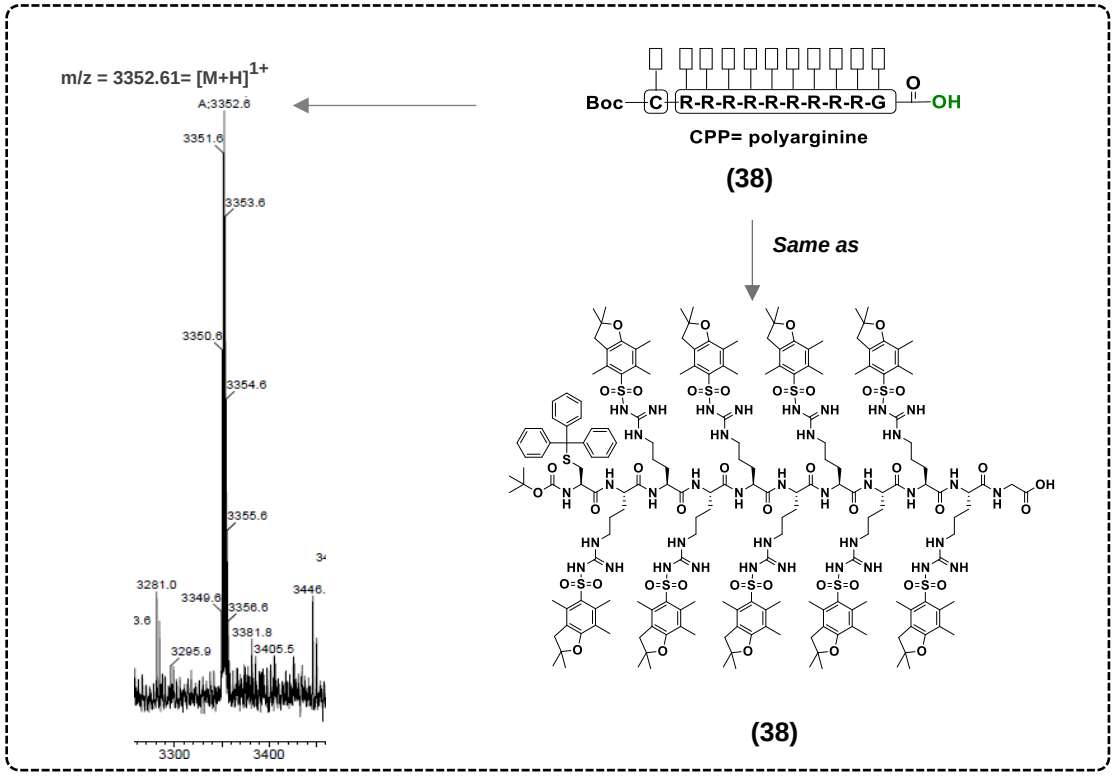

Figure 4.4: A crude MS analysis confirms the expected mass for the fully protected peptide **38** after cleavage from CTC resin with 1% TFA in DCM. The integrity of the protecting groups is preserved while a *C*-terminal COOH group is afforded for further modification.

4.3.4 Attempted convergent SPPS to obtain fusion peptide 41.

After obtaining the fully protected peptide **38** (MS results **Figure 4.4**), with an available COOH group for condensation, and after confirming the full assembly of peptide **40** on rink amide resin (see ESI-MS results **figure 4.2 b**), we tested several coupling reaction conditions to afford the desired peptide **41** (**Scheme 4.4**).

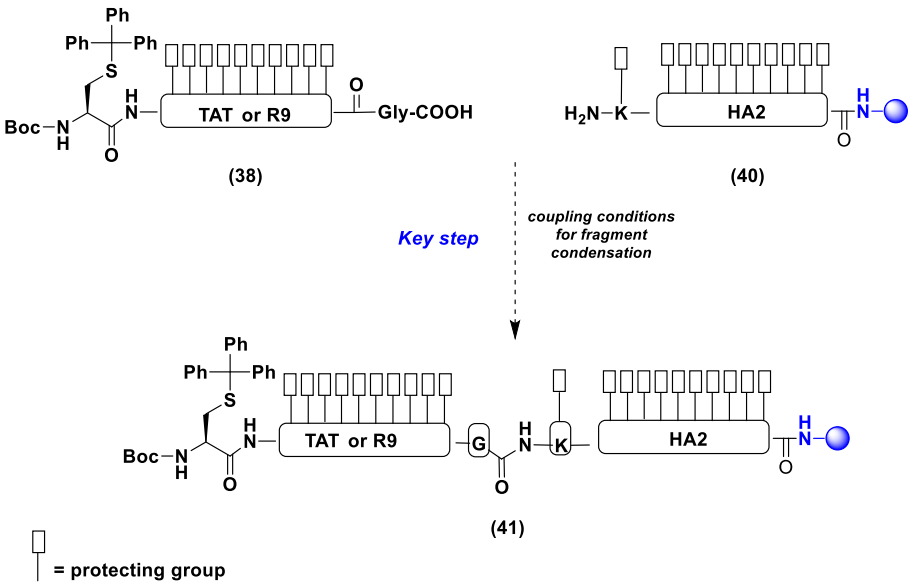

Scheme 4.4: Attempted fragment condensation of fully protected CPP peptide **38** and endosomal escape peptide **40** on ring amide resin.

Because peptide **38** is very hydrophobic, we tried to purify it by flash chromatography on silica gel, at the expense of low product recovery. Then we realized that purification was unnecessary as the crude was mostly clean. Thus, in all reaction conditions, we used excess amount of fragment **38** crude (Table **4.1**).

Entry No.	Scale	Coupling Conditions	Outcome
1	1.0 μmol	HBTU (1.3 μmol), Oxyme (1.3 μmol) DIEA (2.6 μmol) / DMF	No reaction
2	0.5 μmol	HOBT (0.97 μmol), DCC (0.72 μmol) DIEA (2.6 μmol) / DMF	No reaction
3	0.5 μmol	HOBT (0.97 μmol), diisopropylcarbodiimide (0.72 μmol) DIEA (2.6 μmol) / DMF	No reaction
4	0.5 μmol	HOBT (0.97 μmol), EDCI (0.72 μmol) DIEA (2.6 μmol) / DMF	No reaction
5	0.5 μmol	HBTU (2.6 μmol), Oxyme (2.6 μmol) DIEA (5.2 μmol)/ DMF/ double coupling	Inconclusive (insoluble gummy crude material)

Table 4.1. A sample of reaction conditions tested for the fragment condensation of peptides **38** and **40** (Scheme 3.4).

None of the reaction conditions tested (**Table 4.1**) afforded peptide **41**, even though both peptide fragments were almost completely pure. One crucial aspect for a successful coupling of two long peptides is solubility. We observed that peptide **41** was not completely soluble in DMF. Although there are isolated examples of synthesis of long peptides using this strategy,[135-138] there is not a general method.

Also, it is difficult to predict what the solubility of the CTC cleaved peptides will be. After the experience gained, we estimate there are better chances to succeed with peptides made of naturally hydrophobic residues, such as alanine, valine, leucine, isoleucine phenylalanine, as these do not need additional bulky hydrophobic protecting groups. For instance, in entry 5, we did a double coupling under the ordinary amide bond formation conditions (**Table 4.1**), and after the coupling time and the washing step of the resin, we observed a gummy material on the surface of the rink amide beads, which is an indication of aggregation. When protected peptides aggregate on the resin, the participating *C*-terminal COOH and the N-terminal amino group, are hindered and therefore they cannot

react. Additionally, it is worth to note that every consecutive residue on the ten-amino acid long peptide **38**, is protected with a hydrophobic bulky group (see structure in **Figure 4.4**), in contrast, segment **40,** has only five protecting groups which are away from each other.

It is also possible that amide bond formation between **38** and **40** did not take place due to steric hindrance, which could be solved by adding a PEG linker at the *C*-terminus COOH on **38**, and as a bonus, the solubility of **38** in polar SPPS solvents would be improved.

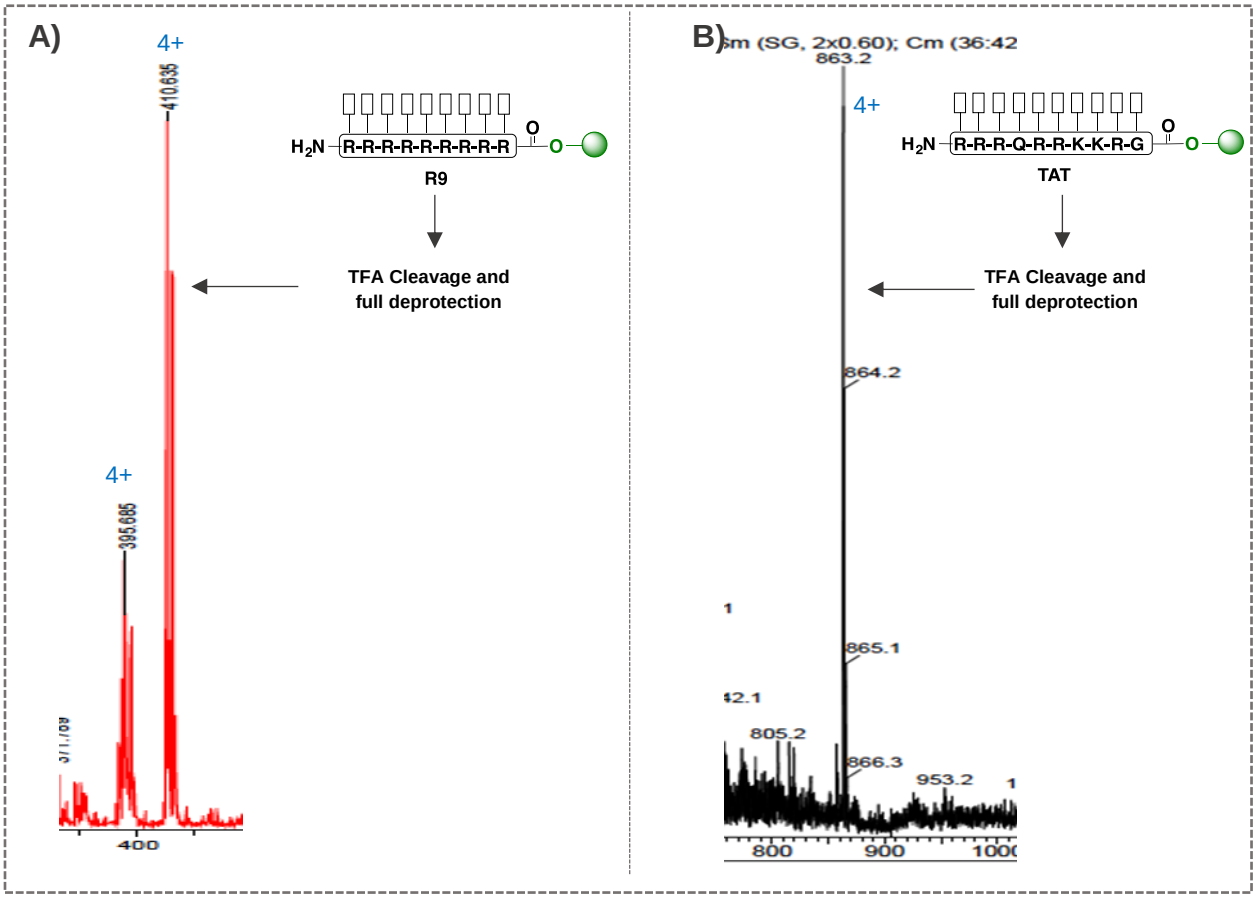

Figure 4.5. When MS analysis of fully protected peptide cleaved from CTC resin is difficult (due to their inherent hydrophobicity and lack of ionization), an alternative solution is to carry out a test cleavage with high TFA concentration for full deprotection. This strategy was employed for polyarginine and TAT peptides as shown in A and B.

Furthermore, MS characterization of fully protected CTC cleaved peptides is not straightforward due to the absence of ionizable groups, as a result, hydrophobic peptides tend to be ‘mass spectrometry invisible’ in both, MALDI and ESI.

Often this problem is solved by doing an N-terminal Fmoc deprotection to provide an ionizable NH_2 group for MS detection. We found that it is best to do an indirect MS detection of hydrophobic peptides by cleaving ~0.5 mg – 1 mg of resin, with 100% TFA to cleave all protection groups, followed by MALDI analysis or ESI (**Figures 4.5 a and b**).

4.4 Stepwise SPPS

Since the convergent SPPS approach did not yield our desired fusion peptide **41**, we tried the alternative stepwise (**Scheme 4.1, route A**) approach for both, Cys-R9-K-HA2 and Cys-TAT-K-HA2 fused peptides Results are discussed next.

4.4.1 SPPS of fused Cys-R9-K-HA2 peptide 41.

Starting from peptide **40** assembled on rink amide resin, we continued the forward synthesis by double coupling each sequential residue until the end (Cysteine). From previous experiments we knew that only Boc-Cys(Trt)-OH was a good coupling partner to be placed at the N-terminus of the fusion peptide.

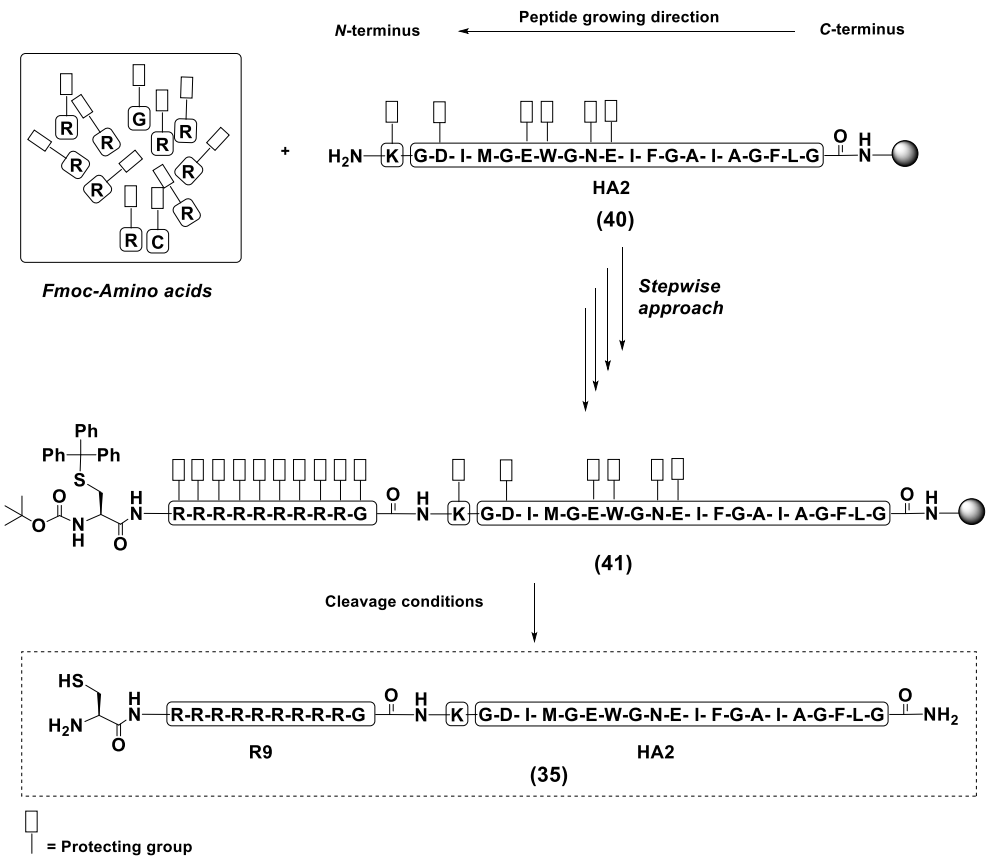

Scheme 4.5. Route A for the solid phase peptide synthesis of fused peptide **35**. Note that the cell penetrating peptide in this case is polyarginine (R9).

Once the SPPS was completed, the resin was washed, high vacuumed overnight to remove residual DMF and further cleaved with 92.5% TFA, 2.5% EDT, 2.5% water, 2.5 % TIPS-H for 2.5 h at r.t. Notably, a cleavage cocktail made of TFA 88%, Phenol 5%, Water 5% and TIPS-H 2% caused methionine oxidation.

EDT is necessary to avoid the oxidation of methionine on HA2. Also, the resin and the cleavage cocktail were flushed with argon. After cleavage of **41** from rink amide resin, crude **35** was precipitated in ether and the crude was analyzed by MALDI (**Figure 4.6**)

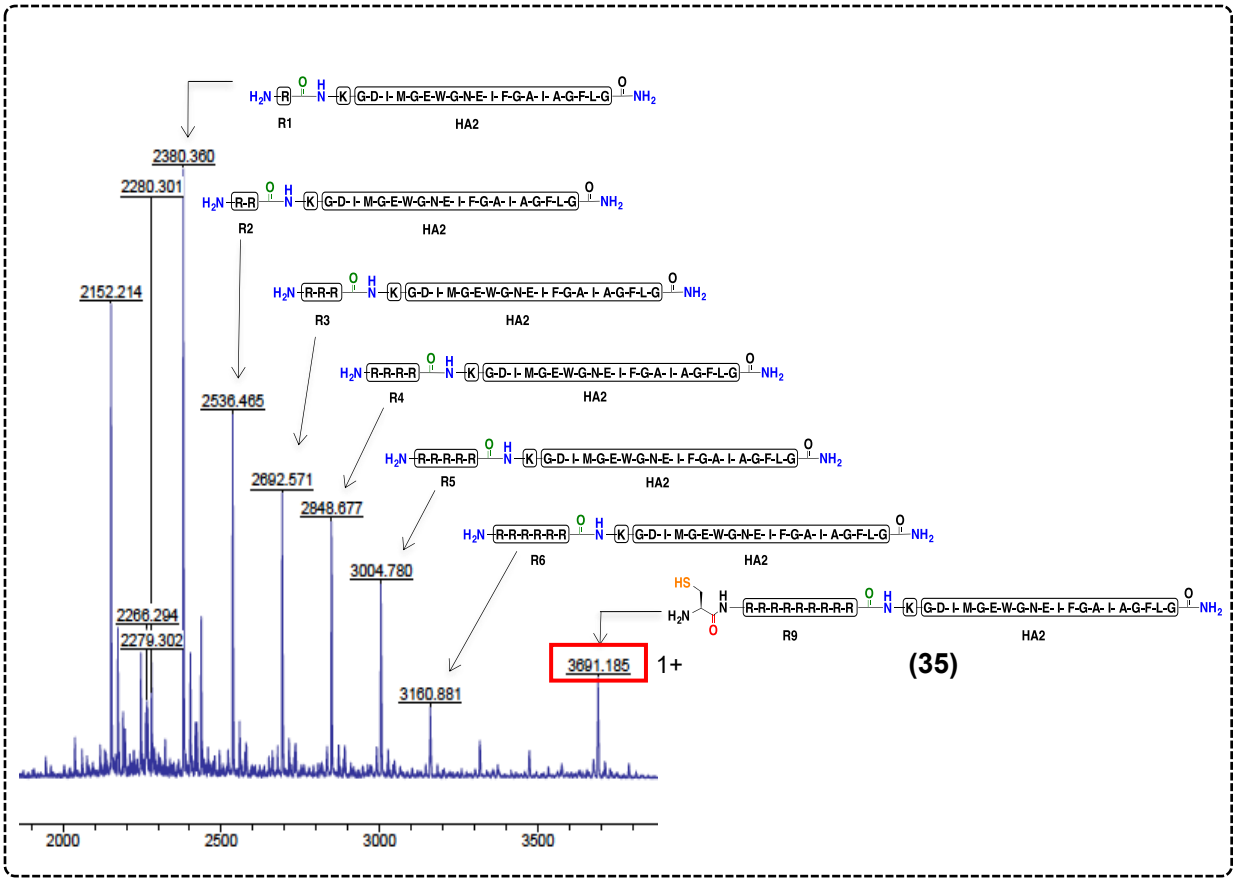

Figure 4.6. MALDI analysis of crude peptide Cys-R9-K-HA2. Note that the cell penetrating peptide in this case is polyarginine (R9).

Surprisingly, this long route afforded the desired fusion peptide Cys-CPP-K-HA2, however, as MALDI data of the crude shows, many truncation products were also generated during the stepwise process. Although the percent yield depends greatly on the peptide sequence and the bulkiness of protecting groups used, formation of truncated peptides is somewhat expected after 12-15 residues. As the peptide chain lengthens, it folds therefore, hindering the last N-terminal residue for further coupling. We tried to decrease this problem by using a low-level substitution resin, so that vicinal peptide chains would not aggregate. Since we performed this synthesis at micromole scale, we

did not isolate the final product **35**, as there were several truncated products which would make separation very difficult.

4.4.2 SPPS of fused Cys-TAT-K-HA2 peptide 41.

Starting from peptide **40** assembled on rink amide resin, we continued the forward synthesis by double coupling each sequential residue until the end (Cysteine). From previous experiments we knew that only Boc-Cys(Trt)-OH was a good coupling partner to be placed at the N-terminus of the fusion peptide.

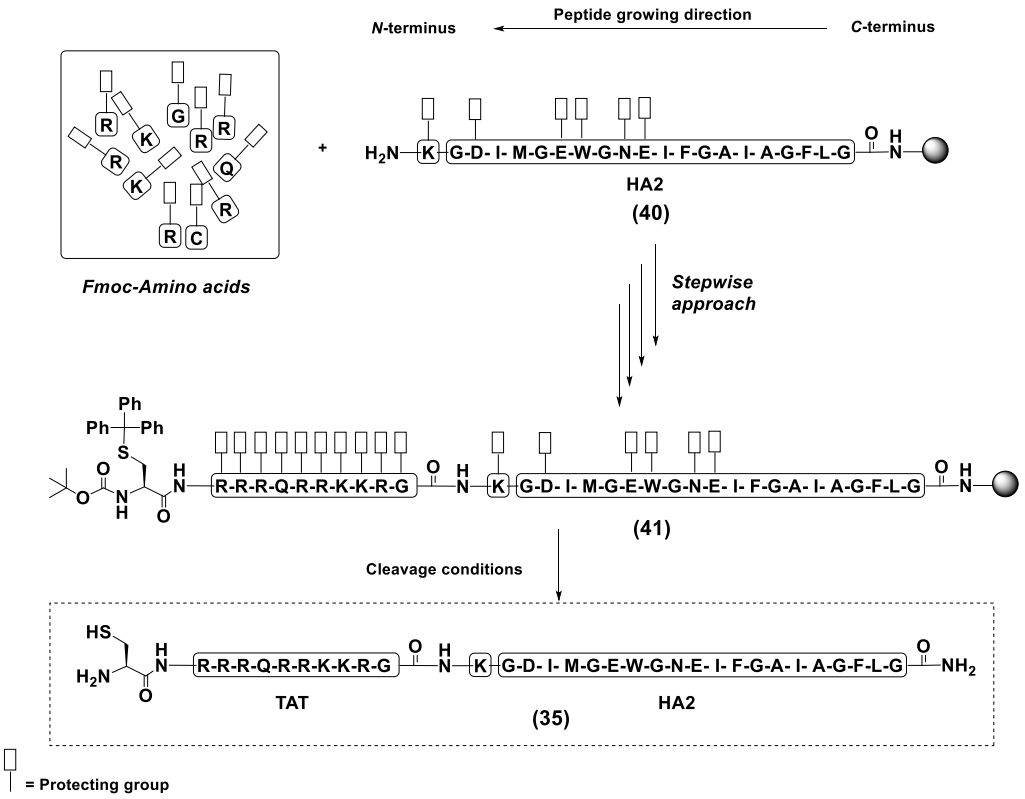

Scheme 4.6. Route A for the solid phase peptide synthesis of fused peptide **35**. Note that the cell penetrating peptide in this case is TAT.

The stepwise SPPS of Cys-TAT-K-HA2 also afforded the desired peptide (**35**), although with high amounts of undesired truncated peptides as shown by MALDI analysis (Figure 4.7).

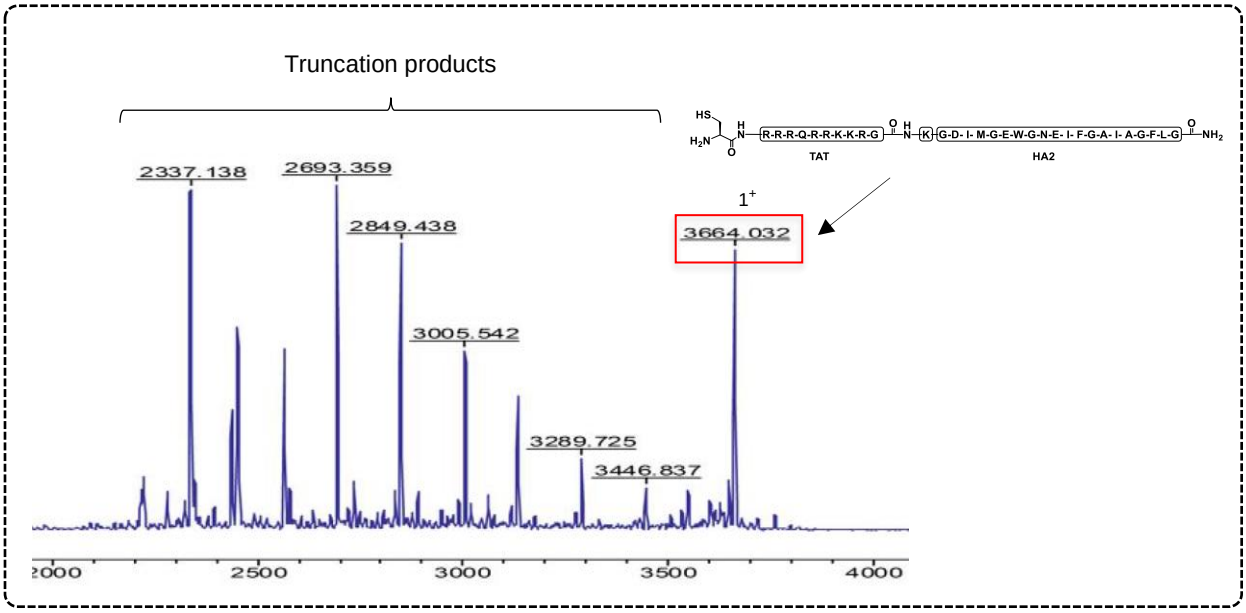

Figure 4.7. MALDI analysis of crude peptide Cys-CPP-K-HA2. Note that the cell penetrating peptide in this case is TAT.

4.4.3 What we learned regarding the assembly of peptide 41.

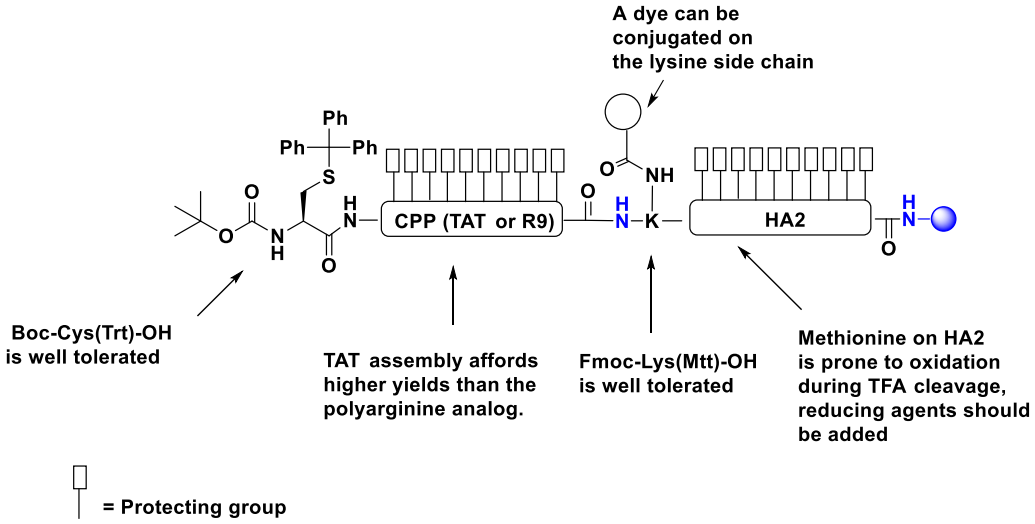

Figure 4.8.: Factors to be considered for the successful synthesis of fused peptide **41**.

In conclusion, two different synthetic strategies were attempted; 1) convergent SPPS, and 2) the conventional stepwise SPPS in which each protected amino acid residue is attached at a time. Only the last afforded the desired fusion peptides, although in very poor yields.

4.4.4 Proposed alternative solution

Peptide **35** (in scheme 4.6**)** could be assembled by relying on a more powerful, high yield reaction. Convergent SPPS could still be a viable choice if the two participating peptides to undergo coupling are completely soluble in the solvent of choice. For example, Bertozzi's lab developed a copper free click reaction by using strained cyclooctyne and azide,[142] (Scheme 4.7).

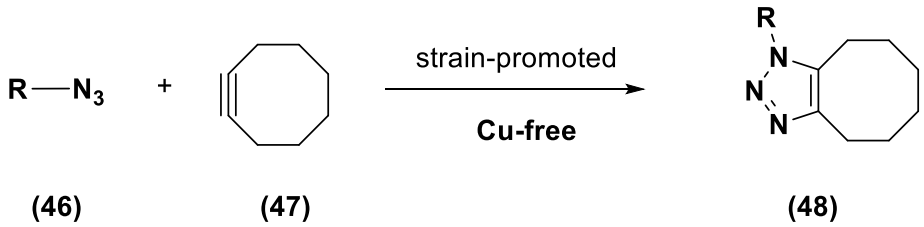

Scheme 4.7: Strain promoted [3+2] cycloaddition of azides and cyclooctynes.

This orthogonal reaction is clean and runs smoothly in water at room temperature, which is why it has been used for selective modification of biomolecules such as glycoproteins, and living cells. This bioconjugation strategy has shown to be effective since it was first reported by Bertozzi's group, as a result, chemical companies are starting to sell more click-chemistry related building blocks that can be easily incorporated in synthesis, thus I have designed a new synthetic route for the assembly of the desired modular CPP-HA2 fusion peptide (**Scheme 4.8**), which will be described in the following section.

4.5 Ongoing synthesis: fragment condensation of two peptides by a Cu-free click reaction.

Building upon the lessons learned from our multiple attempted synthesis of NPys-CPP-TAT peptide, I propose a new synthetic route for its assembly depicted in Scheme 4.8. The key step in the assembly of the fusion peptide, will involve the strain promoted [3+2] cycloaddition of azide-peptide **11** and cyclooctyne-peptide **12**. By incorporating pegylated residues, the water solubility of both peptides will be greatly improved.

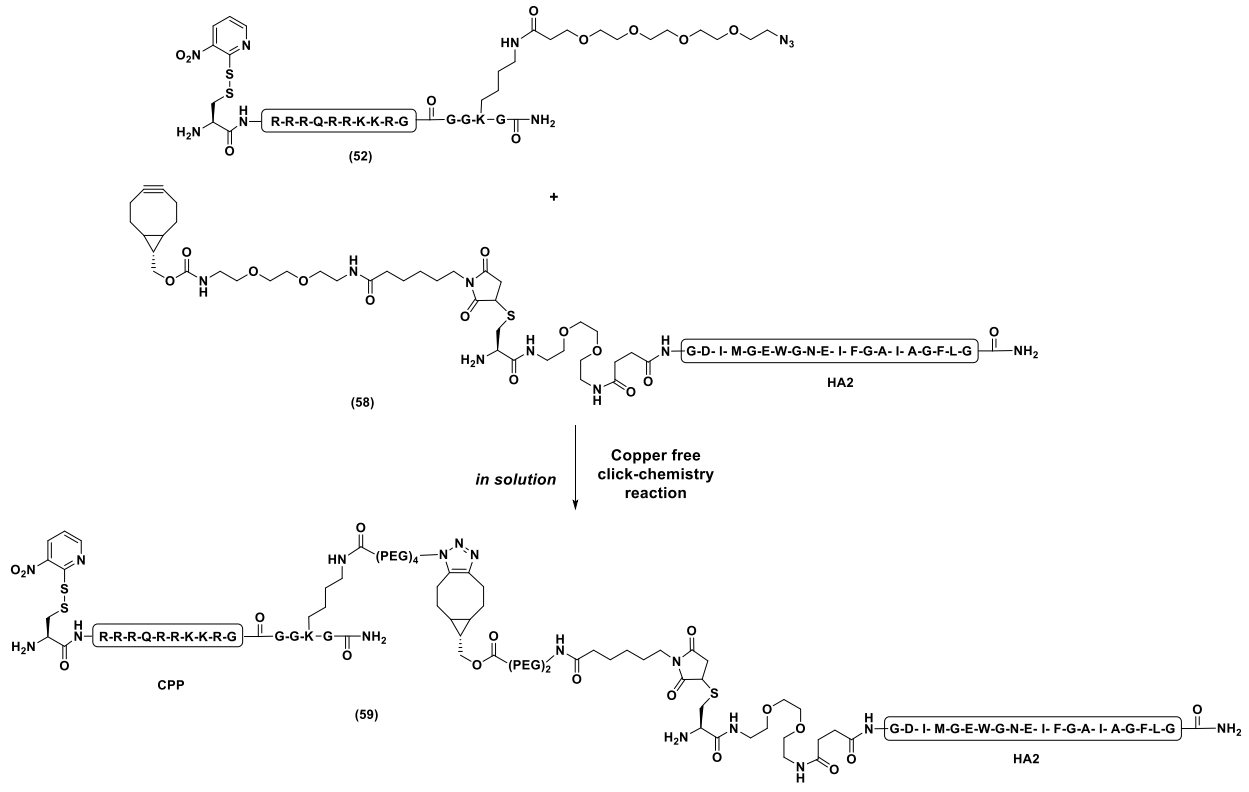

Scheme 4.8. Proposed synthetic route for a fused CPP-HA2 containing peptide **59** equipped with a NPys handle for further conjugation. The key step involves the condensation of two water soluble peptides by means of a well characterized Cu-free cyloaddition reaction under physiological conditions.[142]

4.5.1 Synthetic plan to generate Azide-peptide 52.

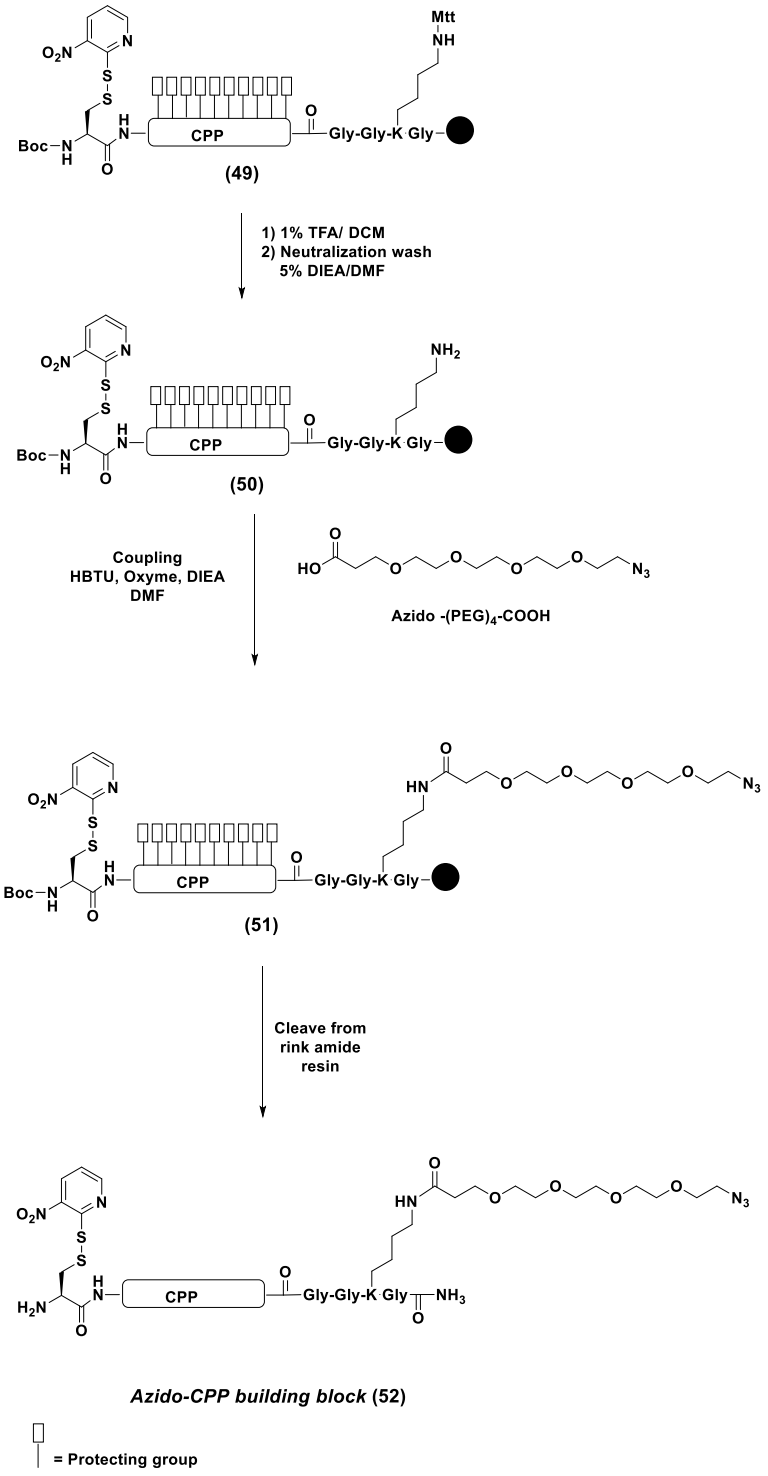

Scheme 4.9. Synthesis of azide building block **52.** Note that all the reagents disclosed in this route are commercially available.

4.5.2 Synthetic plan to generate cyclooctyne-peptide 58.

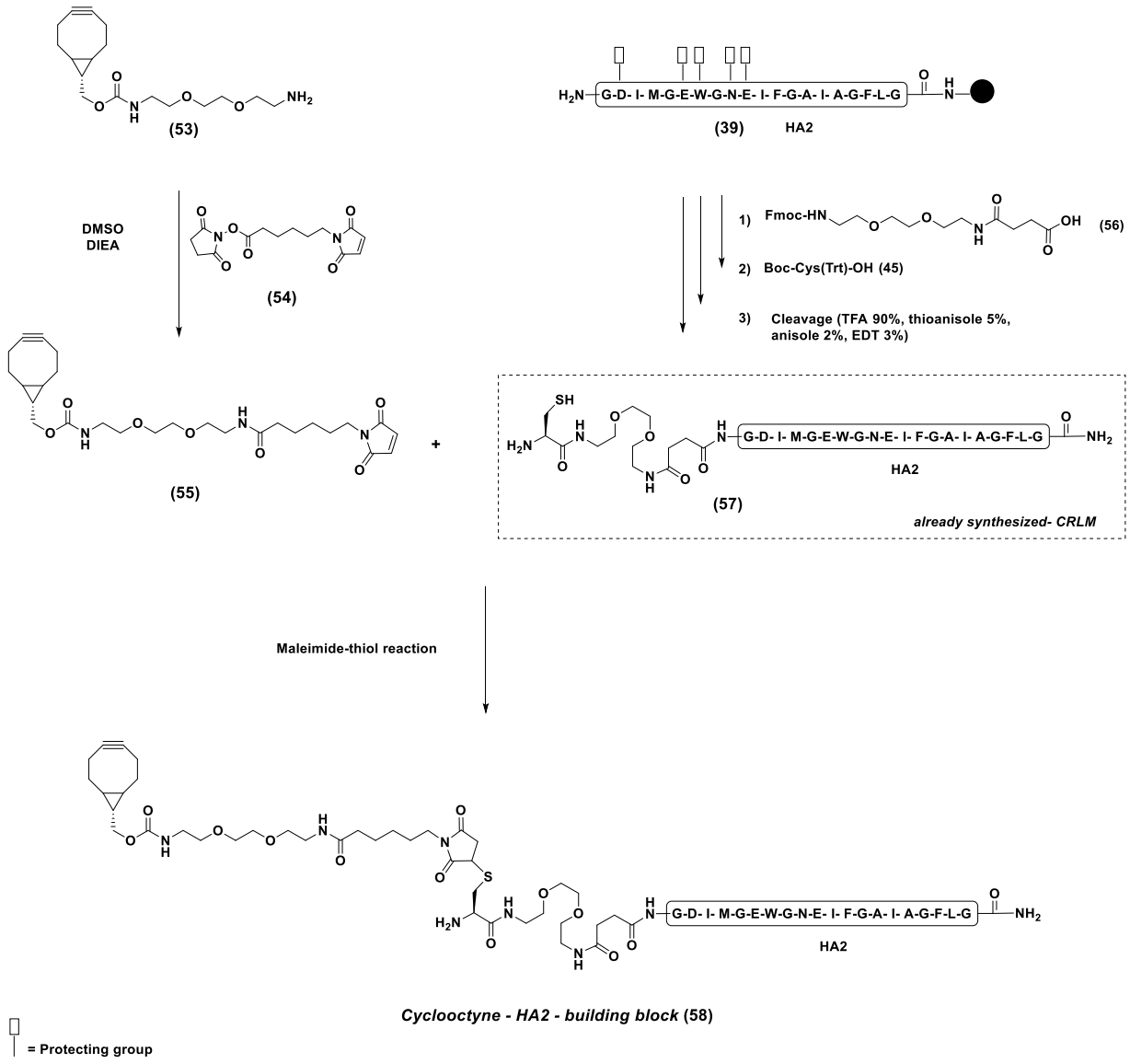

Scheme 4.10. Synthesis of alkyne building block **58**. Note that all the reagents disclosed in this route are commercially available. The HA2 peptide **57** has already been synthesized by our group.

4.6 Motivation to synthesize disulfide-rhodamine FRET acceptor peptide 60

To develop our ratiometric- FRET biosensor (described in chapter 3), it was necessary to synthesize a peptide-based FRET acceptor equipped with a fluorophore capable of absorbing the energy transferred by a green QD donor, thus, the next step was the design of a peptide with the following components: a rhodamine (FRET acceptor) conjugated at the N-terminus, a short peptide linker with a cleavable disulfide bond, and a polyhistidine tag for bioconjugation to the QD surface by affinity coordination. The model we envisioned is shown in **Figure 4.9 a,** and the desired synthetic peptide in **4.9b**.

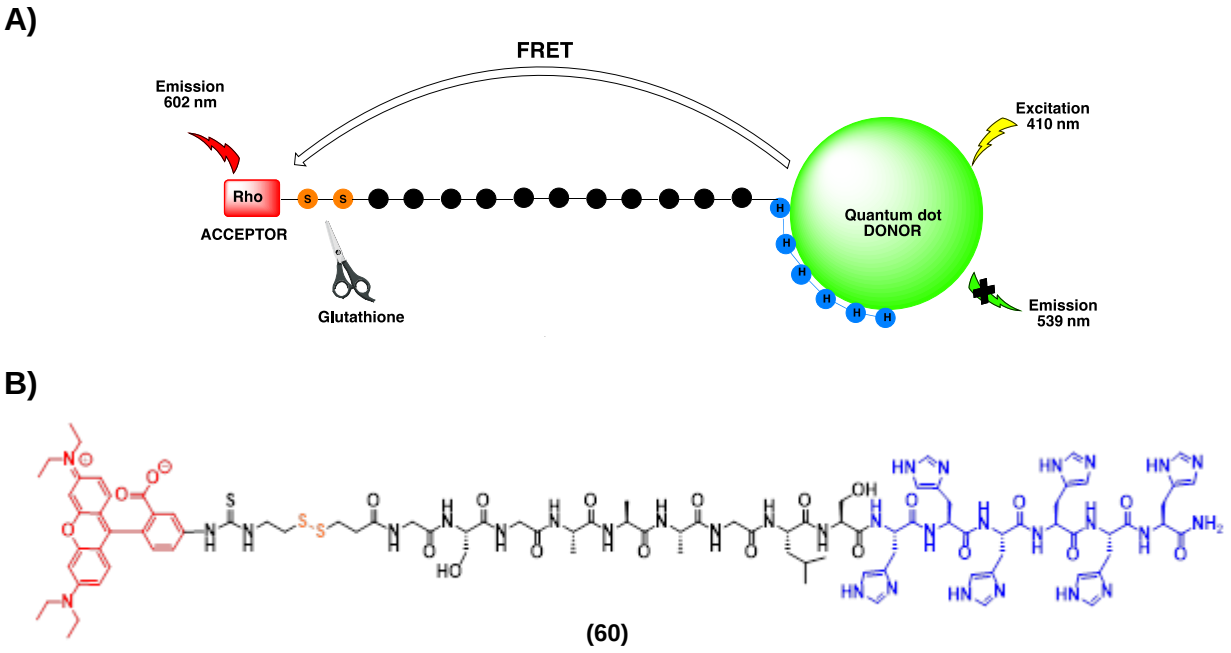

Figure 4.9. A) Features required in a rhodamine FRET acceptor: A rhodamine dye at the N-terminus (red), a cleavable disulfide bond (orange circles), a suitable peptide-based linker (black circles) a polyhistidine tag (blue circles) for affinity coordination on to the QD surface (FRET donor). B) Design of our rhodamine ligand.

4.6.1 Initial strategy: Solution chemistry.

Since we already had several milligrams of pure peptide **59** in hand, we attempted to conjugate it with commercially available rhodamine B isothiocyanate in solution by following standard conjugation protocols for thioamide bond formation. (Figure 4.10).

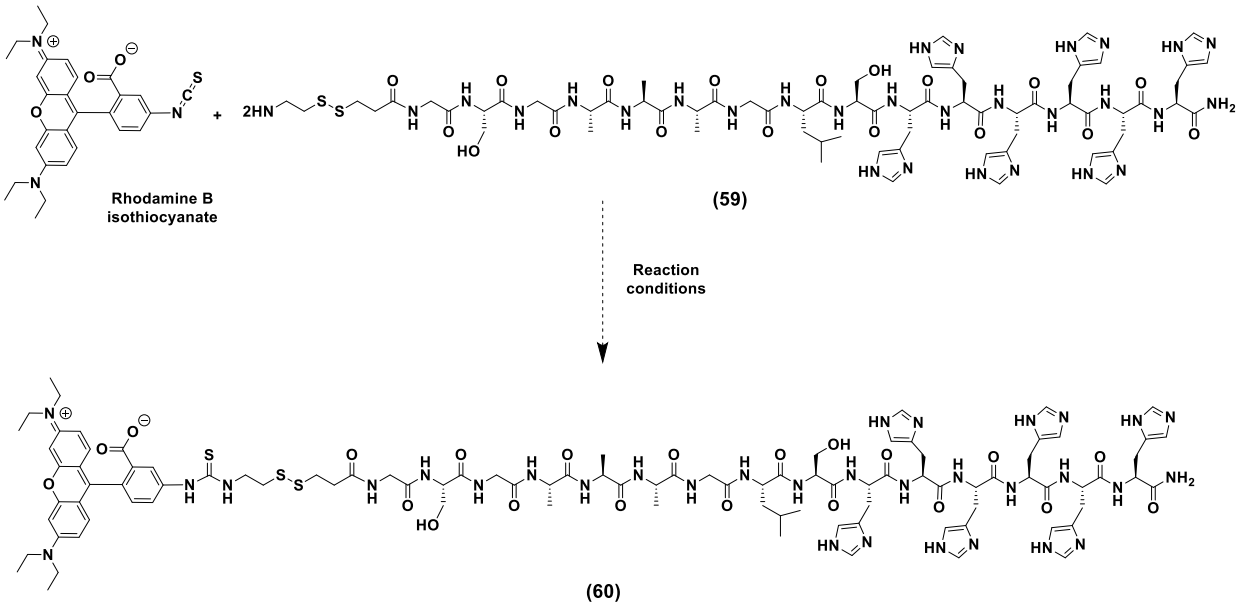

Rxn No.	Scale	Coupling Conditions	Outcome
1	1.19 μmol	Polyhistidine (1.19 μmol, 1.0 equiv), Rhodamine B (11.9 μmol, 10 equiv) DMF/ 24 h / r.t	No reaction
2	1.19 μmol	Polyhistidine (1.19 μmol, 1.0 equiv), Rhodamine B (1.3 μmol, 1.10 equiv) DMAP (1.19 μmol, 1.0 equiv), DMF, 24 h / r.t	No reaction
3	1.19 μmol	Polyhistidine (1.19 μmol, 1.0 equiv), Rhodamine B (1.3 μmol, 1.10 equiv) TEA , DMSO, 24 h / r.t	No reaction

Figure 4.10. Top: Attempted bond forming reaction between rhodamine isothiocyanate and peptide **59** to afford the synthetic target peptide **60**. Bottom: Reaction conditions tested for assembly of peptide **60**.

We monitored each reaction by mass spectrometry and MALDI, and although none of the conditions tested afforded the desired rhodamine-peptide **60**, we consistently observed the same ESI chromatogram upon the analysis of the crude reaction (Figure 4.11).

From left to right in **Figure 4.11**, m/z peaks at 458.4 and 500.5 belong to rhodamine B - isothiocyanate unreacted starting material. Boxed peaks, m/z = 545.2 and 573.1 were found to be new peaks generated in every reaction crude, and they are not the result of instrument background or leftover material from previous samples as we performed several 'washing steps' followed by a blank sample afterwards.

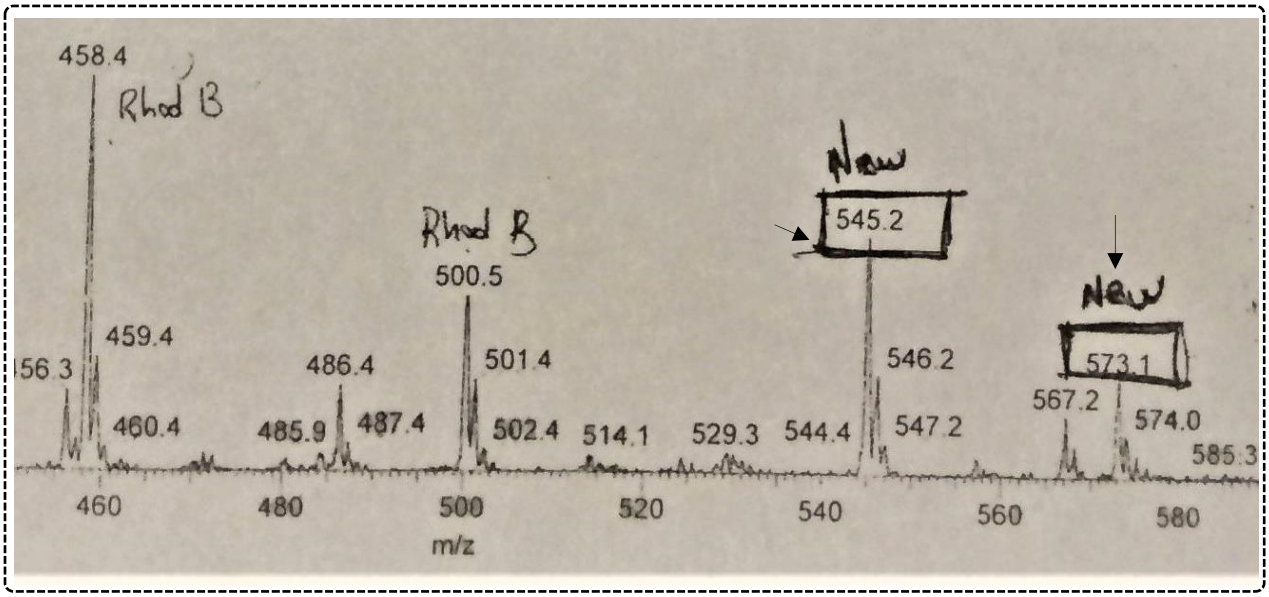

Figure 4.11. A representative MS analysis of a crude reaction to generate peptide **60** shows the presence of two side products (m/z= 542.2 and 573.1).

Also, MALDI analysis revealed in every reaction crude that there was no peptide starting material **59** left, which means that starting material **59** might have decomposed upon

these conditions (the quality of **59** was verified by MALDI before reaction to assure peptide integrity).

We were puzzled by this outcome as isothiocyanate-fluorophores are extensively used to label peptide and proteins in solution, thus, we speculated that maybe the chemical structure of the peptide to be labeled may play a role in the outcome of this bioconjugation reaction.

4.6.2 Possible Edman-like degradation of peptide 60.

Based on a representative MS chromatogram (**Figure 4.11**) we hypothesized the following two plausible degradation pathways (Scheme 4.11). Assuming the desired peptide **60** was assembled in solution, it is possible that nucleophilic attack to C-5 from the neighboring thioamide-sulfur formed compound **62** (Path **A**), while releasing peptide **63**.

We speculated, the generation of **62** might have been driven by formation of the five-membered cycle. Formation of **25** might be explained again by the nucleophilic attack of thioamide-sulfur to sulfur-6 forming a six-membered ring and generating compound **64** while releasing peptide **65**.

Both truncated peptides **62** and **64**, may undergo subsequent degradation reactions in the presence of any rhodamine isothiocyanate excess, to yield more truncated peptides until all the isothiocyanate dye is consumed.

The formation of side products **62** and **64** is supported as their corresponding masses are shown in the MS chromatogram of the reaction crude in **Figure 4.12**.

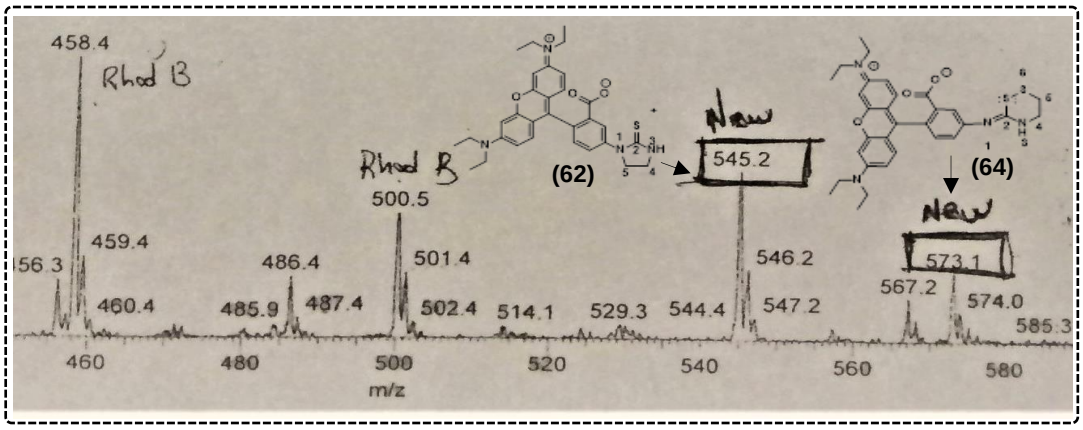

Figure 4.12. Possible chemical structures of side products formed during the assembly of peptide **60** by low resolution ESI-MS.

Note 1:
The instrument was used as it was available without prior calibration.

Note 2:
The calculated exact mass of **62** for $[M+H]^{1+}$= 544.24 (as COOH) and 543.24 (as COO^-).
The calculated exact mass of **64** for $[M+H]^{1+}$= 576.21 (as COOH) and 575.21 (as COO^-).

Thus, the calculated masses for both proposed side products **62** and **64** are slightly off by 2-3 atomic mass units, however, **62** and **64** are only proposed and <u>not</u> definitive structures. To unambiguously determine the structures of **62** and **64**, it would be necessary to isolate them in at least milligram quantities to perform 1D and 2D NMR experiments along with high resolution mass spectrometry studies.

Note 3:
It is hard to predict the ionization state of the purported side products **62** and **64** in the gas phase, therefore it cannot be assured whether the carboxylate or carboxylic acid form would be predominant.

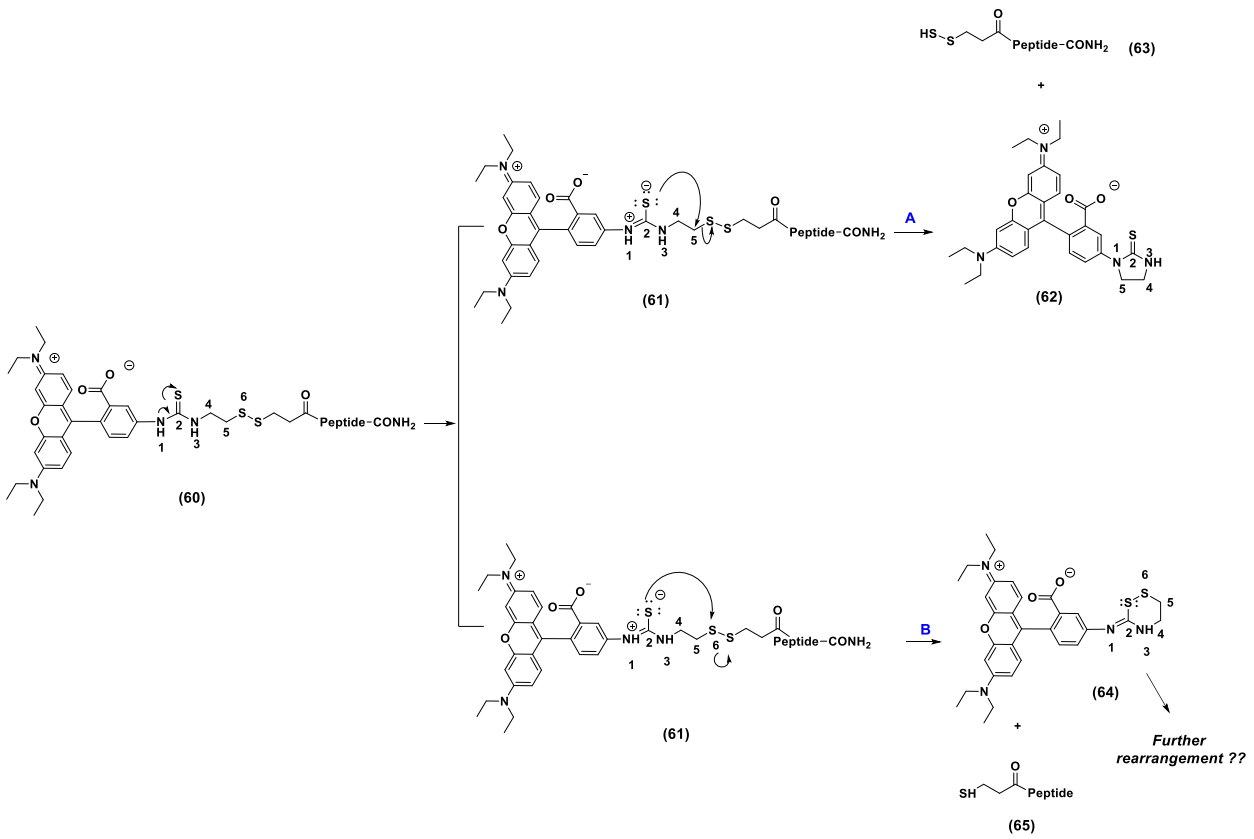

Scheme 4.11. Proposed plausible mechanism for the formation of side-products **62** and **63** by an Edman-like degradation pathway.

We believe that the degradation of our rhodamine disulfide peptide **60** may occur by a mechanism similar to the Edman degradation[143] (**Scheme 4.11**), in which the generation of thiazoline **69** is driven by the formation of a five-member ring when the *N*-terminal residue is an α-amino acid. Upon formation of **69**, peptide **70** is cleaved, and if the last happens to have another α-amino acid at the N-terminus, the cycle repeats until all the thiocyanate is consumed. Thiazolone **69** rapidly isomerizes to the corresponding thiohydantoin **74** derivative.

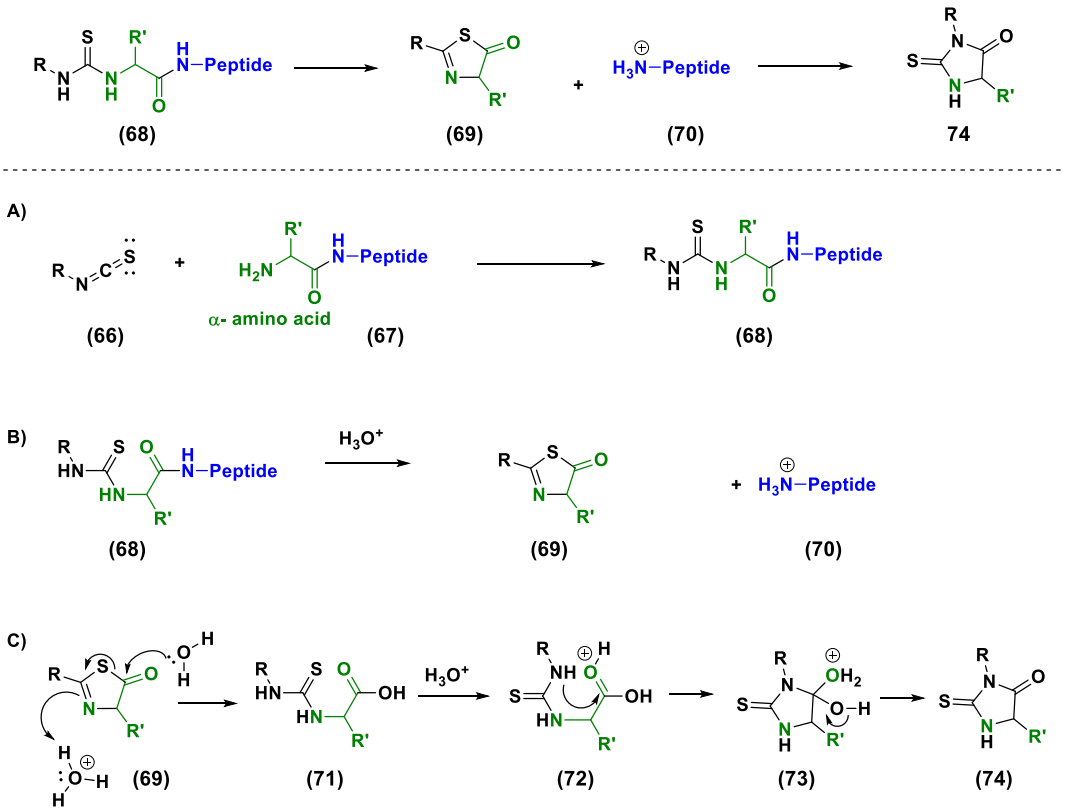

Scheme 4.12. Edman degradation.[143]

Given that the requirement for the Edman degradation is the presence of an α-amino acid at the *N*-terminus, we hypothesized that maybe we could circumvent the similar observed degradation of our rhodamine peptide (Scheme 4.11) by adding a linker between the thioisocyanate and the terminal disulfide amino acid on peptide **59**.

Thus, by adding a linker the thioamide-sulfur would not be able to do a nucleophilic attack on the vicinity of the disulfide bond. Thus, we re-designed the structure of our disulfide rhodamine. The corresponding synthetic route is outlined in the next section.

4.6.3 Adding a linker to avoid disulfide-rhodamine peptide degradation

This time, the synthesis was carried out on solid phase as described on Scheme 4.13. We also used a commercially available PEG linker to improve water solubility as this feature would be crucial for live-cell studies and to avoid using DMSO.

Although incorporating a linker to our rhodamine peptide could solve its early degradation, it was important to also consider the linker length since the goal was to use this rhodamine disulfide peptide as a FRET acceptor. Instead of incorporating a linker, an alternative solution might have been the incorporation of a Fmoc-Lysine (Rhodamine B)-OH amino acid (if it happens to be commercially available).

Also, we avoided using excess amount of rhodamine isothiocyanate, and instead, we used the minimum necessary amount (1.10 equiv) and carried a double coupling. Another crucial detail to improve overall percent yield was the capping (acetylation) step, so that the isothiocyanate dye is not consumed by free unreacted amines. Moreover, the peptide tolerated the cleaving conditions (97% TFA/water). For polyhistidine peptides, TIPS should be avoided if possible.

Fortunately, the new synthetic route shown in scheme 4.13, afforded the desired disulfide rhodamine peptide on rink amide resin without any degradation.

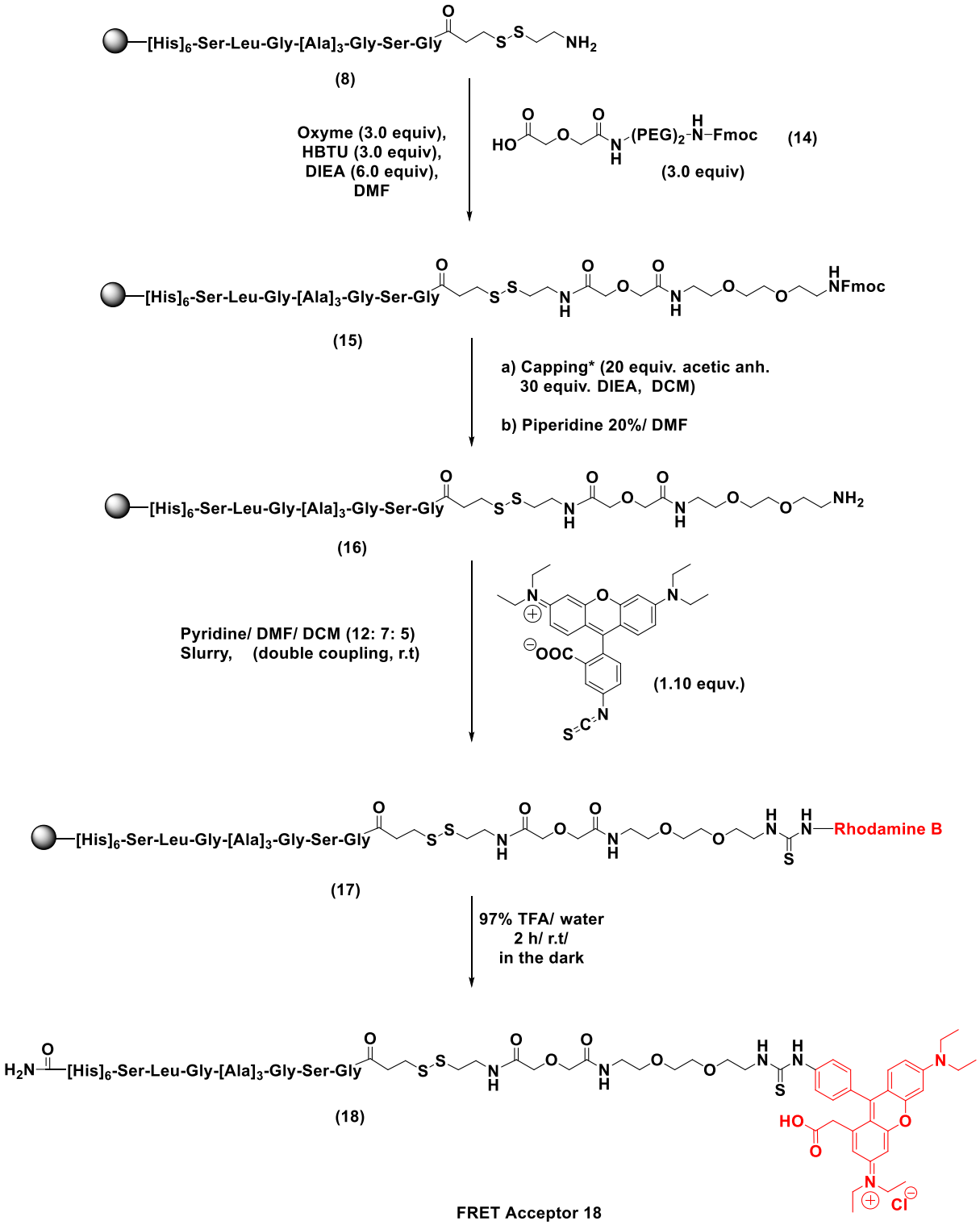

Scheme 4.13. Successful route for the synthesis of Rhodamine B peptide **18** (SPPS). (MS confirmation analysis in chapter 3, scheme 3.2).

4.7 Conclusion

In this chapter I showed the synthetic approaches to assemble a CPP-HA2 fused peptide **35** and the multiple obstacles found along the way. I used solid phase peptide synthesis techniques to generate peptide **35**, through both, a convergent and a stepwise approach. The convergent approach by fragment condensation of protected peptides in solution, has been reported for instance, for the synthesis of the thirty-six amino acid long peptide Enfuvirtide,[144] a membrane fusion inhibitor for the treatment of HIV. Encouraged by this last report, I undertook the task of attempting the fragment condensation of peptides HA2 and CPP (both fully protected) in solution phase as well. Unfortunately, the said condensation did not afford the expected fused peptide **35** under our reaction conditions, mainly due to the poor solubility and high hydrophobicity of the CPP peptide fragment, (fully protected polyarginine or the TAT peptide).

As a lengthy alternative, I tried the conventional stepwise peptide synthesis approach, which afforded the desired fusion peptide **35** in very low yields and with multiple truncated peptides (see Figures 4.6 and 4.7). Cys-TAT-K-HA2 assembly was roughly estimated to be better yielding than the analog Cys-R9-H-HA2 peptide because TAT is easier to assemble on resin, than R9 (due to the bulkiness of the pertinent protecting groups). Finally, for the assembly of the CPP-HA2 fused peptide, I suggested an alternative route in scheme 4.10, which relies on an orthogonal reaction (Copper-free click chemistry reaction) for the fragment condensation of two long and pure peptides, without the need to have any protecting groups on amino acids polar side chains. With the suggested approach in scheme 4.10, there should not be any issues with solubility.

The synthesis of a disulfide rhodamine FRET acceptor **60**, also presented multiple problems in both, solid and solution phase chemistry. I continually observed the decomposition of the peptide starting material **59**, which suggested that an undesired side reaction was taking place during the coupling of **59** and rhodamine isothiocyanate. Based on low resolution mass spectrometry results, I surmised that an Edman-degradation like pathway might have been taking place during the observed undesired decomposition, thus, I added a longer linker (polyethylene glycol) between the disulfide and isothiocyanate functional groups, which solved the problem by avoiding the 5 or 6 membered-ring cyclization to the corresponding degradation products (rational further explained in section 4.6.2) and thus, afforded the desired rhodamine peptide **18** cleanly (scheme 4.13).

Cited literature

1. Bobo, D.; Robinson, K. J.; Islam, J.; Thurecht, K. J.; Corrie, S. R., Nanoparticle-Based Medicines: A Review of FDA-Approved Materials and Clinical Trials to Date. *Pharm Res-Dord* **2016,** *33* (10), 2373-2387.

2. Wegner, K. D.; Hildebrandt, N., Quantum dots: bright and versatile in vitro and in vivo fluorescence imaging biosensors. *Chemical Society Reviews* **2015,** *44* (14), 4792-4834.

3. Jaiswal, J. K.; Goldman, E. R.; Mattoussi, H.; Simon, S. M., Use of quantum dots for live cell imaging. *Nat Methods* **2004,** *1* (1), 73-78.

4. Alivisatos, A. P., Semiconductor clusters, nanocrystals, and quantum dots. *Science* **1996,** *271* (5251), 933-937.

5. Scholes, G. D.; Rumbles, G., Excitons in nanoscale systems. *Nat Mater* **2006,** *5* (9), 683-696.

6. Smith, A. M.; Gao, X. H.; Nie, S. M., Quantum dot nanocrystals for in vivo molecular and cellular imaging. *Photochem Photobiol* **2004,** *80* (3), 377-385.

7. Peng, X. G.; Schlamp, M. C.; Kadavanich, A. V.; Alivisatos, A. P., Epitaxial growth of highly luminescent CdSe/CdS core/shell nanocrystals with photostability and electronic accessibility. *Journal of the American Chemical Society* **1997,** *119* (30), 7019-7029.

8. Dabbousi, B. O.; RodriguezViejo, J.; Mikulec, F. V.; Heine, J. R.; Mattoussi, H.; Ober, R.; Jensen, K. F.; Bawendi, M. G., (CdSe)ZnS core-shell quantum dots: Synthesis and characterization of a size series of highly luminescent nanocrystallites. *Journal of Physical Chemistry B* **1997,** *101* (46), 9463-9475.

9. Wang, Y., Luminescent CdTe and CdSe semiconductor nanocrystals: Preparation, optical properties and applications. *J Nanosci Nanotechno* **2008,** *8* (3), 1068-1091.

10. Talapin, D. V.; Haubold, S.; Rogach, A. L.; Kornowski, A.; Haase, M.; Weller, H., A novel organometallic synthesis of highly luminescent CdTe nanocrystals. *Journal of Physical Chemistry B* **2001,** *105* (12), 2260-2263.

11. Medintz, I. H., Niko *FRET - Förster resonance energy transfer : from theory to applications*. Wiley-VCH Verlag GmbH & Co. KGaA: 2014.

12. Held, P. An Introduction to Fluorescence Resonance Energy Transfer (FRET) Technology and its Application in Bioscience. http://www.labautopedia.org/mw.

13. Förster, T., Intermolecular Energy Migration and Fluorescence. *Annals of Physics* **1948,** *2*.

14. Delehanty, J. B.; Bradburne, C. E.; Medintz, I. L.; Farrell, D.; Pons, T.; Deschamps, J. R.; Brunel, F. M.; Dawson, P. E.; Mattoussi, H., Intracellular delivery of and sensing with quantum dot bioconjugates. *Proc. SPIE* **2009,** *7189* (Colloidal Quantum Dots for Biomedical Applications IV), 71890W/1-71890W/8.

15. Qiu, X.; Guo, J.; Jin, Z.; Petreto, A.; Medintz, I. L.; Hildebrandt, N., Multiplexed Nucleic Acid Hybridization Assays Using Single-FRET-Pair Distance-Tuning. *Small* **2017,** *13* (25), n/a.

16. Algar, W. R.; Medintz, I. L., Concentric energy transfer with quantum dots for multiplexed biosensing. *Nano Rev.* **2013,** *4*, 22428/1-22428/1, 1 pp.

17. Algar, W. R.; Ancona, M. G.; Malanoski, A. P.; Susumu, K.; Medintz, I. L., Assembly of a Concentric Foerster Resonance Energy Transfer Relay on a Quantum Dot Scaffold: Characterization and Application to Multiplexed Protease Sensing. *ACS Nano* **2012,** *6* (12), 11044-11058.

18. Algar, W. R.; Wegner, D.; Huston, A. L.; Blanco-Canosa, J. B.; Stewart, M. H.; Armstrong, A.; Dawson, P. E.; Hildebrandt, N.; Medintz, I. L., Quantum Dots as Simultaneous Acceptors and Donors in Time-Gated Forster Resonance Energy Transfer Relays: Characterization and Biosensing. *J. Am. Chem. Soc.* **2012,** *134* (3), 1876-1891.

19. Jennings, T. L.; Becker-Catania, S. G.; Triulzi, R. C.; Tao, G.; Scott, B.; Sapsford, K. E.; Spindel, S.; Oh, E.; Jain, V.; Delehanty, J. B.; Prasuhn, D. E.; Boeneman, K.; Algar, W. R.; Medintz, I. L., Reactive Semiconductor Nanocrystals for Chemoselective Biolabeling and Multiplexed Analysis. *ACS Nano* **2011,** *5* (7), 5579-5593.

20. Biju, V.; Itoh, T.; Ishikawa, M., Delivering quantum dots to cells: bioconjugated quantum dots for targeted and nonspecific extracellular and intracellular imaging. *Chem. Soc. Rev.* **2010,** *39* (8), 3031-3056.

21. Shamirian, A.; Ghai, A.; Snee, P. T., QD-Based FRET Probes at a Glance. *Sensors* **2015,** *15* (6), 13028-13051.

22. Boeneman, K.; Deschamps, J. R.; Buckhout-White, S.; Prasuhn, D. E.; Blanco-Canosa, J. B.; Dawson, P. E.; Stewart, M. H.; Susumu, K.; Goldman, E. R.; Ancona, M.; Medintz, I. L., Quantum Dot DNA Bioconjugates: Attachment Chemistry Strongly Influences the Resulting Composite Architecture. *ACS Nano* **2010,** *4* (12), 7253-7266.

23. Prasuhn, D. E.; Blanco-Canosa, J.; Susumu, K.; Vora, G. J.; Delehanty, J. B.; Mattoussi, H.; Dawson, P. E.; Medintz, I. L. In *Multivalent display of biomolecules on semiconductor quantum dots utilizing an aniline-mediated chemoselective ligation*, American Chemical Society: 2009; pp COLL-450.

24. Prasuhn, D. E.; Blanco-Canosa, J. B.; Vora, G. J.; Mattoussi, H. M.; Dawson, P. E.; Medintz, I. L., Multivalent display of DNA conjugates on semiconductor quantum dots utilizing a novel conjugation method. *Proc. SPIE* **2009,** *7189* (Colloidal Quantum Dots for Biomedical Applications IV), 71890I/1-71890I/7.

25. Boeneman, K.; Delehanty, J. B.; Susumu, K.; Stewart, M. H.; Medintz, I. L., Intracellular Bioconjugation of Targeted Proteins with Semiconductor Quantum Dots. *J. Am. Chem. Soc.* **2010,** *132* (17), 5975-5977.

26. Prasuhn, D. E.; Blanco-Canosa, J. B.; Vora, G. J.; Delehanty, J. B.; Susumu, K.; Mei, B. C.; Dawson, P. E.; Medintz, I. L., Combining Chemoselective Ligation with Polyhistidine-Driven Self-Assembly for the Modular Display of Biomolecules on Quantum Dots. *ACS Nano* **2010,** *4* (1), 267-278.

27. Prasuhn, D. E.; Deschamps, J. R.; Susumu, K.; Stewart, M. H.; Boeneman, K.; Blanco-Canosa, J. B.; Dawson, P. E.; Medintz, I. L., Polyvalent Display and Packing of Peptides and Proteins on Semiconductor Quantum Dots: Predicted Versus Experimental Results. *Small* **2010,** *6* (4), 555-564.

28. Algar, W. R.; Prasuhn, D. E.; Stewart, M. H.; Jennings, T. L.; Blanco-Canosa, J. B.; Dawson, P. E.; Medintz, I. L., The Controlled Display of Biomolecules on Nanoparticles: A Challenge Suited to Bioorthogonal Chemistry. *Bioconjugate Chem.* **2011,** *22* (5), 825-858.

29. Prasuhn, D. E.; Susumu, K.; Medintz, I. L., Multivalent conjugation of peptides, proteins and DNA to semiconductor quantum dots. *Methods Mol. Biol. (N. Y., NY, U. S.)* **2011,** *726* (Biomedical Nanotechnology), 95-110.

30. Blanco-Canosa, J. B.; Wu, M.; Susumu, K.; Petryayeva, E.; Jennings, T. L.; Dawson, P. E.; Algar, W. R.; Medintz, I. L., Recent progress in the bioconjugation of quantum dots. *Coord. Chem. Rev.* **2014,** *263-264*, 101-137.

31. Walper, S. A.; Turner, K. B.; Medintz, I. L., Enzymatic bioconjugation of nanoparticles: developing specificity and control. *Curr. Opin. Biotechnol.* **2015,** *34*, 232-241.

32. Breger, J.; Delehanty, J. B.; Medintz, I. L., Continuing progress toward controlled intracellular delivery of semiconductor quantum dots. *Wiley Interdiscip. Rev.: Nanomed. Nanobiotechnol.* **2015,** *7* (2), 131-151.

33. Sapsford, K. E.; Pons, T.; Medintz, I. L.; Higashiya, S.; Brunel, F. M.; Dawson, P. E.; Mattoussi, H., Kinetics of Metal-Affinity Driven Self-Assembly between Proteins or Peptides and CdSe-ZnS Quantum Dots. *J. Phys. Chem. C* **2007,** *111* (31), 11528-11538.

34. Duane E. Prasuhn, K. S., and Igor L. Medintz, Multivalent Conjugation of Peptides, Proteins, and DNA to Semiconductor Quantum Dots. In *Biomedical Nanotechnology: Methods and Protocols, Methods in Molecular Biology*, Science, S., Ed. 2011; Vol. 726, pp 95-110.

35. Medintz, I. L.; Uyeda, H. T.; Goldman, E. R.; Mattoussi, H., Quantum dot bioconjugates for imaging, labelling and sensing. *Nat. Mater.* **2005,** *4* (6), 435-446.

36. Medintz, I. L.; Mattoussi, H., Quantum dot-based resonance energy transfer and its growing application in biology. *Phys. Chem. Chem. Phys.* **2009,** *11* (1), 17-45.

37. Berti, L.; D'Agostino, P. S.; Boeneman, K.; Medintz, I. L., Improved peptidyl linkers for self-assembly of semiconductor quantum dot bioconjugates. *Nano Res.* **2009,** *2* (2), 121-129.

38. Sapsford, K. E.; Pons, T.; Medintz, I. L.; Mattoussi, H., Biosensing with luminescent semiconductor quantum dots. *Sensors* **2006,** *6* (8), 925-953.

39. Huotari, J.; Helenius, A., Endosome maturation. *The EMBO Journal* **2011,** *30* (17), 3481-3500.

40. Canton, I.; Battaglia, G., Endocytosis at the nanoscale. *Chemical Society Reviews* **2012,** *41* (7), 2718-2739.

41. Nazarenus, M.; Zhang, Q.; Soliman, M. G.; del Pino, P.; Pelaz, B.; Carregal-Romero, S.; Rejman, J.; Rothen-Rutishauser, B.; Clift, M. J. D.; Zellner, R.; Nienhaus, G. U.; Delehanty, J. B.; Medintz, I. L.; Parak, W. J., In vitro interaction of colloidal nanoparticles with mammalian cells: what have we learned thus far? *Beilstein J. Nanotechnol.* **2014,** *5*, 1477-1490, 14 pp.

42. Sahay, G.; Alakhova, D. Y.; Kabanov, A. V., Endocytosis of nanomedicines. *J Control Release* **2010,** *145* (3), 182-195.

43. Sorkin, A.; von Zastrow, M., Endocytosis and signalling: intertwining molecular networks. *Nature Reviews Molecular Cell Biology* **2009,** *10* (9), 609-622.

44. Iversen, T. G.; Skotland, T.; Sandvig, K., Endocytosis and intracellular transport of nanoparticles: Present knowledge and need for future studies. *Nano Today* **2011,** *6* (2), 176-185.

45. Kumari, S.; Swetha, M. G.; Mayor, S., Endocytosis unplugged: multiple ways to enter the cell. *Cell Research* **2010,** *20* (3), 256-275.

46. Kastl, L.; Sasse, D.; Wulf, V.; Hartmann, R.; Mircheski, J.; Ranke, C.; Carregal-Romero, S.; Martínez-López, J. A.; Fernández-Chacón, R.; Parak, W. J.; Elsasser, H.-P.; Rivera_Gil, P., Multiple Internalization Pathways of Polyelectrolyte Multilayer Capsules into Mammalian Cells. *ACS Nano* **2013,** *7* (8), 6605-6618.

47. Delehanty, J. B.; Mattoussi, H.; Medintz, I. L., Delivering quantum dots into cells: strategies, progress and remaining issues. *Anal. Bioanal. Chem.* **2009,** *393* (4), 1091-1105.

48. Delehanty, J. B.; Bradburne, C. E.; Boeneman, K.; Susumu, K.; Farrell, D.; Mei, B. C.; Blanco-Canosa, J. B.; Dawson, G.; Dawson, P. E.; Mattoussi, H.; Medintz, I. L., Delivering quantum dot-peptide bioconjugates to the cellular cytosol: escaping from the endolysosomal system. *Integr. Biol.* **2010,** *2* (5-6), 265-277.

49. El-Sayed, A.; Futaki, S.; Harashima, H., Delivery of Macromolecules Using Arginine-Rich Cell-Penetrating Peptides: Ways to Overcome Endosomal Entrapment. *Aaps Journal* **2009,** *11* (1), 13-22.

50. Fonseca, S. B.; Pereira, M. P.; Kelley, S. O., Recent advances in the use of cell-penetrating peptides for medical and biological applications. *Adv Drug Deliver Rev* **2009,** *61* (11), 953-964.

51. Selby, L. I.; Cortez-Jugo, C. M.; Such, G. K.; Johnston, A. P. R., Nanoescapology: progress toward understanding the endosomal escape of polymeric nanoparticles. *Wiley Interdiscip Rev Nanomed Nanobiotechnol* **2017,** *9* (5).

52. Christoforidis, S.; McBride, H. M.; Burgoyne, R. D.; Zerial, M., The Rab5 effector EEA1 is a core component of endosome docking. *Nature* **1999,** *397* (6720), 621-625.

53. Beyenbach, K. W.; Wieczorek, H., The V-type H⁺ ATPase: molecular structure and function, physiological roles and regulation. *Journal of Experimental Biology* **2006,** *209* (4), 577-589.

54. Casey, J. R.; Grinstein, S.; Orlowski, J., Sensors and regulators of intracellular pH. *Nat Rev Mol Cell Biol* **2010,** *11* (1), 50-61.

55. Sheff, D. R.; Daro, E. A.; Hull, M.; Mellman, I., The Receptor Recycling Pathway Contains Two Distinct Populations of Early Endosomes with Different Sorting Functions. *The Journal of Cell Biology* **1999,** *145* (1), 123-139.

56. Lübke, T.; Lobel, P.; Sleat, D. E., Proteomics of the lysosome. *Biochimica et Biophysica Acta (BBA) - Molecular Cell Research* **2009,** *1793* (4), 625-635.

57. Pinto-González Howell, D.; Krieser, R. J.; Eastman, A.; Barry, M. A., Deoxyribonuclease II is a lysosomal barrier to transfection. *Mol Ther* **2003,** *8* (6), 957-963.

58. Selby, L. I.; Cortez-Jugo, C. M.; Such, G. K.; Johnston, A. P., Nanoescapology: progress toward understanding the endosomal escape of polymeric nanoparticles. *Wiley Interdiscip Rev Nanomed Nanobiotechnol* **2017**.

59. Patil, M. L.; Zhang, M.; Taratula, O.; Garbuzenko, O. B.; He, H. X.; Minko, T., Internally Cationic Polyamidoamine PAMAM-OH Dendrimers for siRNA Delivery: Effect of the Degree of Quaternization and Cancer Targeting. *Biomacromolecules* **2009,** *10* (2), 258-266.

60. Behr, J. P., The proton sponge: A trick to enter cells the viruses did not exploit. *Chimia* **1997,** *51* (1-2), 34-36.

61. Zhang, B. Q.; Mallapragada, S., The mechanism of selective transfection mediated by pentablock copolymers; Part II: Nuclear entry and endosomal escape. *Acta Biomater* **2011,** *7* (4), 1580-1587.

62. Cufí, S.; Vazquez-Martin, A.; Oliveras-Ferraros, C.; Corominas-Faja, B.; Cuyàs, E.; López-Bonet, E.; Martin-Castillo, B.; Joven, J.; Menendez, J. A., The anti-malarial chloroquine overcomes Primary resistance and restores sensitivity to Trastuzumab in HER2-positive breast cancer. **2013,** *3*, 2469.

63. Funhoff, A. M.; van Nostrum, C. F.; Koning, G. A.; Schuurmans-Nieuwenbroek, N. M. E.; Crommelin, D. J. A.; Hennink, W. E., Endosomal escape of polymeric gene delivery complexes is not always enhanced by polymers buffering at low pH. *Biomacromolecules* **2004,** *5* (1), 32-39.

64. Massignani, M.; LoPresti, C.; Blanazs, A.; Madsen, J.; Armes, S. P.; Lewis, A. L.; Battaglia, G., Controlling Cellular Uptake by Surface Chemistry, Size, and Surface Topology at the Nanoscale. *Small* **2009,** *5* (21), 2424-2432.

65. Lomas, H.; Massignani, M.; Abdullah, K. A.; Canton, I.; Lo Presti, C.; MacNeil, S.; Du, J. Z.; Blanazs, A.; Madsen, J.; Armes, S. P.; Lewis, A. L.; Battaglia, G., Non-cytotoxic polymer vesicles for rapid and efficient intracellular delivery. *Faraday Discuss.* **2008,** *139*, 143-159.

66. White, J. M.; Whittaker, G. R., Fusion of Enveloped Viruses in Endosomes. *Traffic* **2016,** *17* (6), 593-614.

67. Zelphati, O.; Szoka, F. C., Mechanism of oligonucleotide release from cationic liposomes. *P Natl Acad Sci USA* **1996,** *93* (21), 11493-11498.

68. Koltover, I.; Salditt, T.; Rädler, J. O.; Safinya, C. R., An Inverted Hexagonal Phase of Cationic Liposome-DNA Complexes Related to DNA Release and Delivery. *Science* **1998,** *281* (5373), 78-81.

69. Jones, R. A.; Cheung, C. Y.; Black, F. E.; Zia, J. K.; Stayton, P. S.; Hoffman, A. S.; Wilson, M. R., Poly(2-alkylacrylic acid) polymers deliver molecules to the cytosol by pH-sensitive disruption of endosomal vesicles. *Biochem J* **2003,** *372*, 65-75.

70. Nakase, I.; Kobayashi, S.; Futaki, S., Endosome-Disruptive Peptides for Improving Cytosolic Delivery of Bioactive Macromolecules. *Biopolymers* **2010,** *94* (6), 763-770.

71. Li, W. J.; Nicol, F.; Szoka, F. C., GALA: a designed synthetic pH-responsive amphipathic peptide with applications in drug and gene delivery. *Adv Drug Deliver Rev* **2004,** *56* (7), 967-985.

72. Danial, M.; Perrier, S.; Jolliffe, K. A., Effect of the amino acid composition of cyclic peptides on their self-assembly in lipid bilayers. *Org Biomol Chem* **2015,** *13* (8), 2464-2473.

73. Qian, S.; Wang, W. C.; Yang, L.; Huang, H. W., Structure of the alamethicin pore reconstructed by x-ray diffraction analysis. *Biophys J* **2008,** *94* (9), 3512-3522.

74. Tian, W. D.; Ma, Y. Q., Insights into the endosomal escape mechanism via investigation of dendrimer-membrane interactions. *Soft Matter* **2012,** *8* (23), 6378-6384.

75. Leroueil, P. R.; Berry, S. A.; Duthie, K.; Han, G.; Rotello, V. M.; McNerny, D. Q.; Baker, J. R.; Orr, B. G.; Holl, M. M. B., Wide varieties of cationic nanoparticles induce defects in supported lipid bilayers. *Nano Lett* **2008,** *8* (2), 420-424.

76. Hong, S. P.; Leroueil, P. R.; Janus, E. K.; Peters, J. L.; Kober, M. M.; Islam, M. T.; Orr, B. G.; Baker, J. R.; Holl, M. M. B., Interaction of polycationic polymers with supported lipid bilayers and cells: Nanoscale hole formation and enhanced membrane permeability. *Bioconjugate Chem* **2006,** *17* (3), 728-734.

77. Kichler, A.; Leborgne, C.; Coeytaux, E.; Danos, O., Polyethylenimine-mediated gene delivery: a mechanistic study. *The Journal of Gene Medicine* **2001,** *3* (2), 135-144.

78. Suma, T.; Miyata, K.; Anraku, Y.; Watanabe, S.; Christie, R. J.; Takemoto, H.; Shioyama, M.; Gouda, N.; Ishii, T.; Nishiyama, N.; Kataoka, K., Smart Multilayered Assembly for Biocompatible siRNA Delivery Featuring Dissolvable Silica, Endosome-Disrupting Polycation, and Detachable PEG. *ACS Nano* **2012,** *6* (8), 6693-6705.

79. Maier, K.; Martin, I.; Wagner, E., Sequence defined disulfide-linked shuttle for strongly enhanced intracellular protein delivery. *Mol Pharmaceut* **2012,** *9* (12), 3560-3568.

80. Yuba, E.; Kojima, C.; Harada, A.; Tana; Watarai, S.; Kono, K., pH-Sensitive fusogenic polymer-modified liposomes as a carrier of antigenic proteins for activation of cellular immunity. *Biomaterials* **2010,** *31* (5), 943-951.

81. Hama, S.; Akita, H.; Ito, R.; Mizuguchi, H.; Hayakawa, T.; Harashima, H., Quantitative Comparison of Intracellular Trafficking and Nuclear Transcription between Adenoviral and Lipoplex Systems. *Mol Ther* **2006,** *13* (4), 786-794.

82. Gilleron, J.; Querbes, W.; Zeigerer, A.; Borodovsky, A.; Marsico, G.; Schubert, U.; Manygoats, K.; Seifert, S.; Andree, C.; Stoter, M.; Epstein-Barash, H.; Zhang, L.; Koteliansky, V.; Fitzgerald, K.; Fava, E.; Bickle, M.; Kalaidzidis, Y.; Akinc, A.; Maier, M.; Zerial, M., Image-based analysis of lipid nanoparticle-mediated siRNA delivery, intracellular trafficking and endosomal escape. *Nat Biotech* **2013,** *31* (7), 638-646.

83. Manunta, M.; Izzo, L.; Duncan, R.; Jones, A. T., Establishment of subcellular fractionation techniques to monitor the intracellular fate of polymer therapeutics II. Identification of endosomal and lysosomal compartments in HepG2 cells combining single-step subcellular fractionation with fluorescent imaging. *J Drug Target* **2007,** *15* (1), 37-50.

84. M Colin, M. M., G Trugnan, M Kornprobst, R P Harbottle, A Knight, R G Cooper, A D Miller, J Capeau, C Coutelle and M C Brahimi-Horn, Cell delivery, intracellular trafficking and expression of an integrin-mediated gene transfer vector in tracheal epithelial cells. *Gene Ther* **2000,** *7* (2), 139-152.

85. Richardson, S. C. W.; Pattrick, N. G.; Lavignac, N.; Ferruti, P.; Duncan, R., Intracellular fate of bioresponsive poly(amidoamine)s in vitro and in vivo. *J Control Release* **2010,** *142* (1), 78-88.

86. Mellert, K.; Lamla, M.; Scheffzek, K.; Wittig, R.; Kaufmann, D., Enhancing Endosomal Escape of Transduced Proteins by Photochemical Internalisation. *Plos One* **2012,** *7* (12), e52473.

87. JONES, R. A.; CHEUNG, C. Y.; BLACK, F. E.; ZIA, J. K.; STAYTON, P. S.; HOFFMAN, A. S.; WILSON, M. R., Poly(2-alkylacrylic acid) polymers deliver molecules to the cytosol by pH-sensitive disruption of endosomal vesicles. *Biochem J* **2003,** *372* (1), 65-75.

88. Basha, G.; Novobrantseva, T. I.; Rosin, N.; Tam, Y. Y. C.; Hafez, I. M.; Wong, M. K.; Sugo, T.; Ruda, V. M.; Qin, J.; Klebanov, B.; Ciufolini, M.; Akinc, A.; Tam, Y. K.; Hope, M. J.; Cullis, P. R., Influence of Cationic Lipid Composition on Gene Silencing Properties of Lipid Nanoparticle Formulations of siRNA in Antigen-Presenting Cells. *Mol Ther* **2011,** *19* (12), 2186-2200.

89. Benjaminsen, R. V.; Mattebjerg, M. A.; Henriksen, J. R.; Moghimi, S. M.; Andresen, T. L., The Possible Proton Sponge Effect of Polyethylenimine (PEI) Does Not Include Change in Lysosomal pH. *Mol Ther* **2013,** *21* (1), 149-157.

90. Martens, T. F.; Remaut, K.; Demeester, J.; De Smedt, S. C.; Braeckmans, K., Intracellular delivery of nanomaterials: How to catch endosomal escape in the act. *Nano Today* **2014,** *9* (3), 344-364.

91. Garaiova, Z.; Strand, S. P.; Reitan, N. K.; Lélu, S.; Størset, S. Ø.; Berg, K.; Malmo, J.; Folasire, O.; Bjørkøy, A.; de L. Davies, C., Cellular uptake of DNA–chitosan nanoparticles: The role of clathrin- and caveolae-mediated pathways. *International Journal of Biological Macromolecules* **2012,** *51* (5), 1043-1051.

92. Serda, R. E.; Mack, A.; van de Ven, A. L.; Ferrati, S.; Dunner, K.; Godin, B.; Chiappini, C.; Landry, M.; Brousseau, L.; Liu, X.; Bean, A. J.; Ferrari, M., Logic-Embedded Vectors for Intracellular Partitioning, Endosomal Escape, and Exocytosis of Nanoparticles. *Small* **2010,** *6* (23), 2691-2700.

93. Mohandessi, S.; Rajendran, M.; Magda, D.; Miller, L. W., Cell-Penetrating Peptides as Delivery Vehicles for a Protein-Targeted Terbium Complex. *Chemistry - A European Journal* **2012,** *18* (35), 10825-10829.

94. Petryayeva, E.; Algar, W. R.; Medintz, I. L., Quantum dots in bioanalysis: a review of applications across various platforms for fluorescence spectroscopy and imaging. *Appl. Spectrosc.* **2013,** *67* (3), 215-252.

95. Afsari, H. S.; Dos Santos, M. C.; Linden, S.; Chen, T.; Qiu, X.; Henegouwen, P.; Jennings, T. L.; Susumu, K.; Medintz, I. L.; Hildebrandt, N.; Miller, L. W., Time-gated

FRET nanoassemblies for rapid and sensitive intra- and extracellular fluorescence imaging. *Science Advances* **2016,** *2* (6).

96. Shamirian, A.; Afsari, H. S.; Hassan, A.; Miller, L. W.; Snee, P. T., In Vitro Detection of Hypoxia Using a Ratiometric Quantum Dot-Based Oxygen Sensor. *Acs Sensors* **2016,** *1* (10), 1244-1250.

97. Shamirian, A.; Afsari, H. S.; Wu, D. H.; Miller, L. W.; Snee, P. T., Ratiometric QD-FRET Sensing of Aqueous H2S in Vitro. *Anal Chem* **2016,** *88* (11), 6050-6056.

98. Medintz, I. L.; Pons, T.; Delehanty, J. B.; Susumu, K.; Dawson, P. E.; Mattoussi, H., Assembly and intracellular delivery of quantum dot-fluorescent protein bio-conjugates. *Proc. SPIE* **2008,** *6866* (Colloidal Quantum Dots for Biomedical Applications III), 68660B/1-68660B/10.

99. Delehanty, J. B.; Medintz, I. L.; Pons, T.; Brunel, F. M.; Dawson, P. E.; Mattoussi, H., Self-Assembled Quantum Dot-Peptide Bioconjugates for Selective Intracellular Delivery. *Bioconjugate Chem.* **2006,** *17* (4), 920-927.

100. Martin, I.; Teixido, M.; Giralt, E., Intracellular fate of peptide-mediated delivered cargoes. *Curr. Pharm. Des.* **2013,** *19* (16), 2924-2942.

101. Boeneman Gemmill, K.; Delehanty, J. B.; Stewart, M. H.; Susumu, K.; Blanco-Canosa, J. B.; Dawson, P. E.; Huston, A.; Medintz, I., Further progress in cytosolic cellular delivery of quantum dots. *Proc. SPIE* **2012,** *8232* (Colloidal Nanocrystals for Biomedical Applications VII), 82320B/1-82320B/7.

102. Delehanty, J. B.; Bradburne, C. E.; Susumu, K.; Boeneman, K.; Mei, B. C.; Farrell, D.; Blanco-Canosa, J. B.; Dawson, P. E.; Mattoussi, H.; Medintz, I. L., Spatiotemporal Multicolor Labeling of Individual Cells Using Peptide-Functionalized Quantum Dots and Mixed Delivery Techniques. *J. Am. Chem. Soc.* **2011,** *133* (27), 10482-10489.

103. Dalal, C.; Jana, N. R., Multivalency Effect of TAT-Peptide-Functionalized Nanoparticle in Cellular Endocytosis and Subcellular Trafficking. *The Journal of Physical Chemistry B* **2017,** *121* (14), 2942-2951.

104. Dalal, C.; Saha, A.; Jana, N. R., Nanoparticle Multivalency Directed Shifting of Cellular Uptake Mechanism. *The Journal of Physical Chemistry C* **2016,** *120* (12), 6778-6786.

105. Ishikawa, M.; Biju, V., In vitro imaging of cells using peptide-conjugated quantum dots. *Proc. SPIE* **2010,** *7575* (Colloidal Quantum Dots for Biomedical Applications V), 75750R/1-75750R/8.

106. Anas, A.; Okuda, T.; Kawashima, N.; Nakayama, K.; Itoh, T.; Ishikawa, M.; Biju, V., Clathrin-Mediated Endocytosis of Quantum Dot-Peptide Conjugates in Living Cells. *ACS Nano* **2009,** *3* (8), 2419-2429.

107. Chen, B.; Liu, Q.; Zhang, Y.; Xu, L.; Fang, X., Transmembrane Delivery of the Cell-Penetrating Peptide Conjugated Semiconductor Quantum Dots. *Langmuir* **2008,** *24* (20), 11866-11871.

108. Delehanty, J. B.; Medintz, I. L.; Pons, T.; Dawson, P. E.; Brunel, F. M.; Mattoussi, H., Selective cellular delivery of self-assembled quantum dot-peptide bioconjugates. *Proc. SPIE-Int. Soc. Opt. Eng.* **2007,** *6448* (Colloidal Quantum Dots for Biomedical Applications II), 64480U/1-64480U/10.

109. Walters, R.; Kraig, R. P.; Medintz, I.; Delehanty, J. B.; Stewart, M. H.; Susumu, K.; Huston, A. L.; Dawson, P. E.; Dawson, G., Nanoparticle targeting to neurons in a rat hippocampal slice culture model. *ASN Neuro* **2012,** *4* (6), 383-392.

110. Boeneman, K.; Delehanty, J. B.; Blanco-Canosa, J. B.; Susumu, K.; Stewart, M. H.; Oh, E.; Huston, A. L.; Dawson, G.; Ingale, S.; Walters, R.; Domowicz, M.; Deschamps, J. R.; Algar, W. R.; Dimaggio, S.; Manono, J.; Spillmann, C. M.; Thompson, D.; Jennings, T. L.; Dawson, P. E.; Medintz, I. L., Selecting improved peptidyl motifs for cytosolic delivery of disparate protein and nanoparticle materials. *ACS Nano* **2013,** *7* (5), 3778-96.

111. Agarwal, R.; Domowicz, M. S.; Schwartz, N. B.; Henry, J.; Medintz, I.; Delehanty, J. B.; Stewart, M. H.; Susumu, K.; Huston, A. L.; Deschamps, J. R.; Dawson, P. E.; Palomo, V.; Dawson, G., Delivery and Tracking of Quantum Dot Peptide Bioconjugates in an Intact Developing Avian Brain. *ACS Chem. Neurosci.* **2015,** *6* (3), 494-504.

112. Walters, R.; Medintz, I. L.; Delehanty, J. B.; Stewart, M. H.; Susumu, K.; Huston, A. L.; Dawson, P. E.; Dawson, G., The role of negative charge in the delivery of quantum dots to neurons. *ASN Neuro* **2015,** *7* (July-Aug.), 1-12.

113. Getz, T.; Qin, J.; Medintz, I. L.; Delehanty, J. B.; Susumu, K.; Dawson, P. E.; Dawson, G., Quantum dot-mediated delivery of siRNA to inhibit sphingomyelinase activities in brain-derived cells. *J. Neurochem.* **2016,** *139* (5), 872-885.

114. Liu, B. R.; Huang, Y.-w.; Winiarz, J. G.; Chiang, H.-J.; Lee, H.-J., Intracellular delivery of quantum dots mediated by a histidine- and arginine-rich HR9 cell-penetrating peptide through the direct membrane translocation mechanism. *Biomaterials* **2011,** *32* (13), 3520-3537.

115. Guarnieri, D.; Muscetti, O.; Falanga, A.; Fusco, S.; Belli, V.; Perillo, E.; Battista, E.; Panzetta, V.; Galdiero, S.; Netti, P. A., Surface decoration with gH625-membranotropic peptides as a method to escape the endo-lysosomal compartment and reduce nanoparticle toxicity. *Nanotechnology* **2015,** *26* (41), 415101/1-415101/12.

116. Falanga, A.; Vitiello, M. T.; Cantisani, M.; Tarallo, R.; Guarnieri, D.; Mignogna, E.; Netti, P.; Pedone, C.; Galdiero, M.; Galdiero, S., A peptide derived from herpes simplex virus type 1 glycoprotein H: membrane translocation and applications to the delivery of quantum dots. *Nanomedicine: Nanotechnology, Biology and Medicine* **2011,** *7* (6), 925-934.

117. Dudu, V.; Rotari, V.; Vazquez, M., Sendai virus-based liposomes enable targeted cytosolic delivery of nanoparticles in brain tumor-derived cells. *J. Nanobiotechnol.* **2012,** *10*, 9.

118. Safi, M.; Domitrovic, T.; Kapur, A.; Zhan, N.; Aldeek, F.; Johnson, J. E.; Mattoussi, H., Intracellular Delivery of Luminescent Quantum Dots Mediated by a Virus-Derived Lytic Peptide. *Bioconjugate Chem.* **2017,** *28* (1), 64-74.

119. Koshman, Y. E.; Waters, S. B.; Walker, L. A.; Los, T.; de Tombe, P.; Goldspink, P. H.; Russell, B., Delivery and visualization of proteins conjugated to quantum dots in cardiac myocytes. *J. Mol. Cell. Cardiol.* **2008,** *45* (6), 853-856.

120. Li, M.; Tao, Y.; Shu, Y.; LaRochelle, J. R.; Steinauer, A.; Thompson, D.; Schepartz, A.; Chen, Z. Y.; Liu, D. R., Discovery and characterization of a peptide that enhances endosomal escape of delivered proteins in vitro and in vivo. *J Am Chem Soc* **2015,** *137* (44), 14084-93.

121. Liu, B. R.; Huang, Y.-W.; Chiang, H.-J.; Lee, H.-J., Cell-penetrating peptide-functionalized quantum dots for intracellular delivery. *J. Nanosci. Nanotechnol.* **2010,** *10* (12), 7897-7905.

122. Duan, H.; Nie, S. In *Cell-penetrating quantum dots based on multivalent and endosomolytic surface coatings*, American Chemical Society: 2007; pp COLL-157.

123. Tan, R. S.; Naruchi, K.; Amano, M.; Hinou, H.; Nishimura, S.-I., Rapid Endolysosomal Escape and Controlled Intracellular Trafficking of Cell Surface Mimetic Quantum-Dots-Anchored Peptides and Glycopeptides. *ACS Chem. Biol.* **2015,** *10* (9), 2073-2086.

124. Wadia, J. S.; Stan, R. V.; Dowdy, S. F., Transducible TAT-HA fusogenic peptide enhances escape of TAT-fusion proteins after lipid raft macropinocytosis. *Nat Med* **2004,** *10* (3), 310-315.

125. Kaplan, I. M.; Wadia, J. S.; Dowdy, S. F., Cationic TAT peptide transduction domain enters cells by macropinocytosis. *J Control Release* **2005,** *102* (1), 247-53.

126. Richard, J. P.; Melikov, K.; Vives, E.; Ramos, C.; Verbeure, B.; Gait, M. J.; Chernomordik, L. V.; Lebleu, B., Cell-penetrating peptides. A reevaluation of the mechanism of cellular uptake. *J Biol Chem* **2003,** *278* (1), 585-90.

127. Susumu, K.; Oh, E.; Delehanty, J. B.; Blanco-Canosa, J. B.; Johnson, B. J.; Jain, V.; Hervey, W. J.; Algar, W. R.; Boeneman, K.; Dawson, P. E.; Medintz, I. L., Multifunctional Compact Zwitterionic Ligands for Preparing Robust Biocompatible Semiconductor Quantum Dots and Gold Nanoparticles. *Journal of the American Chemical Society* **2011,** *133* (24), 9480-9496.

128. Smrt, S. T.; Draney, A. W.; Lorieau, J. L., The influenza hemagglutinin fusion domain is an amphipathic helical hairpin that functions by inducing membrane curvature. *J Biol Chem* **2015,** *290* (1), 228-38.

129. Clare, E. R.; Carl, W. B., III; Igor, L. M.; James, B. D., Intracellular FRET-based probes: a review. *Methods Appl Fluores* **2015,** *3* (4), 042006.

130. H Stewart, M.; L Huston, A.; Scott, A.; Efros, A.; S Melinger, J.; Boeneman, K.; Trammell, S.; Blanco Canosa, J. B.; E Dawson, P.; L Medintz, I., *Complex Forster Energy Transfer Interactions between Semiconductor Quantum Dots and a Redox-Active Osmium Assembly*. 2012; Vol. 6, p 5330-47.

131. Le Reste, L.; Hohlbein, J.; Gryte, K.; Kapanidis, Achillefs N., Characterization of Dark Quencher Chromophores as Nonfluorescent Acceptors for Single-Molecule FRET. *Biophys J* **2012,** *102* (11), 2658-2668.

132. Eichmann, C.; Orts, J.; Tzitzilonis, C.; Vogeli, B.; Smrt, S.; Lorieau, J.; Riek, R., Intermolecular detergent-membrane protein noes for the characterization of the dynamics of membrane protein-detergent complexes. *J Phys Chem B* **2014,** *118* (49), 14288-301.

133. Sun, Q.; Cai, S.; Peterson, B. R., Selective Disruption of Early/Recycling Endosomes: Release of Disulfide-Linked Cargo Mediated by a N-Alkyl-3β-Cholesterylamine-Capped Peptide. *Journal of the American Chemical Society* **2008,** *130* (31), 10064-10065.

134. Lundin, P.; Johansson, H.; Guterstam, P.; Holm, T.; Hansen, M.; Langel, U.; Andaloussi, S. E. L., Distinct Uptake Routes of Cell-Penetrating Peptide Conjugates. *Bioconjugate Chem* **2008,** *19* (12), 2535-2542.

135. Dalcol, I.; Rabanal, F.; Ludevid, M.-D.; Albericio, F.; Giralt, E., Convergent Solid Phase Peptide Synthesis: An Efficient Approach to the Synthesis of Highly Repetitive Protein Domains. *The Journal of Organic Chemistry* **1995,** *60* (23), 7575-7581.

136. Riniker, B.; Flörsheimer, A.; Fretz, H.; Sieber, P.; Kamber, B., A General Strategy for the Synthesis of Large Peptides: The Combined Solid-Phase and Solution Approach. *Tetrahedron* **1993,** *49* (41), 9307-9320.

137. Vasileiou, Z., Barlos, K. and Gatos, D., Convergent solid-phase and solution approaches in the synthesis of the cysteine-rich Mdm2 RING finger domain. *J. Peptide Sci.* **2009,** *15*, 824-831.

138. Bray, B. L., Large-scale manufacture of peptide therapeutics by chemical synthesis. *Nat Rev Drug Discov* **2003,** *2* (7), 587-593.

139. Hansen, P. R.; Oddo, A., Fmoc Solid-Phase Peptide Synthesis. In *Peptide Antibodies: Methods and Protocols*, Houen, G., Ed. Springer New York: New York, NY, 2015; pp 33-50.

140. Schwab, L. S., 14-(Arylhydroxyamino)codeinones and derivatives as analgetics and antagonists. *J Med Chem* **1980,** *23* (6), 698-702.

141. Silvia, V.; Baldisserotto, A.; Scalambra, E.; Malisardi, G.; Durini, E.; Manfredini, S., Novel molecular combination deriving from natural aminoacids and polyphenols: Design, synthesis and free-radical scavenging activities. *European Journal of Medicinal Chemistry* **2012,** *50*, 383-392.

142. Agard, N. J.; Prescher, J. A.; Bertozzi, C. R., A Strain-Promoted [3 + 2] Azide−Alkyne Cycloaddition for Covalent Modification of Biomolecules in Living Systems. *Journal of the American Chemical Society* **2004,** *126* (46), 15046-15047.

143. Edman, P., Mechanism of the Phenyl Isothiocyanate Degradation of Peptides. *Nature* **1956,** *177* (4510), 667-668.

144. Bray, B. L., Large-scale manufacture of peptide therapeutics by chemical synthesis. *Nature Reviews Drug Discovery* **2003,** *2*, 587.

VITA

Education

Ph.D.: The University of Illinois at Chicago – Chemistry 2017
Chicago, **IL**, **USA**
Focus: Synthetic Organic and Peptide Chemistry

Master of Science: University at Buffalo,
The State University of New York – Chemistry 2009
Buffalo, **NY**, **USA**
Focus: Medicinal Chemistry

Bachelor of Science: University of Veracruz –
Chemistry, Pharmacy and Biology 2003
Orizaba, **Veracruz**, **Mexico**
Graduated with Distinction

Highlights

- Design, synthesis, purification, and characterization of small molecules and peptides.
- Solid phase peptide synthesis.
- Structure elucidation of small molecules by nuclear magnetic resonance (NMR) techniques.
- Transition metal catalysis.
- Execution of multi-step synthesis and scale-up.
- Expertise in standard purification and characterization techniques.

Technical Skills

- Purification techniques: High-pressure liquid chromatography (HPLC), flash chromatography, crystallization, and distillation.
- Mass spectrometry techniques: Electrospray ionization (ESI), Gas chromatography-mass spectrometry (GC-MS), Matrix-assisted laser desorption ionization (MALDI), Liquid chromatography-mass spectrometry (LC-MS).
- Nuclear magnetic resonance (NMR) techniques: Execution and interpretation of 1D NMR for example H1, C13, DEPT, and 2D NMR techniques such as COSY, NOESY, HMQC, HMBC.
- Infrared spectroscopy (IR) , UV-VIS spectrometer (UV) and fluorimeter.

- Skilled on the execution of humidity and air sensitive reactions and in the use of glove box.
- Extensive hands-on experience in the design and execution of multi-step syntheses.
- Ample experience in the optimization of chemical processes and scale-up methodologies.
- Highly skilled on peptide synthesis on solid phase
- Strong understanding of peptide chemistry and organic chemistry, with the ability to merge both fields.

Professional Experience

NMR Technician and Teaching Assistant, Chemistry Department
The University of Illinois at Chicago, Chicago, IL (08/201– 05/2017)

- Trained students enrolled in the Physical Chemistry Laboratory course on the execution of 1D and 2D NMR experiments (H1, C13, DEPT, COSY, HMBC, HMQC) as a tool for structure elucidation of small molecules.
- Maintained Varian NMR magnets by nitrogen and helium fillings.

Research Assistant for Prof. Lawrence Miller, Chemistry Department
The University of Illinois at Chicago, Chicago, IL (08/2013 – 09/2017**)**

- Synthesized peptide ligands for coating semiconductor quantum dots and monitor their intracellular delivery by microscopy.
- Multi-step synthesis, purification and characterization of fluorescent peptide for live-cell imaging applications.
- Designed and synthesized modular peptide probes as tools for their intracellular delivery and imaging studies.

Research Assistant for Prof. Vladimir Gevorgyan, Chemistry Department
The University of Illinois at Chicago, Chicago, IL (08/2009 - 04/2013)

- Developed a methodology for the synthesis of furans and pyrroles by gold catalysis.
- Developed a highly enantioselective methodology for the synthesis of silyl aldehydes by carbenoid insertion reactions into silicon-hydrogen bonds.
- Developed a practical and high yield methodology for the synthesis of alkyl silyl propargylic aldehydes.
- Collaborated on the synthesis of medicinally relevant triazoles catalyzed by copper.

Research Assistant for Prof. Qing Lin, Chemistry Department
University at Buffalo, The State University of New York,
Buffalo, NY (08/2005 - 05/2009)

- Demonstrated the utility of photochemistry to synthesize a series of pyrazole and pyrazoline analogs of anti-cancer inhibitor Nutlin-3.
- Discovered a lead pyrazole compound inhibitor of MDM2-p53 interaction.
- Validated the use of photochemistry for the macrocyclization or 'peptide stapling' of linear peptides.
- Investigated the inhibitory activities of staples peptides in protein-protein interactions.
- Developed and validated a robust ELISA assay to measure the inhibitory activities of small molecules to disrupt protein-protein interactions.
- Synthesized a biotinylated tetrazole probe, which served to confirm the metabolic incorporation of homoallylglycine (HAG) as a viable bioorthogonal chemical reporter for selective protein modification.

Published Work

- Shiroodi, R. K.; **Vera, C. I. R.**; Dudnik, A. S.; Gevorgyan, V., Synthesis of furans and pyrroles via migratory and double migratory cycloisomerization reactions of homopropargylic aldehydes and imines. *Tetrahedron Lett.* 2015, 56 (23), 3251-3254. (Special issue, symposium-in-print: Harry Wasserman).
- Chattopadhyay, B.; **Vera, C. I. R.**; Chuprakov, S.; Gevorgyan, V., Fused Tetrazoles as Azide Surrogates in Click Reaction: Efficient Synthesis of N-Heterocycle-Substituted 1,2,3-Triazoles. *Org.Lett.* 2010, 12 (9), 2166-2169.
- Song, W.; Wang, Y.; Yu, Z.; **Vera, C. I. R.**; Qu, J.; Lin, Q., A Metabolic Alkene Reporter for Spatiotemporally Controlled Imaging of Newly Synthesized Proteins in Mammalian Cells. *ACS Chem.Biol.* 2010, 5 (9), 875-885. (Cover Article) Evaluated by Biology Faculty of 1000 as "Must Read", October 14, 2010.
- Madden, M. M.; **Vera, C. I. R.**; Song, W.; Lin, Q., Facile synthesis of stapled, structurally reinforced peptide helices via a photoinduced intramolecular 1,3-dipolar cycloaddition reaction. Chem. Commun. 2009, (37), 5588-5590.
- Wang, Y.; **Vera, C. I. R**.; Lin, Q., Convenient synthesis of highly functionalized pyrazolines via mild, Photoactivated 1,3-dipolar cycloaddition. Org.Lett. 2007, 9 (21), 4155-4158.

- M.S. dissertation**: Rivera Vera, C. I**. Applications of the 1,3-dipolar cycloaddition reaction towards the target-guided synthesis of small molecule inhibitors and towards peptide stapling. The state University of New York at Buffalo, June 2009.
- Poster session: Chattopadhyay, B.; **Vera, C. I. R.**; Chuprakov, S.; Gevorgyan, V. Fused Tetrazoles as Azide Surrogates in Click Reaction: Efficient Synthesis of N-Heterocycle-Substituted 1,2,3-Triazoles, Presented at 27th Herbert C. Brown Lectures in Organic Chemistry, West Lafayette, Indiana, April 2010.
- Patent application: Lin, Q.; Madden, M.; **Rivera Vera, C. I**. Stapled Peptides and Method of Synthesis. Patent Application WO 2010/033617, Sep 16, 2009.

APPENDIX

OHN WILEY AND SONS LICENSE TERMS AND CONDITIONS

This Agreement between University of Illinois at Chicago -- Claudia Rivera Vera ("You") and John Wiley and Sons ("John Wiley and Sons") consists of your license details and the terms and conditions provided by John Wiley and Sons and Copyright Clearance Center.

License Number	4174010711037
License date	Aug 22, 2017
Licensed Content Publisher	John Wiley and Sons
Licensed Content Publication	Wiley Interdisciplinary Reviews - Nanomedicine and Nanobiotechnology
Licensed Content Title	Nanoescapology: progress toward understanding the endosomal escape of polymeric nanoparticles
Licensed Content Author	Laura I. Selby,Christina M. Cortez-Jugo,Georgina K. Such,Angus P.R. Johnston
Licensed Content Date	Feb 3, 2017
Licensed Content Pages	1
Type of Use	Dissertation/Thesis
Requestor type	University/Academic
Format	Print and electronic
Portion	Figure/table
Number of figures/tables	2
Original Wiley figure/table number(s)	Figure 1, Figure 2
Will you be translating?	No
Title of your thesis / dissertation	Peptide-based strategies of delivering semiconductor nanocrystals into living cells
Expected completion date	Sep 2017
Expected size (number of pages)	120
Requestor Location	University of Illinois at Chicago 845 west taylor st Chemistry dept SES building CHICAGO, IL 60607 United States Attn: claudia
Publisher Tax ID	EU826007151
Billing Type	Invoice
Billing Address	University of Illinois at Chicago 845 west taylor st Chemistry dept SES building CHICAGO, IL 60607 United States Attn: claudia
Total	0.00 USD
Terms and Conditions	

ELSEVIER LICENSE
TERMS AND CONDITIONS

This Agreement between University of Illinois at Chicago -- Claudia Rivera Vera ("You") and Elsevier ("Elsevier") consists of your license details and the terms and conditions provided by Elsevier and Copyright Clearance Center.

License Number	4181620119425
License date	Sep 03, 2017
Licensed Content Publisher	Elsevier
Licensed Content Publication	Nano Today
Licensed Content Title	Intracellular delivery of nanomaterials: How to catch endosomal escape in the act
Licensed Content Author	Thomas F. Martens,Katrien Remaut,Jo Demeester,Stefaan C. De Smedt,Kevin Braeckmans
Licensed Content Date	Jun 1, 2014
Licensed Content Volume	9
Licensed Content Issue	3
Licensed Content Pages	21
Start Page	344
End Page	364
Type of Use	reuse in a thesis/dissertation
Portion	figures/tables/illustrations
Number of figures/tables /illustrations	1
Format	both print and electronic
Are you the author of this Elsevier article?	No
Will you be translating?	No
Original figure numbers	Table 3
Title of your thesis/dissertation	Peptide-based strategies of delivering semiconductor nanocrystals into living cells
Expected completion date	Sep 2017
Estimated size (number of pages)	120
Requestor Location	University of Illinois at Chicago 845 west taylor st Chemistry dept SES building CHICAGO, IL 60607 United States Attn: claudia
Publisher Tax ID	98-0397604
Total	0.00 USD

Terms and Conditions